DEVELOPMENT OF A **POOL AND SLOT FISHWAY**

Laboratory Measurements and Numerical Simulation

BY **DAVID DERFLINGER**, B.Sc.

GRAZ UNIVERSITY OF TECHNOLOGY

Institute for Hydraulic Engineering and Water Resources Management

Provided to obtain the academic degree of a

Master of Civil Engineering

GRAZ, SEPTEMBER 2021

AUTHOR
David Derflinger, MSc candidate
david.derflinger@hotmail.com
Geotechnical and Hydraulic Engineering

SUPERVISOR
Assoc.Prof. Dipl.-Ing. Dr.nat.techn. Josef Schneider

SUPERVISING ASSISTANT
Dr.techn. M.Sc. Shervin Shahriari

DECLARATION OF HONOR

I declare that this thesis has been composed solely by myself and that it has not been submitted, in whole or in part, in any previous application for a degree. Except where stated otherwise by reference or acknowledgement, the work presented is entirely my own.

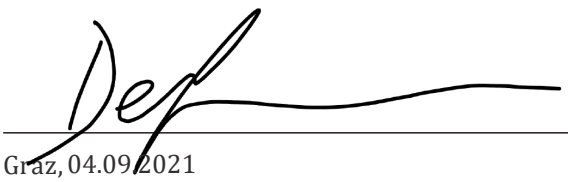

Graz, 04.09.2021

ACKNOWLEDGEMENTS

I would like to take the opportunity and thank those who supported me during the process of writing this thesis.

First and foremost, I would like to thank Assoc.Prof. Josef Schneider who, not only made this thesis possible, but also gave valuable advice and feedback throughout the entire process. Both the laboratory measurements and the theoretical approach would have not been as manageable without his support.

Equally, Dr. Shervin Shahriari has played a major role during the setup and analysis of the numerical simulations. His advice and engagement not only made a significant portion of this thesis possible, but also provided indispensable information about the topic as a whole.

Special thanks go out to DDipl.-Ing Georg Seidl who has provided numerous counts of subject-specific advice and has shown such a high degree of personal involvement, which unquestionably pushed the quality of the thesis at hand to what it is.
I also want to mention MSc. Markus Haslwanter, who provided valuable data and insights from a previously conducted thesis on the same topic, which I am very grateful for.

Additionally, I would like to thank the staff of the Institute for Hydraulic Engineering and Water Resources Management at TU Graz, starting with the head of office Univ.-Prof. Gerald Zenz, who has, together with Assoc.Prof. Josef Schneider, provided the opportunity to work at the Institute and gather knowledge in the field, ultimately leading to this thesis. As well as the laboratory staff Martin Koch and Walter Felgitsch, who regularly lend a helping hand during the measurement process.

Last but not least, I would like to express my loving thanks to my family and partner, who made sure that at least some rest was found in between the hours spent working on this thesis and who supported me to an extent that I can't do justice in just those few words.

THANK YOU.

ABSTRACT

The necessity for fishways, where the natural flow of a river has been disturbed by artificial means, is based on nature conservation efforts and tied to Austrian law by the *Water Framework Directive*. The process of ensuring a biodiversity least disturbed by human influence is supported by the analysis of the structures making it achievable. For this reason, a methodical study of a particular type of fishway, the Pool and Slot Fishway (PSF), was conducted utilizing both laboratory measurements and Computational Fluid Dynamics.

The fundamentals for the ecological assessment and general fishway design were based on the Austrian Guideline for Fishway Design, published by the Austrian Federal Ministry for Agriculture, Regions and Tourism. The subsequent investigation was carried out using an Acoustic Doppler Velocimeter for the laboratory measurements and the application ANSYS Fluent for the numerical simulations. Additionally, the flow behaviour was compared between two similar versions of the geometry, differing only in slot-width, for a better understanding of its influence.

The general flow within the measurement domain was visualized and described in detail, providing a large set of reference images for further assessment and comparison.

In succession to a previously conducted work on the same topic, the hypothesis of an advantageous flow behaviour, in comparison to a conventional vertical-slot fishway, was repeatably shown and validated by measurement and simulation data. Flow velocities, as well as the Turbulent Kinetic Energy (TKE) was plotted at horizontal and vertical planes, supported by line measurements, describing their spatial distribution and quantitative range.

01 INTRODUCTION

The topic of river connectivity, for aquatic life, is a major indicator for the ecological quality of a river system. Since its implementation into Austrian law, in 2003, the so-called *Water Framework Directive* has set requirements on the quality of overground flows and has thereby created a demand for improvement, regulated by law and based on nature conservation efforts. Although leaving natural rivers as they are and minimizing human involvement would certainly be best for the ecosystem, some disruption is practically unavoidable. Hydro-power plants, dams and all sort of artificial blockages are justifiably built but separate the natural river flow. To counteract the disadvantages to the river system introduced by such structures, installations like fishways have to be constructed. All over Europe, and ultimately all across the world, fishways will have to be implemented in high numbers to improve and stabilize the ecological situation within and around lotic systems. For that reason, a better understanding of the intricate details within the different types of fishways is essential to both optimize existing layouts and progress towards even better alternatives. One of those existing types is the Pool and Slot Fishway (PSF), a variant of the vertical-slot fishway and the focus of this body of work.

A previously conducted thesis on the topic of PSFs (HASLWANTER, 2020) indicated a flow behaviour, theoretically superior to that of a conventional vertical-slot fishway. To expand the investigation, gather more data and possibly confirm the hypothesis, this follow-up thesis was brought to light.

Due to the preceding efforts, a laboratory model of the fishway in question already existed and so did reference data to draw comparisons from. It is worth noting that all the measurements included within this thesis were gathered after the previous one had already been finished and are there to either reinforce or question the advantages a PSF has over similar build-types.

As part of understanding the flow dynamics of fishways, the ecological framework in which they exist has to be understood. Therefore, aspects of the ecological situation are described with the help of the *Austrian Guideline for Fishway Design* (AG-FAH 2012), published by the Austrian Federal Ministry for Agriculture, Regions and Tourism (BMNT). Although this particular fishway does not exist as such in nature, the ecological fundamentals from which the design is derived, are drawn from an existing location so that its layout resembles a reasonably implemented structure.

Laboratory measurements and the subsequent visualizations give an overview of the flow characteristics and offer data for comparison, as well as evaluations concerning potential efficacy, design specifics and assumed theory.

On top of the physical measurements, numerical simulations were performed to both test their performance when applied to such structures, and provide a complete picture of the entire water body within the PSF. The combination of laboratory and Computational Fluid Dynamics (CFD) data provided a diverse set of results, each with their own pros and cons, offering the opportunity for cross-examination at points with high uncertainty.

After all, the goal of this thesis was to provide an analysis of the PSF, which improves the understanding of its general behaviour and tests a range of aspects critical to its effectiveness.

02 BASICS OF A FISHWAY

ECOLOGY
INTRODUCTION

During their evolution, fish have adopted to the four-dimensional nature of lotic ecosystems, consisting of a longitudinal, lateral and vertical connectivity, as well as a temporal variability of that connectivity. Therefore, the migration behaviour fish show throughout most of their life stages, is closely tied to said connectivity (WARD 1989; JUNGWIRTH et al. 2000). In natural river systems fish migrate both up- and downstream as well as in lateral direction. The general goal of their movement is to find resources regarding nutrition, growth, reproduction, shelter from predators and similar (NORTHCOTE 1978). A disruption of those migration paths therefore has a substantial negative effect on most fish species (ZITEK et al. 2007).

The connection between different habitats within a larger lotic ecosystem benefits the fish stocks. Not only does a diverse habitat provide the essentials mentioned before, but also stabilizes otherwise isolated fish stocks after events impacting the local fish population. A large-scale connectivity of the lotic ecosystem is key to the long-term conservation of most fish species and with that the ecological state of the rivers involved. Preventing populations from acquiring new habitats while further dividing existing ones will most likely lead to a significant impact on both fish stocks and diversity (AG-FAH 2012).

For this reason, preserving and restoring the natural river passage has to be considered especially at locations where it previously has been disturbed. During the last century countless constructions like hydro-power plants and dams have been built without a sufficient way of providing fish with a way of passage. In 2003 the *EU Water Framework Directive* from the year 2000 was implemented in the *Wasserrechtsgesetz 1959* (BGBl. Nr. 215/1959 i.d.g.F.) of Austria, making it national law and enforcing, among other goals, a certain quality of the lotic ecosystem. A factor in this quality rating is the river connectivity, increasing efforts to improve critical locations and preventing more to come.

Avoiding building disadvantageous structures in the first place, would be a way of approaching such a connectivity. This in itself would create the dilemma of weighing e.g renewable energy of flood safety against the ecological situation. Therefore, fishways are constructed to ease the impact of necessary river installations on the environment around them. These fishways provide the fish with means of passage, while still allowing an almost complete shut-off from the natural river flow.

Generally, fishways are constructions which allow the existing fish stock and/or other aquatic animals to overcome man-made obstacles on their way upstream (JUNGWIRTH and PELIKAN 1989).

Many different types of fishways have been developed, each with their own set of pros and cons. To support the construction efforts, the Austrian Federal Ministry for Agriculture, Regions and Tourism has created a design guideline called *Leitfaden zum Bau von Fischaufstiegshilfen* (AG-FAH 2012), which has also provided the framework for the following design decisions. For the purpose of this thesis, only the PSF, a variation of the vertical-slot fishway, will be reviewed.

SWIMMING PERFORMANCE

A major limiting factor for fishways are the swim speeds of the different fish species. The construction allows the upstream movement via a succession of pools and slots with alternating water velocities. The fish must overcome the higher velocities around the slots which are then followed by a low velocity pool area. Whether or not a fish can overcome the critical points and ascend the fishway depends mostly on its swim speed and the duration for which it is sustainable. These separate swimming performances can be roughly divided into the following categories (according to JENS et al. 1997, later expanded by CLOUGH and TURNPENNY 2001):

Sustained swimming speed

The regular speed at which a fish commonly moves through waters and which it can sustain for a long period of time (>200 min) without showing signs of fatigue.

Prolonged swimming speed

The swimming speed that can only be held for a shorter duration (20s – 200 min) leading to a certain muscle fatigue.

Burst swimming speed

The swimming speed that can only be achieved for a very limited amount of time (<20s) and is followed by a recovery period.

Critical burst speed

According to CLOUGH and TURNPENNY (2001) it is the swimming speed that is, after a short time (<20s), followed by an involuntary drift off. It is also the swimming speed that is crucial for eco-hydraulic planning.

Maximum swimming speed

A theoretical maximum possible swimming speed for a fish species.

The following figure shows a schematic of the interaction between swimming speeds and duration.

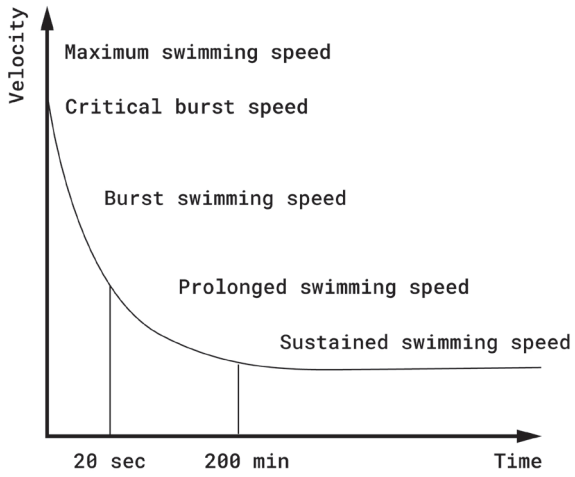

Figure 1: Maximum speed and duration (PAVLOV 1989)

For the design of a fishway, the burst- and critical burst swimming speeds are the deciding factors. If flow rates exceed the swimming performance for a prolonged period of time without offering opportunities for rest, fish are unable to overcome the obstacle and are forced to take a rest before repeating the attempt. Different species show a natural difference in their critical burst speed. For example, salmonoids reach a speed of about 10 BL/s (body lengths per second) for trout this usually means around 2–3 m/s, while others like cyprinids and breams fall short of that with about 4–5 BL/s. The weakest among the migrating fish are usually juvenile or small fish species, limited by burst swim speeds of approximately 0.35–0.6 m/s (JENS et al. 1997). For those, a rough bottom should provide flow conditions that enable a fishway ascend even with higher velocities within the main flow. Generally, the maximum flow rates should not exceed 1 m/s in the potamal and 1.5–2 m/s in the rhithral, according to JUNGWIRTH and PEKIKAN (1989). (AG-FAH 2012)

ORIENTATION

To achieve the primary goal of connecting the up- and downstream regions of an insurmountable structure, a fishway has to not only create a flow which allows for a variety of fish to move upstream, but first and foremost has to be found. Fish primarily find orientation by sensing the water flow rate and direction. According to JENS et al. (1997), fish sense only the currents close to their body, while weaker secondary flows are often unnoticed. If a flow rate exceeds the manageable limit, the fish will search for a more adequate streamline. Turbulent flow conditions might put additional strain on the migration. To precisely navigate towards a leading flow, the flow rate has to be above about 0.3 m/s, below that fish continuously lose their sense of direction. An optimum for most of the fish home to the potamal is a flow rate of about 70–100 cm/s according to PAVLOV (1989). Additionally, the flow rate at the outflow of the fishway should be higher than the one in the mainstream to be detectable (AG-FAH 2012).

DESIGN

The overall design of the fishway is meant to create conditions that cater to the needs of the migrating fish population—considering aspects as mentioned before. Depending on the local specifics, the design usually follows the guidelines set in the *Leitfaden zum Bau von Fischaufstiegshilfen* (AG-FAH 2012) and is adjusted for the situation. The main principles of findability and passability are at the forefront of the decision-making process. Each type of fishway has its own way of solving the main problems. One of those, the PSF, will be discussed in detail in the following chapters.

POOL AND SLOT FISHWAY

INTRODUCTION

The measurements and calculations conducted throughout this thesis are centred around a PSF—a specific type of vertical-slot fishway defined by its straight wall elements devoid of any 'hook-elements' at the slot boundaries. Previous work has been provided concerning a comparison of a standard vertical-slot fishway and the aforementioned PSF. After indications arose that the simplistic design of the PSF might bring benefits to the structure's behaviour, while reducing the geometric complexity, more research was initiated, leading to this body of work. Although the concept of how a fishway works is generally consistent, the different types each bring their own strengths and weaknesses. For the sake of simplicity, this thesis holds its focus on the PSF, describing its properties in as much detail as possible and opening up the potential for comparisons without itself providing an evaluation of such. The value therefore lies in a better understanding of the specifics, making it easier to judge whether or not a PSF fits a certain situation.

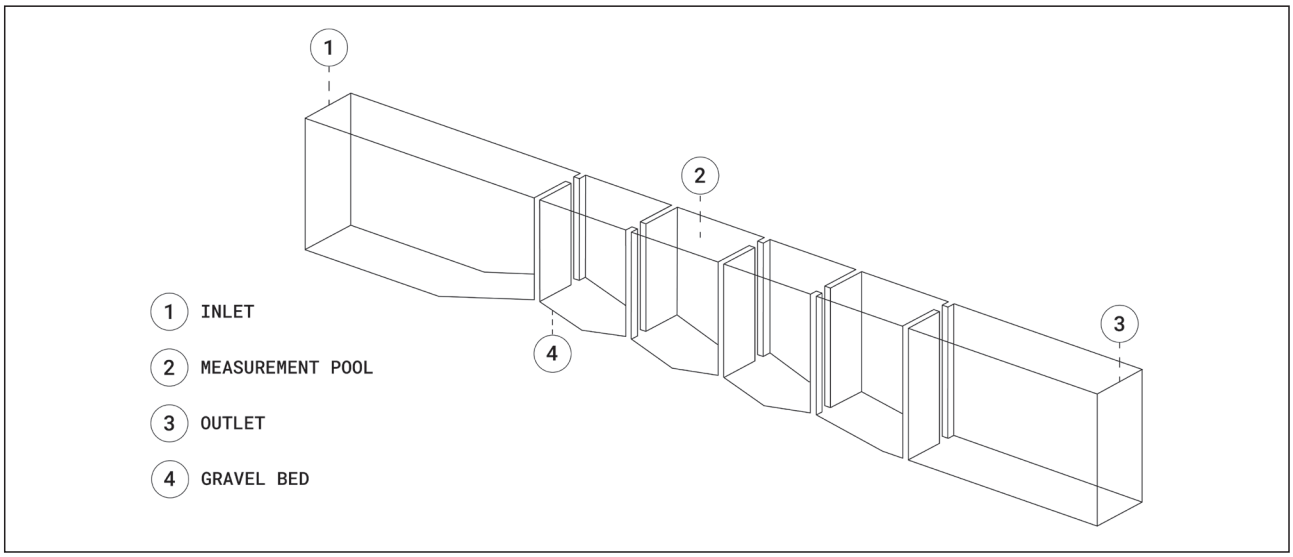

Figure 2: Pool and Slot Fishway sketch

The general design of a PSF can be seen in Figure 2. Note that the design lacks any sort of small-scaled elements, making the construction an easier task compared to a standard vertical-slot fishway including hooked elements at the slot boundaries. Another design property that is essential to the PSF is its bottom design. Rather than having a constant inclination, the PSF forms small basins between the pool-separating walls. Similar to other fishways, the pool boundaries are alternating from side to side, creating a specific flow behaviour.

The specific PSF in focus was designed around the previously mentioned guideline (AG-FAH 2012) and is therefore closely related to the dominant fish species, targeted by the construction. The design should allow for the passage of as many fish, common in the area, as possible. Targeting not only bigger and stronger species, but also smaller and weaker fish who might experience troubles surpassing more intense water flows. For this purpose, the hydraulic behaviour of the fishway will be further investigated with the goal of creating a surrounding best fit for the local fish migration. To test whether or not specific design decisions have a beneficial effect on the system behaviour and to generally have a better understanding of PSF, a downscaled flume was constructed in the laboratory of the *Institute for Hydraulic Engineering and Water Management* (TU GRAZ). Measurements taken in the laboratory can then be scaled back to a real-life situation and evaluated using existing guidelines and comparable fishways. The detailed measurement setup, including the measurement device, exact geometry and overall methodology will be explained in the following chapters.

ECOLOGICAL SITUATION

Since the laboratory measurement setup had to be based on an ecological situation, the river Mur around the city of Graz (AUT) builds the framework for the design of the testing flume. Most of the geometry is therefore chosen based on the occurring fish population, as its sole purpose is to cater to their needs. First and foremost, the river type and with it the size-determining fish species has to be determined. The river Mur, for which the fishway was designed, was narrowed down to specifically target the section around the city of Graz. In the guideline (AG-FAH 2012), the river Mur is classified as a river of the type 'Epipotamal large' and the size-determining fish species is the Danube salmon (Huchen), with a length of up to 100 cm. In the following table, the different river types can be seen with the relevant one being highlighted. Further understanding of the fish diversity comes from a report done for the Styrian state govern-

Table 1: River Region (AG-FAG 2012)

FISHREGION	DECISIVE FISH-SPECIES AND -LENGTH
EPIRHITHRAL	
Epirhithral, MQ < 2 m^3/s	30 cm River Trout
Epirhithral, MQ > 2 m3/s	40 cm River Trout
METARHITHRAL	
Metarhithrall, MQ < 2 m3/s	40 cm River Trout
Metarhithrall, MQ > 2 m3/s	50 cm River Trout, Grayling
HYPORHITHRAL	
Hyporhithral small, MQ < 2 m3/s	50 cm Chub, Grayling, 50 cm Burbot
Hyporhithral large without Huchen, MQ > 2 m3/s	60 cm Burbot, Barbel/ Nase
Hyporhithral large with Huchen, MQ > 2 m3/s - 20 m3/s	80 cm Huchen
Hyporhithral large with Huchen, MQ > 20 m3/s	100 cm Huchen
EPIPOTAMAL	
Epipotamal medium without Pike, without Huchen	60 cm Barbel/ Nase
Epipotamal medium with Pike, without Huchen	90 cm Pike, 50 cm Bream
Epipotamal medium with Huchen	90 cm Huchen, 50 cm Bream
Epipotamal large with Huchen	100 cm Huchen
Epipotamal large without Huchen, with Catfish	120 cm Catfish
Epipotamal large without Huchen, without Catfish	90 cm Pike, 50 cm Bream

ment titled *Fischökologische Zustandserhebung der Mur im Stadtgebiet von Graz 2012* (WOSCHITZ et al. 2013). The report confirms the river type as epipotamal large and lists not only the largest species, but divides all occurring fish into categories, labelled 'leading species', 'typical accompanying species' and 'rare accompanying species'. The table to the right was translated from the aforementioned report and is further based on an investigation done at the river section Gratkorn to Wildon (WOSCHITZ et al. 2007). The table is furthermore expanded by an ecological condition rating, reaching from 1 (very good) to 5 (bad). The rating system was introduced by the BMNT, in their report titled *Leitfaden zur Erhebung der Biologischen Qualitätselemente Teil A1 – Fische* (BMNT 2019). The rating is composed of three separate rating criteria: species composition, region index and age structures. The index table has also been translated and is shown in addition to the species diversity list.

Table 2 : Fish Ecological Condition Index (WOSCHITZ et al. 2013)

Fish Ecological Condition Index	
1	Very Good
2	Good
3	Mediocre
4	Unsatisfactory
5	Bad

Finally, the largest fish, the Danube salmon (the size-determining species), provides the basis for the minimum dimensions of the fishway. What will later be discussed in the geometry section is then based on the following fish dimensions.

Table 3 : Huchen body measurement (AG-FAH 2012)

SIZE DEFINING FISH SPECIES	Length (cm)	Height (cm)	Width (cm)
Huchen	80	13	10
	90	14	12
	100	16	12
	120	19	14

Table 4 : Fish Ecological Diversity Mur (WOSCHITZ et al. 2013)

RIVER	MUR	
Fish Region	EP large	
Name	type	index
Aalrutte	a	4
Aitel	l	5
Äsche	a	4
Bachforelle	a	4
Bachschmerle	a	4
Barbe	l	5
Bitterling	r	3
Brachse	r	3
Elritze	a	4
Flussbarsch	a	4
Frauennerfling	a	4
Giebel	r	3
Goldsteinbeißer	r	3
Gründling	l	5
Güster	r	3
Hasel	a	4
Hecht	a	4
Huchen	a	4
Karausche	r	3
Kesslergründling	r	3
Koppe	a	4
Laube	a	4
Moderlieschen	r	3
Nase	l	5
Nerfling	r	3
Neunauge	a	4
Rotauge	a	4
Rotfeder	r	3
Rußnase	r	3
Schied	r	3
Schlammpeitzger	r	3
Schleie	r	3
Schneider	l	5
Schrätzer	r	3
Semling	r	3
Steinbeißer	a	4
Steingreßling	r	3
Sterlet	r	3
Streber	a	4
Strömer	l	5
Weißflossengründli	a	4
Wildkarpfen	r	3
Zander	r	3
Zingel	r	3

l = leading species, a = typical accompanying species
r = rare accompanying species

GEOMETRY

The basic geometry of the PSF, as mentioned before, is related to both sides of the fish size spectrum. The size-determining fish species is setting the minimum dimensions for the pools and slots while the juvenile and small fish species are limiting the flow rate as well as the turbulence, expressed as energy dissipation [W/m3].

For PSFs the pool length must exceed three times the body length of the size-determining species and the pool width two times their body length. For the vertical slots at the pool boundaries, the width can be reduced to three times their body width but must be greater than 15 cm (AG-FAH 2012).

Applied to the situation at hand, the minimum dimensions are set by the Danube salmon (huchen) with a body length of 100 cm, a body height of 16 cm and a body width of 12 cm (according to JÄGER et al. 2010). Resulting in the following structure dimensions:

Pool length:	3.10 m	(min. 3.00 m)
Pool width:	2.10 m	(min. 2.00 m)
Slot width:	0.36–0.46 m	(min. 36 cm)

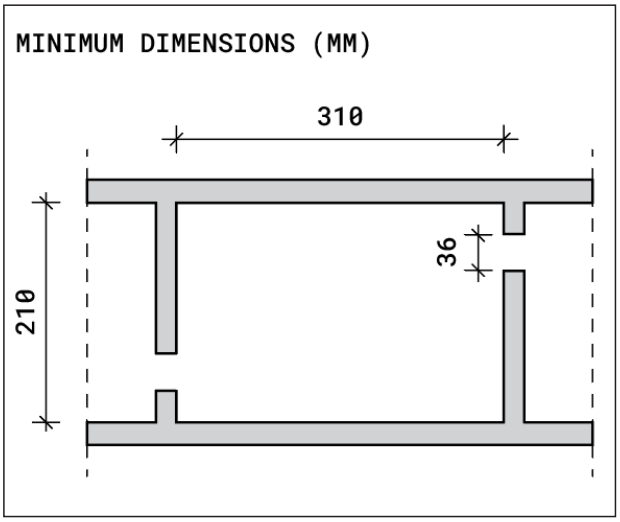

Figure 3: Minimum dimensions

Table 5: Minimum dimensions (FG-FAH 2012)

FISHREGION	DECISIVE FISH-SPECIES	FISH LENGTH [cm]	MAX. LEVEL DIFFERENCE BETWEEN POOLS [cm]	ENERGYDISSIPATION [W/m³]	SLOT WIDTH [cm]	MIN. POOL LENGTH [cm]	MIN. POOL WIDTH [cm]
Epirhithral, MQ < 2 m³/s	River Trout (RT)	30	20	160	15	210	140
Epirhithral, MQ > 2 m³/s	River Trout	40	20	160	15	210	140
Metarhithral, MQ < 2 m³/s	River Trout	40	18	140	15	200	130
Metarhithral, MQ > 2 m³/s	Grayling, River Trout	50	18	130	20	250	170
Hyporhithral, MQ < 2 m³/s	RT, Chub, Grayling, Burbot	50	15	120	20	230	150
Hyporhithral, MQ > 2 m³/s	Burbot, Barbel	60	15	120	25	250	170
Hyporhithral, 2 < MQ < 20 m³/s	Huchen	80	15	120	30	280	190
Hyporhithral, MQ > 20 m³/s	Huchen	100	15	120	35	310	210
Epipotamal medium	Barbel	60	13	100	25	250	170
Epipotamal medium	Pike	90	13	100	27	270	180
Epipotamal medium	Huchen	90	13	100	32	290	190
Epipotamal large	Huchen	100	13	100	35	310	210
Epipotamal large	Catfish	120	13	100	50	370	250

Additionally, the water depth has to be regulated, as fish need a certain volume around them—or rather their tail fin—to be able to swim properly. Different literature list a variety of minimum depths, for the purpose of this dimensioning process the same boundary values are used as described in AG-FAH (2012). Therefore, the lowest acceptable water depth is 2.5 times the body height of the size-determining fish species but must always exceed 20 cm (AG-FAHG 2012). For this particular case this means a depth of:

Minimum water depth: 40 cm

The same is true for the pool boundaries. The water depth within the slot should exceed the same minimum and the bottom should connect smoothly to those of the pools. Jumps in the bottom altitude should generally be avoided as it disturbs the migration path of fish moving close to the ground (AG-FAH 2012).

Table 5 showed the minimum dimensions for vertical-slot fishways according to AG-FAH (2012). It is noted that for the minimum pool length and width, a minimum volume has been the limiting factor, setting the values slightly above those calculated from the size-determining fish species. This has been considered in the model dimensions.

Another specific aspect of the PSF variation of the vertical-slot fishway, is the bottom geometry. In contrast to having a constant inclination, the pool bottoms each have a small basin like shape, with its maximum depth in the middle of the pool, rising towards the pool boundaries. Those basins create an area with low flow velocities and should in theory provide a space in which fish can survive, should the water flow be interrupted for a period of time (SEIDL 2018).

HYDRAULIC BEHAVIOUR

The hydraulic behaviour of the PSF is the core subject of the investigations carried out, both in the laboratory and the numerical model. It is essential to understand the flow mechanisms to ensure conditions that fit the aforementioned framework. The crucial points hereby are the slot areas where maximum flow velocities occur, as well as the overall flow dynamics, energy dissipation and discharge. In particular, the velocities should allow even for weaker fish to migrate through the fishway. Flow dynamics should behave in a way that fish can move between the calm sections of the pools without being excessively subjected to the main flow currents—needing their burst swim speeds only to overcome the short slot section and being met with lower flow velocities right after. The energy dissipation and with it the turbulence are an indicator for how much fish are subjected to challenging swimming situations. High turbulence might interfere with the orientation and makes the ascent more difficult, especially for weaker fish. Last but not least, the discharge is not only influencing all of the other factors but is itself important for creating a guiding flow detectable at the outflow into the natural waters. If the discharge is too low, fish might not find the entrance to the fishway in the first place.

The basic principle of how the fishway works is by transporting water from a higher elevation to a lower one, while transferring potential energy into kinetic energy, hence the flow velocities between the pools. From this relationship, first evaluations can be made about the flow velocities and the type of flow.

$$E_{pot} = m\ g\ h \quad [\frac{kg\ m^2}{s^2}] \tag{1}$$

$$E_{kin} = \frac{1}{2}\ m\ v^2 \quad [\frac{kg\ m^2}{s^2}] \tag{2}$$

$$E_{kin} = E_{pot} \rightarrow v = \sqrt{2\ g\ \Delta h} \quad [\frac{m}{s}] \tag{3}$$

From the relationship between velocity and converted height difference, another common flow parameter can be derived, the Froude number (see equation 15). This value describes the flow condition as either subcritical (below 1.0), meaning that the wave propagation speed is higher than the surface flow velocity, or supercritical (above 1.0), meaning that surface waves can only travel downstream. While an evaluation of the flow behaviour is more complicated than the sheer wave velocity, the Froud number can give first indications of its properties. Usually for the pool boundaries a lower Froude number is desirable.

When taking a closer look at the overflow behaviour at the pool boundary, the Poleni equation [4] is one way of obtaining further quantifiable values. Especially the overflow coefficient μ is used to compare the flow condition between different structures.

$$Q = \frac{2}{3}\,\mu\, b\,\sqrt{2\,g}\,h^{\frac{3}{2}} \quad [\frac{m^3}{s}] \qquad [4]$$

The basic Poleni equation [4] as seen above, although only describes a complete weir overflow and is for that reason not adequate for the situation. The overflow at the pool boundary is influenced by the downstream water level because of its depth and therefore has to be considered in the calculation. Which is done by reducing the overflow coefficient with the value α, expanding the equation like follows:

$$Q = \frac{2}{3}\,\mu\,\alpha\, b\,\sqrt{2\,g}\,h^{\frac{3}{2}} \quad [\frac{m^3}{s}] \qquad [5]$$

For the implementation of this reduction, μ and α are combined to μ_v and calculated taking in consideration both the upstream water depth h_o and the downstream water depth h_u. This backwater influenced overflow coefficient can be calculated as follows according to DWA (2014):

$$\mu_v = 0.59\,(1 - [\frac{h_u}{h_o}]^{4.5})^{0.48} \quad [-] \qquad [6]$$

The following figure shows the relationship between the backwater influenced overflow coefficient μ_v and h_u/h_o.

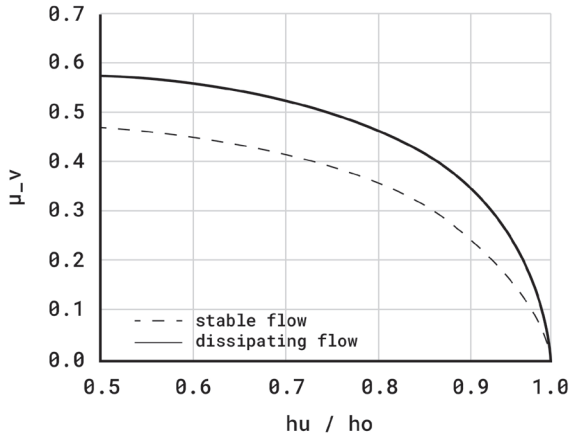

Figure 4: Overflow coefficient $\mu_v = f(hu/ho)$

Analysing the overflow even closer, the turbulence plays a major role in the flow behaviour. The critical zone hereby is in short succession of the vertical slot, where the discharge from the upper water level meets the lower downstream water level. What can be described as a water jet from upstream creates turbulences as it collapses shortly after the pool boundary. The turbulence itself can be described via the Turbulent Kinetic Energy (TKE), which is composed of the three spatial velocity components. The essential property hereby is the fluctuation of those velocity components around their mean value. This is quantified by the Root Mean Squares (RMS) as can be seen below. The velocity components in x, y and z direction are defined as u, v and w respectively.

$$u_{RMS} = \sqrt{\frac{1}{n}\sum_{i=1}^{n}(u_i - \bar{u})^2}\;;\;\; \bar{u} \ldots mean\ velocity\ u \qquad [7]$$

$$v_{RMS} = \sqrt{\frac{1}{n}\sum_{i=1}^{n}(v_i - \bar{v})^2}\;;\;\; \bar{v} \ldots mean\ velocity\ v \qquad [8]$$

$$w_{RMS} = \sqrt{\frac{1}{n}\sum_{i=1}^{n}(w_i - \bar{w})^2}\;;\; \bar{w} \ldots mean\ velocity\ w \qquad [9]$$

These RMS values, usually obtained from measurements or simulations, can then be combined to the TKE in the form as follows (according to POPE 2000):

$$k = \frac{1}{2} \left({u_{RMS}}^2 + {v_{RMS}}^2 + {w_{RMS}}^2 \right) \quad \left[\frac{m^2}{s^2} \right] \qquad [10]$$

Higher values of the TKE indicate more turbulence. A depiction of the spatial distribution will follow in the chapters about the physical and the numerical model.

Another way of describing the general turbulent behaviour is the power density. Due to the incoming water flow, power is first added to the system, scaling with the discharge and potential difference. Dividing it by the specific volume of a single pool you receive the specific power density of the following form (DWA 2014):

$$p_D = \rho_w \, g \, Q \, \frac{\Delta h}{V} \quad \left[\frac{W}{m^3} \right] \qquad [11]$$

In the epipotamal large the power density should not exceed 100 W/m³ (AG-FAH 2012), limiting either the incoming discharge or the pool dimensions.

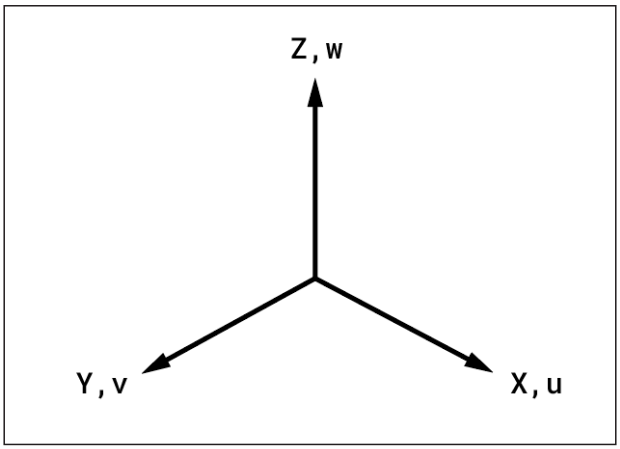

Figure 5: Coordinate System

Describing the overall flow dynamics, the velocity components show the direction and magnitude of the different fluid volumes which were measured. Cumulatively, these volumes show the flow behaviour within the fishway. The goal hereby is, to guide the flow in a way that creates conditions most advantageous for fish to ascend. Locating the main current and its magnitude as well as quantifying the rest of the water flow is the basis for further investigations. The three-dimensional flow is thereby defined by the velocity components u, v and w for the special directions x, y and z respectively (as shown in Figure 5).

For evaluating the flow velocities, the three velocity components are combined to build a velocity vector. Since each component is not a single value, but a cumulation of data points, an average value has to be calculated. This can be done in two ways, either by obtaining the velocity magnitude (V_{MAG}) (see equation 12) by determining the velocity vector for each measurement and calculating the arithmetic mean from there. Or by obtaining the average velocity (V_{AVG}) (see equation 13), calculating the arithmetic mean for each of the velocity components and after that combining them to a velocity vector. Both options are shown with the following equations. Since the average velocity approach achieves a higher accuracy, it is commonly preferred.

$$V_{MAG} = \frac{1}{n} \sum_{i=1}^{n} \sqrt{{u_{x,i}}^2 + {v_{y,i}}^2 + {w_{z,i}}^2} \qquad [12]$$

$$V_{AVG} = \sqrt{\left(\frac{1}{n}\sum_{i=1}^{n} u_{x,i}\right)^2 + \left(\frac{1}{n}\sum_{i=1}^{n} v_{y,i}\right)^2 + \left(\frac{1}{n}\sum_{i=1}^{n} w_{z,i}\right)^2} \qquad [13]$$

For the design process of a fishway, these hydraulic fundamentals have to be evaluated and balanced to a point where the flow condition does not produce values exceeding the limits established earlier, based on the biological capabilities of the relevant fish species.

To summarize, the main considerations target the maximum velocities within the pool boundaries, governed by the overflow equations, the turbulent behaviour and power density. Each effected by the specific pool volume, flow rate and potential difference as well as the minimum dimensions of the structure, set by the size-determining fish species and the guiding current that has to be produced.

03 LABORATORY MEASUREMENTS

INTRODUCTION

After discussing the fundamentals of how a fishway works, the logical next step of the analysis process is a physical model to test the theory in a controlled environment. For that matter, an already existing flume in the *Institute for Hydraulic Engineering and Water Resources Management* of the TU Graz was used to set up the fishway model. The dimensions and design, as well as the ecological base conditions, were determined considering the theory previously discussed. Although, the model was scaled down to fit the testing environment. Therefore, model laws have to be applied for making comparisons between the different scales, which will be discussed in detail later on. The flume with a length of about 13.50 m harbours four connected pool sections, separated by five wall elements. An additional inflow as well as outflow section should stabilize the inflow and outflow water levels. The bottom inclination is achieved by a rough gravel bed and shaped to form separate basins between the wall elements, each peaking in height at the pool boundaries. The incoming discharge is provided by the institutes closed pipe system, building pressure by means of an elevated reservoir. At the outflow boundary, the model has an adjustable gate, controlling the downstream water level and with that the potential difference between the pool sections.

Since the planned investigations required a variable slot width, dismountable blocks were added at the slots, allowing for two variations of the same fishway, one with a slot width of 12.7 cm the other with 16.7 cm. Additionally, the last wall element is composed of a wooden sheet, which can be both widened and closed requiring only a limited amount of work.

To increase the efficiency of the measuring process, a programmable, mechanical arm was installed, capable of moving along three axes. Attaching the measurement probe to the device allowed for an autonomous operation, supported by a guiding script and the corresponding applications.

To understand the fluid dynamics across the pool area, horizontal planes parallel to the base-ground were measured, as well as certain vertical planes and particular points of interest. Together they depict the fluid motion in three-dimensional space, although not over the complete volume due to time constraints and the repetitive nature of the measurement.

The measurement probe used for the experiments is an Acoustic Doppler Velocimeter (ADV) from the brand NORTEK, which measures a fluid volume by means of acoustic impulses paired with the principle of the Doppler Frequency Shift. Working with a probe of such type offered a set of advantages and disadvantages. Most notably, the reflecting properties of the side walls, when measuring at certain distances from the boundary, created areas of low accuracy. Something that was known beforehand and mentioned in the device manual, but still challenging to adjust for. The invasive nature of such measurements was limited by the use of a side looking probe, which on the other hand meant that some parts of the geometry where inaccessible for measurements. The exact measurement grids are subsequently shown in the respective chapter.

Interpreting the collected data played another major role in the evaluation process. Different measurement settings produced a set of varying data behaviour, requiring a number of test cases to adjust for a variety of flow sections. Balancing the measurement intervals in particular produced a noticeable difference in the data quality. Overall, the ADV produced satisfactory results, with the exception of certain critical areas, which required some careful adjustments to be viable.

MEASUREMENT SETUP

The measurement setup, as roughly described before, is a combination of many distinct parts. The following chapter will expand on the information already given and explain in detail the specifics of each segment.

MODEL LAW

The scale of the laboratory model is primarily set by the already existing flume and the target minimum dimensions of the life-sized fishpass. The limiting factor hereby being the width of the flume, from which the length scale was calculated (see equation 14). The model pool length was then adjusted accordingly, and the overall number of pools was reduced to fit the testing environment. The effect of which was deemed neglectable since stable flow conditions were still established.

$$M_L = \frac{L_{NATURE}}{L_{MODEL}} = \frac{2.10\,m}{0.76\,m} \cong 2.76 \qquad [14]$$

If a hydraulic model is dominated by inertia and gravity forces, Froude's Model Law is commonly used to relate properties in nature with their counterpart in the model. The assumption is made, that the ratio between inertia and gravity is equal in nature as in the model. The Froude number itself relates the flow velocity *u* to the surface wave propagation speed, written as square root over gravity times flow depth (STROBL, ZUNIC 2006):

$$F_r = \frac{u}{\sqrt{g\,h}} \qquad [15]$$

From there, the following relationships can be established:

$$\frac{u_{NATURE}}{\sqrt{g\,h_{NATURE}}} = \frac{u_{MODEL}}{\sqrt{g\,h_{MODEL}}} \qquad [16]$$

Assuming that the gravitational force is constant and that $h_{MODEL} = h_{NATURE} / M_L$:

$$\frac{u_{NATURE}}{\sqrt{h_{NATURE}}} = \frac{u_{MODEL}}{\sqrt{\frac{h_{NATURE}}{M_L}}} \quad or \quad \frac{u_{NATURE}}{u_{MODEL}} = \sqrt{M_L} \qquad [17]$$

Therefore, the ratio between velocities in nature and in the model is $\sqrt{(M_L)}$. This further concludes that the following scales are applicable:

$$M_L = 2.76 \qquad [18]$$

$$M_t = M_L^{1/2} = 1.66 \qquad [19]$$

$$M_u = M_L/M_t = M_L/M_L^{1/2} = M_L^{1/2} = 1.66 \qquad [20]$$

$$M_Q = M_L^{3}/M_t = M_L^{3}/M_L^{1/2} = M_L^{5/2} = 12.69 \qquad [21]$$

$$M_F = M_\rho\, M_L^{4}/M_t^{2} = M_L^{4}/M_L = M_L^{3} = 21.10 \qquad [22]$$

This means that the flow behaves 1.66 times faster in nature compared to the model. Measured velocities in the model have to be multiplied by 1.66 to be comparable and the discharge in the actual fishway has to be divided by 12.69 to behave similar in the model. Finally, any forces measured in the model must be scaled up by a factor of 21.10 to match those theoretically measured in nature (STROBL, ZUNIC 2006).

GEOMETRY

After establishing the relationships between the life-sized fishway and the model, all the installations were made in the laboratory flume, according to the dimensions as described earlier. The main construction elements hereby are the 7 cm thick walls, which were installed with a 1.13 m spacing between them. Leaving an inflow length of about 5 m and an outflow length of about 3.6 m. Four pools are setup this way, though measurements were primarily taken from the second pool, where flow conditions were stable and mostly devoid of inflow disturbances. The slots are alternating between left and right, starting at the left (streamwise), with a width of 12.7 cm. At a later stage the width was increased to 16.7 cm by removing pre-installed elements at the slots. Both versions as well as the calculated minimum dimensions can be seen in the figures on the following page (Figure 6 - 8).

The inflow is controlled by a manual slider at the top end of the flume in combination with an induction flow meter. The water depth at the outflow boundary, on the other hand, is controlled by a vertically adjustable gate. Throughout the measurement stages water levels were kept constant, adjusting only the slot width and discharge to remain at the desired levels. This was meant to simulate a fixed potential difference between the up- and downstream, where a wider slot would not change the water levels but the discharge, as it would in nature.

The entire flume is horizontal, therefore a bed inclination had to be installed via a rough gravel bed. The exact layout of which can be seen in the longitudinal sketch (Figure 10).

On top of the flume, two rails were installed holding the guiding equipment for the measurement probe. The layout allowed for a streamwise movement covering almost the entire length of the flume, except for the direct in- and outflow sections. Spanwise the arm can move up to about 8 cm close to each wall, allowing for measurement up to about 3 cm close to the wall. A sketch of the equipment can be seen in Figure 12.

MEASUREMENT POINTS

Measurements in the laboratory flume were mostly taken at fixed locations to be comparable throughout the investigation. To cover as much of the flow behaviour as possible, three horizontal planes, as well as a vertical plane were situated in the second pool section. The horizontal planes, consisting of 344 measurement points each, are set at three different water depths, 4 cm and 8 cm apart. The planes are well submerged at about half the water depth, depending on the discharge, and are inclined to be parallel to the bottom inclination. Since the general flow behaviour inside the pools appeared to be qualitatively constant over the depth, plane (1) was chosen for the main representation of the results, paired with vertical measurements giving a more detailed view over the depth. The vertical plane stretches over the entire length of the second pool, crosses the third slot and reaches into the third pool. This way, measurements were taken in the calm recirculation areas as well as the slot, covering the critical sections shortly after the pool boundary. Due to geometrical restraints, only a certain depth was covered by the vertical plane. To have additional information about the depth dependent velocity behaviour, vertical line measurements were conducted at the slot, showing velocities until about 2 cm close to the bottom.

The majority of the measurement points are aligned in a grid and measured utilizing the guiding equipment installed on top of the flume. This way a large quantity of points could be targeted autonomously only by providing a coordinate file. For that process the Arduino software was used to control and synchronize the Vectrino software, conducting the actual measurements, and the guiding apparatus, holding and moving the ADV probe in place.

The general position of the measurement planes is shown in Figure 9. The depth therefore is measured from the bottom up, relative to a theoretical parallel bottom surface since the actual bottom varies in depth due to its basin like form.

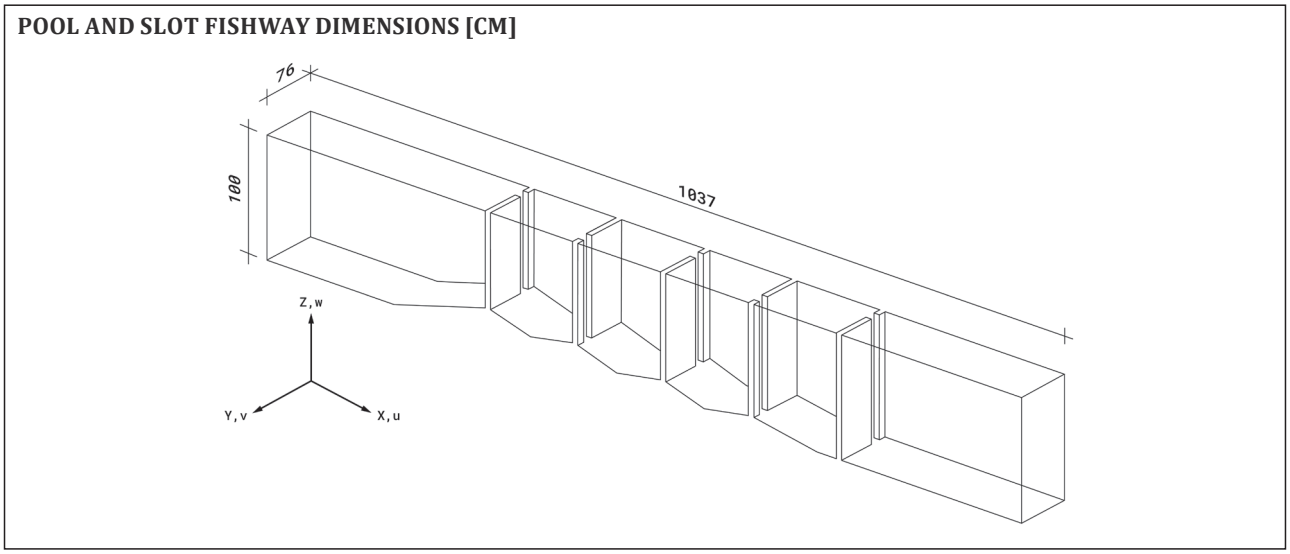

Figure 6: PSF Dimensions

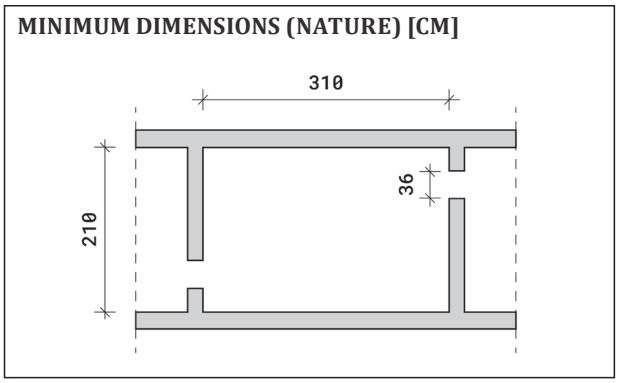

Figure 7: Minimum Dimensions

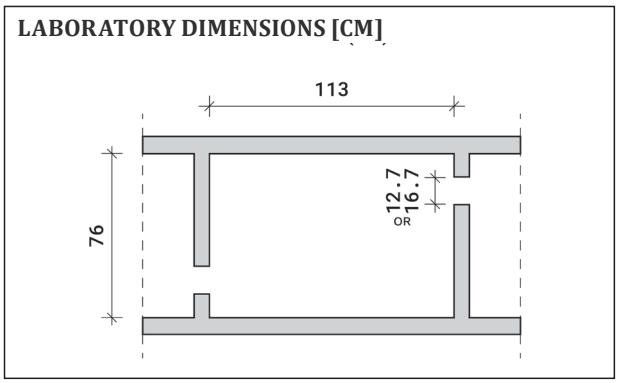

Figure 8: Laboratory Dimensions

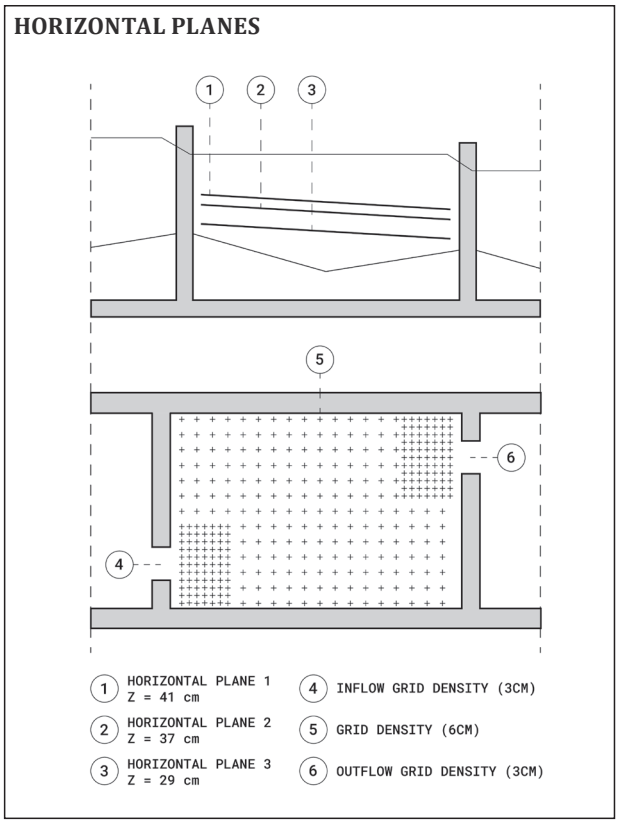

Figure 9: Horizontal Planes

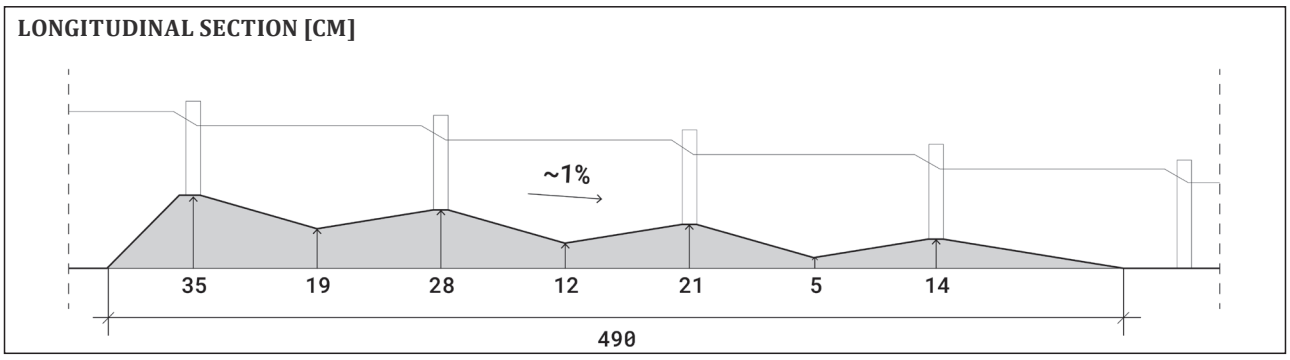

Figure 10: Longitudinal Section

MATERIALS

The laboratory flume was built using a variety of materials from steel to polymers, though the only ones relevant for the flow evaluation are the inner surfaces. Most notably the gravel, shaping the bottom, has an influence while the smooth wall surfaces are rather negligible. Therefore, the gravel was randomly measured and documented. The resulting average sieving width, as the shortest mesh size a stone would fit through, was found to be around 5 cm (d_m = 4.7 cm). Usually, bed roughness is expressed as a Manning's or Strickler roughness coefficient and is implemented in numerical models as such. Therefore, the following equation was used to calculate the Strickler value, according to STROBL, ZUNIC (2006). The Manning's value, if needed, is then the inverse of the Strickler value.

$$k_{St} = \frac{21}{{d_m}^{1/6}} \cong 35\ [m^{1/3}/s] \qquad [23]$$

This roughness coefficient was then used for the numerical simulation, although in a diminished form.

DISCHARGE

The discharge for the experiments was controlled by a manual slider and the quantity of water was displayed on an induction flow meter. To produce comparable results, discharge had to be relatively constant over time. To ensure the systems reliability, the fluctuations were recorded and are shown in the following figure.

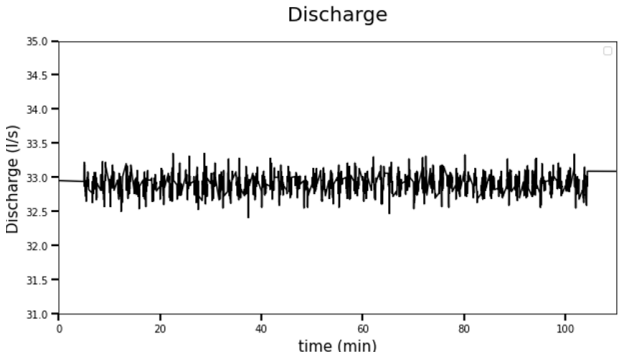

Figure 11: Example plot of Discharge at the inflow

The exemplary discharge behaviour was recorded while conducting one of the measurements at the version one, with a set discharge of 33 l/s. It stayed constant over the full duration, which was repeatably observed during the measurements, with only minor fluctuations between roughly 32.5 l/s and 33.3 l/s. At rare occasions the different models in the laboratory can influence each other, especially during the start and stop processes—due to the nature of the experiment these only had a neglectable impact but were still avoided if possible.

Data was collected from two different cases, one with a discharge of 33 l/s and a slot width of 12.7 cm, another with 42 l/s and a slot width of 16.7 cm. Both cases resulted in roughly the same water levels throughout the model.

GUIDING EQUIPMENT

The aforementioned guiding equipment for the measurement probe consists of a vertical arm connected to a rail reaching spanwise over the flume. Two additional rails on top of each longitudinal wall allow for movement in the x direction while the rest of the construction covers the y and z component. Together they allow for a three-dimensional positioning of the ADV probe, which is mounted on the vertical arm. The positioning itself is controlled by two separate programs, one for manual movement, the other for an automated operation. The following sketch gives an overview of the laboratory setup:

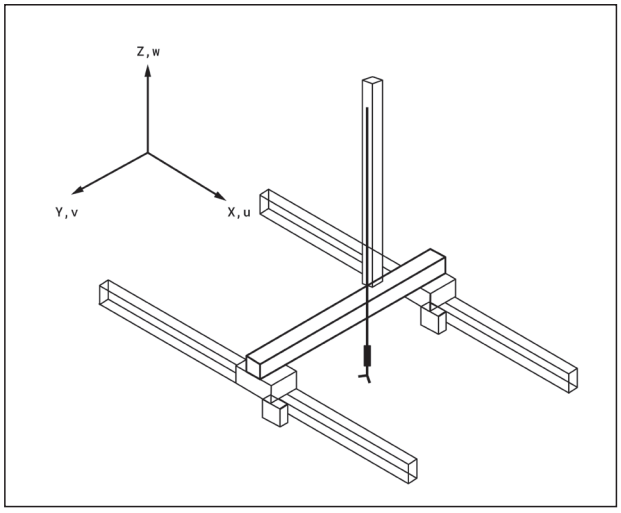

Figure 12: Guiding Equipment

THE MEASUREMENT PROBE

The device used for taking point measurements in the laboratory flume was a NORTEK velocimeter, to be specific, the Vectrino side-looking probe. As the name indicates, this probe has a measurement head pointed to the side, therefore aiming at a flow volume that is minimally disturbed by the presence of the probe. Working with such a device presents a set of advantages but is also tied to a number of disadvantages that have to be considered.

First and foremost, the geometrical indications of working with a side-looking probe will be mentioned. In a rectangular flume, like the one at hand, it is possible to gather point data very close to the vertical boundaries, although weak spots have to be considered—more on this later. What is an advantage in the spacious pool areas of the flume, proposes considerable difficulties in the slots between them. The volume at which the probe is aiming must be set at a certain distance range, making manoeuvring within tight spaces challenging. Another major factor are signal reflections from the surrounding boundaries, which can induce critical signal errors and might even render the measurement unusable.

When it comes to the vertical component, the side-looking probe is very flexible and can theoretically measure from the point where it touches the bottom up to the water surface, even in a half-submerged state, in which it would only gather x and y data. In a fully submerged state it measures 3D data, although not each velocity component is treated the same. For example, the vertical component has a higher instrument noise than the horizontal ones and it also depends on how the main flow is oriented in relation to the instrument—the handbook notes that flow from the back of the probe '*is causing an awful response*' (NORTEK 2018).

Generally, it can be noted that the quality of the measurement is strongly dependent on choosing the right settings for a certain situation and surrounding. Factors like flow behaviour and the geometrical properties of the nearest obstacles can greatly influence the needed settings.

Circumstances can already vary within a set of points in close proximity, which lead to situations where a majority of points in a measurement set were of good quality, while some of them were practically unusable. Measurement repetitions of certain subsections are usually a necessity and some data points proposed a very difficult measurement environment.

In the following sections, the instrument's specifics will be covered in more detail, offering a better understanding of its capabilities and limitations.

The following figure shows the ADV transmitter and receiver end of the probe plus the according axes.

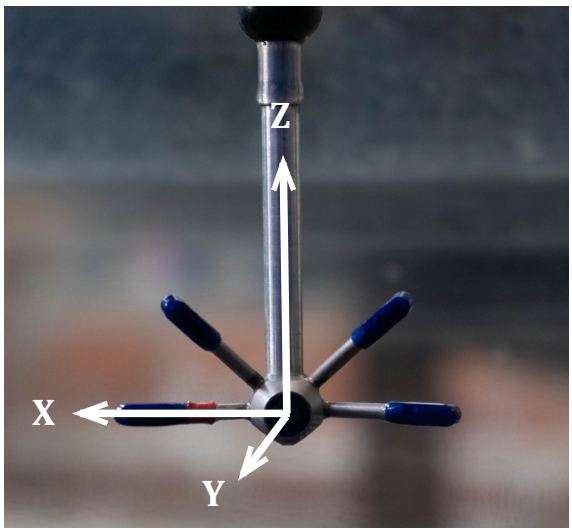

Figure 13: ADV Probe

WORKING PRINCIPLE

The Vectrino measures the velocity of water by utilizing the physical principles of the Doppler Effect. The so-called *Doppler Shift*, which makes this measurement procedure work, is the change of the wave frequency by movement of the source relative to the observer or vice versa. The stationary probe is emitting a pair of sound pulses of a specific frequency aimed at a certain water volume. When the sound waves are reflected, their frequency shifts according to the velocity of particles which it is reflected off. In the case of measuring water, it is not the fluid itself that reflects the waves but passive tracers that are

suspended in it. Under laboratory conditions, those tracers are usually dirt particles—if the water is 'too clean', the reflection signal might not be strong enough, therefore a certain degree of impurities in the water is desirable.

As already mentioned, the Vectrino probe is utilizing a pair of acoustic pulses, the use of two rather than one pulse is commonly referred to as a pulse-to-pulse coherent method. These pulses, aimed at a specific volume, have an expected reflection time dependent on the speed of sound within the fluid. Therefore, calculating an appropriate speed of sound is crucial. The Probe achieves this by measuring the water temperature and applying a standard salinity—it is worth mentioning that the speed of sound is more sensitive to temperature variations than to salinity, justifying this approach, according to NORTEK's judgement. Knowing this, the reflection signal is measured at the four sidearms of the probe needed for a 3D assessment of the point data. The actual velocity is then calculated by comparing the phase shifts of the two return signals. Combinations of the four measured pulse pairs, one for each arm, are used to calculate the three orthogonal velocity components (NORTEK 2018).

"*The phase difference between the two reflected pulses is a direct measure of the velocity, and can be expressed as*:

$$V = \frac{\Delta\varphi\ C}{4\pi\ F_{source}\ \Delta t} \qquad [24]$$

Here, V is the current velocity, Δϕ is the phase difference, F_{source} is the transmitter frequency and Δt is the time difference between two consecutive pulses." (NORTEK 2018)

The measurement volume, which is the target of the acoustic pulses, is located at a distance of approximately 50 mm from the transmitter. The volume is defined by the intersection of the four beams, two of which are horizontal and the other two slanted by 65 degrees from the vertical. The horizontal ones are responsible for the u_x and v_y measurements, while the slanted ones are two separate w_z measurements.

The volume is additionally adjustable between 3–15 mm in length, allowing for adjustments (NORTEK 2018). A larger volume hereby seemed to smoothen measurements in a highly turbulent environment, while a smaller volume might result in a more precise point measurement, although harder to detach from influences of noise.

SETTINGS

The settings used for the point measurements were thoroughly tested in the beginning stages of the project. Although certain advantageous settings were indicated by previous measurements, a range of adjustments were tested with varying degrees of success. Adjustments were primarily done by balancing three main settings: sampling rate (Hz), nominal velocity range (m/s) and sampling volume (mm).

The sampling rate appeared to have by far the highest influence on the overall data quality. The challenge lied in finding a spot where the rate was high enough to detect as much of the turbulent behaviour as possible while not being affected by excessive noise. For that matter the power spectral density plot of a 200 Hz (maximum) measurement was analysed with the conclusion that the signal is excessively affected by noise at values above approximately 50–70 Hz. This was indicated by the signal flattening out in the log-log scale, around the 50–70 Hz mark, after previously following the expected k–5/3 line of Kolmogorov's hypotheses, as described in the book *Turbulent Flows* (POPE S. B. 2000).

The following figures show two point-measurements applying the already adjusted sampling rate of 50 Hz. The data is shown as both the unfiltered and filtered signal. Data filtering was done using the Modified Phase-Spacing Thresholding described in *Estimation of Power Spectra of Acoustic-Doppler Velocimetry Data Contained with intermittent spikes* (PARSHEH et al. 2010), with additional prefilters on correlation of < 50 and Signal to Noise Ratio (SNR) of > 5. Note that the first plot is showing a point with lower initial quality, where filtering did adjust the signal notably and the second plot is showing a point with high quality unfiltered data.

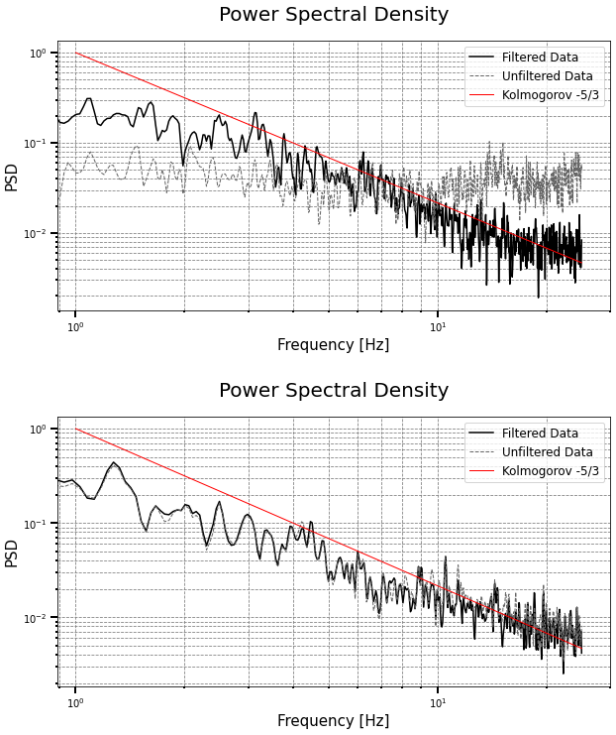

Figure 14: Power Sprectral Density

The second adjustable setting is the nominal velocity range in meters per second. This one should be set as close to the expected maximum velocities as possible. An unnecessarily high value will introduce excessive noise. Additionally, the velocity range is connected to the internal sampling rate of the probe. Since maximum velocities between 1–2 m/s were expected, the range was set to ±2.50 and by that to a internal sampling rate of 125 Hz. Each vector measurement takes advantage of all the available samples, independent of the manually set rate. If the sample rate, like in this case, is set to 50 Hz, each output will be averaged by two samples and every second output by 3 (125/50 = 2.5) (NORTEK 2018). A nominal velocity range of ±1.00 was tested, since the value should be as low as possible for a higher accuracy, but ultimately failed to produce satisfying results.

The third value that produced a noticeable difference in the measurement behaviour is the sampling volume size in millimetres. Most of the measurements were conducted using a medium value of 6.1 mm, for some critical locations with a comparably high turbulence, the volume was set up to 7.6 mm. While this did not enormously improve the data, it helped, among other changes, to gather viable point data. A number of other settings can be seen in the following figure, those not discussed were set to their recommended state according to the manual.

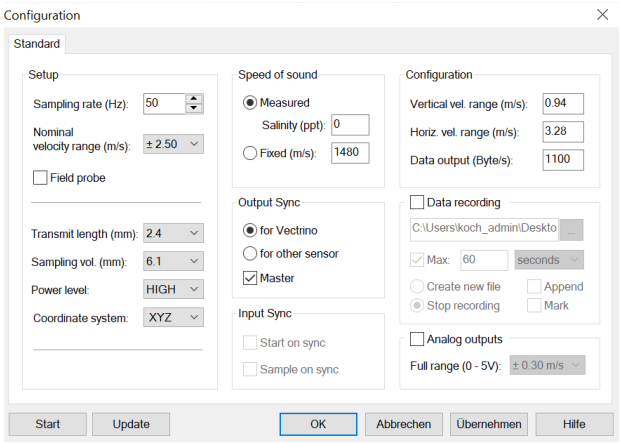

Figure 15: ADV Settings

Aside from the ADV settings themselves, the duration of the measurement played a significant role during the calibration stages and later on when troubleshooting certain points. The filtered data, in many cases, was reduced to a fraction of the whole sample set. Therefore, a longer measurement provided a generally larger sample size for values to be averaged from. To evaluate which measurement duration would provide both a stable average value and an appropriate time expenditure, a 4 min (50 Hz) test sample was taken at a comparably turbulent part of the domain. From that, the moving average was plotted, and the appropriate time was set to 60 s.

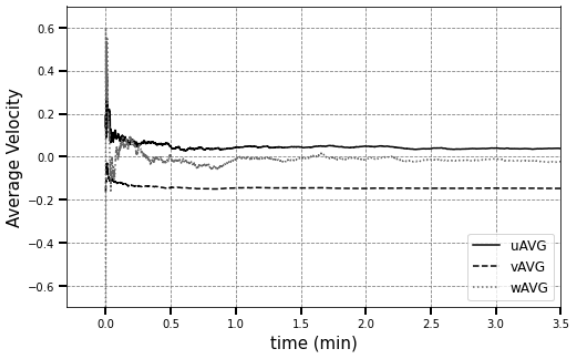

Figure 16: Moving Average

WEAK SPOTS

Weak spots are documented in the ADV manual as regions with low SNR and correlation values due to pulse interference near the boundaries. Depending on the velocity range settings, the distance from the boundaries where the weak spots occur, changes. For ±2.50 m/s the manual lists the distances 0.03 m and 0.10 m. Experience shows that the type of wall material influences that distance, which makes quality predictions difficult. The following figure shows the data quality of a horizontal measurement plane, with red marking areas of high data quality and blue those of low quality (1). Note that at the top a line of low quality runs parallel to the boundary, indicating pulse interference. Data of those 'low quality areas' was then reviewed, showing only a minor influence on the velocity magnitudes. Since velocities around the prominent pulse interference zone (1) were comparably low, the quality shift had no considerable effect and the data was therefore included in the visualization.

Figure 17 additionally shows the orientation of the ADV probe, with orientation (2) being used at every measurement point possible, only switching to orientation (3) at points along the left boundary (in streamwise direction), marked by the area (4).

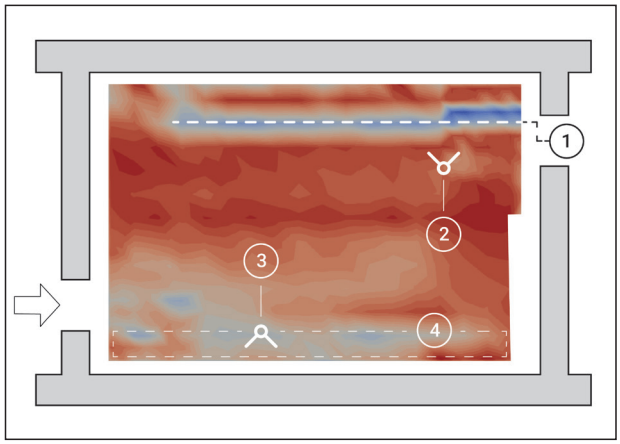

Figure 17: Weak Spots

DATA POST PROCESSING

Collecting point measurements alone is deemed as insufficient for analysing the flow behaviour. A crucial step, before the data can be discussed, is the post processing via appropriate programs. In this case, WinADV from the *United States Bureau of Reclamation* was used. The data was subsequently filtered and compressed into summary files for the visualization step. The filtering process was governed by the data correlation and the *Signal-to-Noise Ratio* (SNR). For most of the data, a correlation higher than 50 % was targeted, although at certain critical locations, for example right after the pool boundaries, the correlation limit had to be reduced to 30 %. The SNR cut-off at 20 dB on the other hand was reliably exceeded, imposing barely any data loss. The challenge throughout the measurement period was handling the correlation and the reflection overlay at specific point sets.

After filtering the data, it could be visualized using ParaView by Kiteware and the Adobe Creative Cloud. During this process certain values were marked as failed measurements and were manually sorted out. For illustrative purposes those values were usually replaced by interpolation, as far as they were not deemed crucial.

04 COMPUTATIONAL FLUID DYNAMICS

INTRODUCTION

In addition to the laboratory measurements, a numerical study of the PSF was performed. For that matter the laboratory flume was virtually modelled after its original geometry and subjected to the same discharges according to the slot width. By including measurements of the real-life counterpart, the model was validated, and the flow behaviour could be compared to what was shown in the laboratory investigation. Further than that, the numerical model allowed for a detailed view of the entire domain, allowing for assessments concerning critical locations as well as qualitative information about the flow behaviour.

The calculation was done using ANSYS Fluent with additional pre-processing of the mesh via the according 'Workbench' tools. The settings and numerical schemes were chosen on the basis of what has previously been proven effective at similar projects, according to literature and research papers (e.g. MENTER 1994).

The numerical results were then used to support the laboratory measurements. The goal hereby lied in confirming and expanding the data, giving a more complete picture of the flow within the fishway. Especially locations that were hard, or even impossible to reach with the ADV probe, could then be included with the application of Computational Fluid Dynamics (CFD).

The overall simulation structure followed the same logic as the laboratory measurements, where two similar versions, distinguished only by their slot width and discharge, were analysed. The simulation types are shown in the following table.

Table 6: PSF Versions

VERSION	SLOT WIDTH	DISCHARGE
1	12.7 cm	33 l/s
2	16.7 cm	42 l/s

NUMERICAL SIMULATION
SETTINGS

The quality of the numerical simulation is greatly influenced by its settings and the chosen numerical schemes. Therefore, research papers were examined, and established setups were implemented. References were taken from KEVIN B. MULLIGAN et al. (2016), JASON M. DUNGUAY (2016), IMAN H. HAMEED (2020) as well as the ANSYS Fluent User's Guide of 2018. The open channel flow was therefore modelled using the multiphase Volume of Fluid (VOF) approach. Volume Fraction Parameters were set to implicit and two phases, air and water, were introduced.
The numerical calculation solves the Reynolds Averaged Navier-Stokes (RANS) equation with the two-equation eddy-viscosity model, k-omega. The Shear Stress Transport (SST) formulation which then switches from the k-omega model, near the walls, to a k-epsilon model in the free surface flow. This is due to the increased performance of the k-omega model near the boundary including the viscous sub-layers. Common problems of the k-omega model in the free-stream sections are then avoided by switching to the k-epsilon model (MENTER F.R. 1993/4). The Semi-Implicit Method for Pressure-Linked Equations (SIMPLE) scheme was used for pressure-velocity coupling (PATANKAR and SPALDING 1972). The conservation of the momentum equation was solved using a Second Order Upwind method while the TKE equation was solved using a First Order Upwind method. Additionally, the Transient Formulation was set to Bounded Second Order Implicit. The following table summarizes the numerical settings applied to ANSYS Fluent:

Table 7: CFD Settings

Time	Transient
Type	Pressure-Based
Multiphase Model	Volume of Fluid
Viscous Model	k-omega SST
Pres.-Vel. Coupling	SIMPLE
Momentum Equation	Second Order Upwind
TKE Equation	First Order Upwind
Transient Formulation	Bounded Second Order Implicit

GEOMETRY

The geometry for the numerical model was directly taken from the construction plans of the laboratory flume. A simplified version of which was drawn using AutoCAD. Therefore, only the inner dimensions of the flume were relevant, since only the fluid body, extended by an air-filled buffer zone, had to be modelled. Installations that were necessary for the flow behaviour of the laboratory flume could be ignored and only an adequately long in- and outflow section was modelled. This established the zone of interest (pool number two) at a sufficient distance from the boundaries. The layout was then imported to ANSYS and extrapolated using the SpaceClaim module, adding the bottom geometry in the process. The product of this can be seen in the next figure.

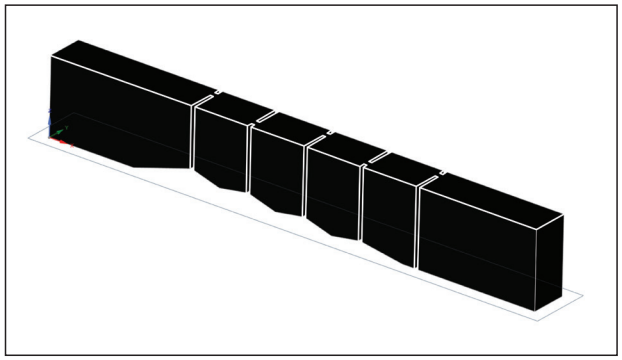

Figure 18: SpaceClaim Model

From there, the geometry was exported and first meshed with the Fluent-internal automatic meshing tool, which was later manually improved.

MESH

Due to the geometrically simple nature of the PSF, a high-quality mesh with a highly regular element size could be set up. Rectangular elements were chosen, with an average size of roughly 3 cm resulting in a minimum orthogonal quality of 0.57 (ANSYS internal metric describing the mesh shape quality as skewness of mesh structures, with 0 being the worst and 1 the best). Additionally, three boundary elements of a smaller size were implemented near the walls, since velocity gradients towards a non-slip boundary are usually steep. A sample view of the mesh can be seen in the following figure, showing the second pool section where the laboratory measurements were taken.

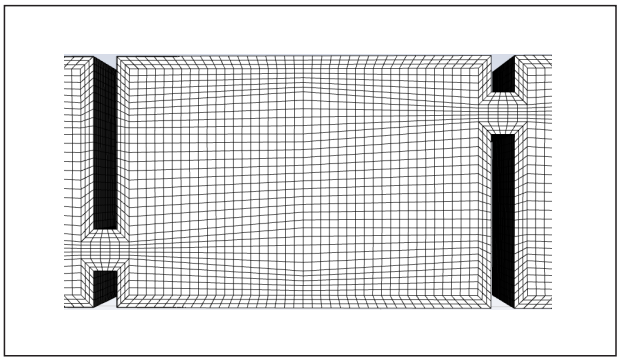

Figure 19: CFD Mesh

The regularity of the mesh improved the data quality further after preliminary calculations were done, using an automatically generated hexagonal mesh.

BOUNDARY CONDITIONS

Essential for the numerical calculation are the boundary conditions applied to the mesh. These define the behaviour at the outer surfaces of the mesh and set the environment for any following calculations. For a simple case like this, basically three main conditions with slight variations were enough to define the domain. First the inlet boundary, defined as a mass-flow-inlet, sets the discharge at the top of the flume. The two phases were separately set, water as 33 or 42 kg/s, depending on the PSF version, and air as placeholder value, which in the calculation will be scaled accordingly. The obvious second boundary condition was the outlet, defined as a pressure-outlet, allowing for any phase to leave the domain without the option of returning back in. Here the water level at the end of the flume was fixed to 41 cm according to the laboratory measurements. The pressure-outlet boundary was additionally applied to the top of the mesh, letting air out of the system. The final conditions are two types of wall boundaries. One smooth wall for the vertical walls and some of the bottom, as well as a rough wall boundary at the gravel bed. The roughness height was set to 5 mm in the early stages of the calculation and left as such due to a satisfactory behaviour of the model. The flow indicated no sensitive behaviour regarding the bed roughness, therefore no significant improvements were expected from increased roughness values.

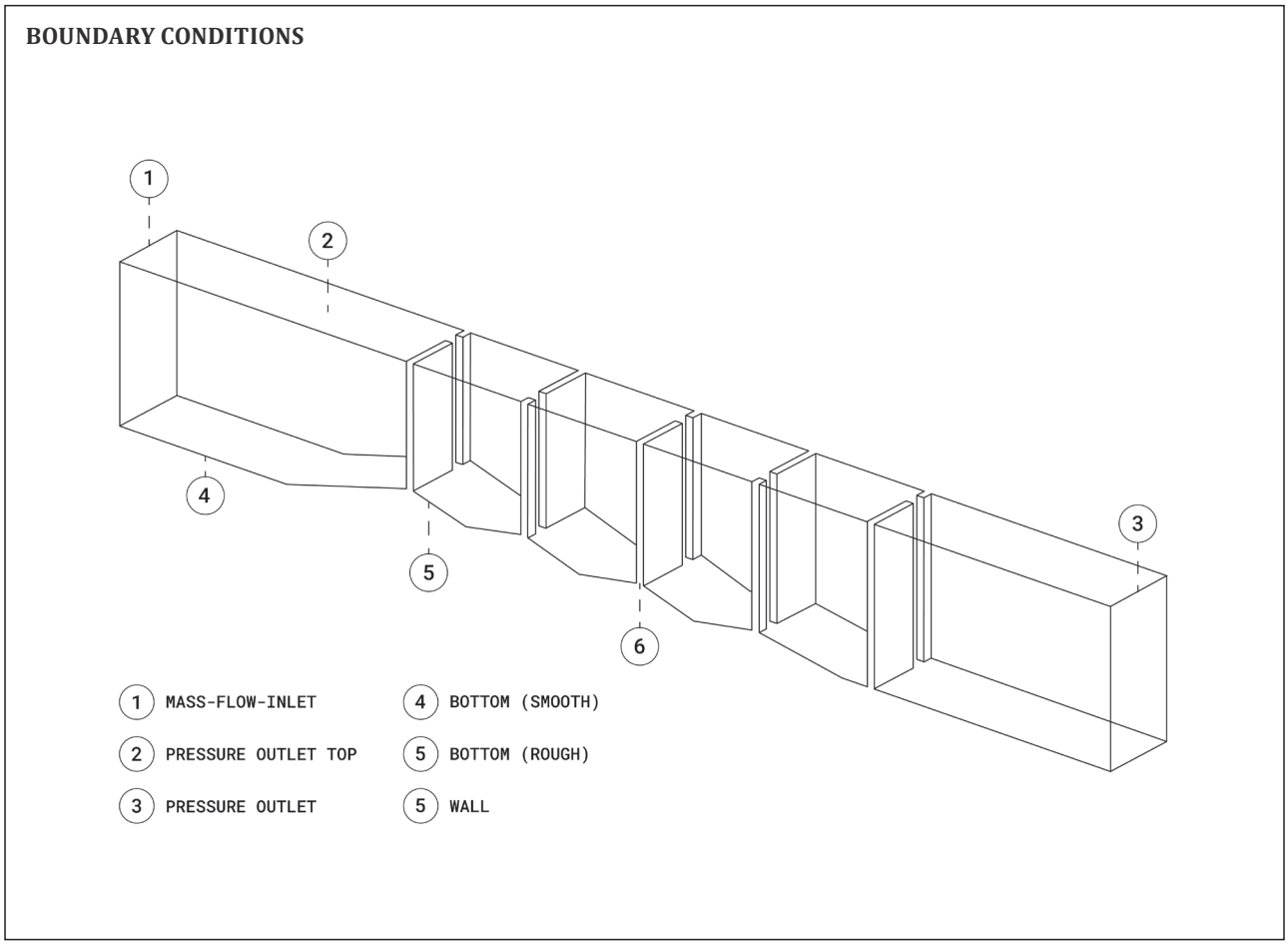

Figure 20: Boundary Conditions

VALIDATION

After achieving stable conditions in the numerical simulation, the case was transitioned to the 'Results' tool of ANSYS, initiating the post-processing step. From there, planes were added at the according locations related to the laboratory measurements and data was mapped onto them, producing data sets which could then be compared to the previous measurements. Additionally, line data was exported at known locations and plotted together with the measurement data for a better representation of the model correlations. Although, the first step in the validation process was comparing the water levels throughout the domain. Outflow depth was, as expected, equal to what was measured in the laboratory, due to the fixed outflow depth set for the simulation. The inflow depth, and therefore also the level differences between the pools, were within 1–2 cm of the laboratory measurements. This was evaluated as sufficiently precise, since water levels in the real-life flume were subjected to unavoidable natural fluctuations of a similar amount.

Further validation was done in two major steps. First of all, comparing the flow behaviour of both the laboratory measurements and the numerical model via contour plots and velocity magnitudes. And in the second step, comparing detailed line data at certain sections for a quantitative comparison of the data sets. Even though most of the collected data was compared during the validation, only an exemplary set of it will be shown here. A comprehensive collection of the visualized data can be found in the appendix.

The figures on the following page will each compare the results of the CFD simulation, at appropriate locations, with those of the laboratory measurements (Version 2).

Velocity magnitudes of the second layer show a similar flow path along the right wall in flow direction (Y/B = 1). Maximum velocities occur shortly after the slot and are almost identical, with 1.25 m/s in the simulation and measured maximum of 1.19 m/s. The central recirculation zone is well defined in both cases and secondary flow separations can be observed in the corner X/L = 0, Y/B = 1 and under certain measurement conditions also in the corner X/L = 1.5, Y/B = 1—similar to those shown in the CFD simulation at the same locations. The following validation concerning the separate velocity components refers to imagines which can be found in the appendix and are not shown on the following page.

Looking at the velocities in x-direction (u_x), an almost identical behaviour can be observed. The pool is divided into two main flow sections, one main flow current in positive x direction, from the inflow slot along the right wall (Y/B = 1), and another secondary flow in negative x direction along the opposite wall (Y/B = 0). Combined they form a flow circulation throughout the whole pool with a strong separation of high and low velocity areas. Velocities in y-direction repeatably show the correlation between the numerical model and the laboratory measurements. Here the second component of the two-dimensional circulating flow can be observed. While the flow, led by the inflow current, is drawn in positive y-direction from approximately X/L = 0 to X/L = 0.8, the second half is affected by the outflow current, moving the flow in negative y-direction. The separation between the two zones is located at a similar X/L coordinate between 0.7 and 1.0. While velocities in x- and y-direction were matching notably well, velocities in z-direction appeared more difficult to compare. This could, in part, be due to the higher sensitivity to noise and reflections of the ADV probe in z-direction.

Qualitatively the contour plots give a good indication of the validity of the numerical simulation. To additionally support this case, data was exported along certain lines (Figure 25) and compared to measurements taken in the laboratory. Therefore, two horizontal lines were chosen, one parallel to the x-axis (1) and the other parallel to the y-axis (2), supported by a third vertical line (3) at the outflow slot. Data of all three velocity components was analysed during this process, although only the velocity magnitude is shown on the following page, the full velocity spectra can be found in the appendix.

The first comparison (Figure 22) along the line of approximately Y/B = 0.8 (1) in streamwise direction follows a trend that has already been indicated by the contour plots. The two-dimensional velocity components of u_x and v_y as well as the velocity vector are closely matched by the simulation data. Only velocities along the z-direction w_z fluctuate within the laboratory measurement data and are only occasionally matched. Since the two-dimensional flow behaviour is dominant and velocity vectors are only slightly affected by the vertical component, valid statements can still be made with minor restrictions.

The second plot (Figure 23) compares data along the spanwise direction at approximately X/L = 0.1. Velocity peaks at the slot outflow are pronounced within both data sets. The specific outflow behaviour shows minor differences between the simulation and the measurements, therefore certain data trends occur similarly but not always at the exact same location.

The third comparison (Figure 24) shows the vertical line within the outflow slot (3). Velocity magnitudes are matched along about 2/3 of the depth, only varying slightly towards the bottom.

Summarizing the validation process, all indications point at a simulation output that satisfyingly matches the measured flow behaviour. Particularly the 2D flow in x- and y-direction is mirrored throughout the investigation and shows sufficient qualitatively and quantitatively matching data. At this point it was decided that a further fine-tuning of the numerical model was not necessary and that results could be analysed to support the laboratory measurements.

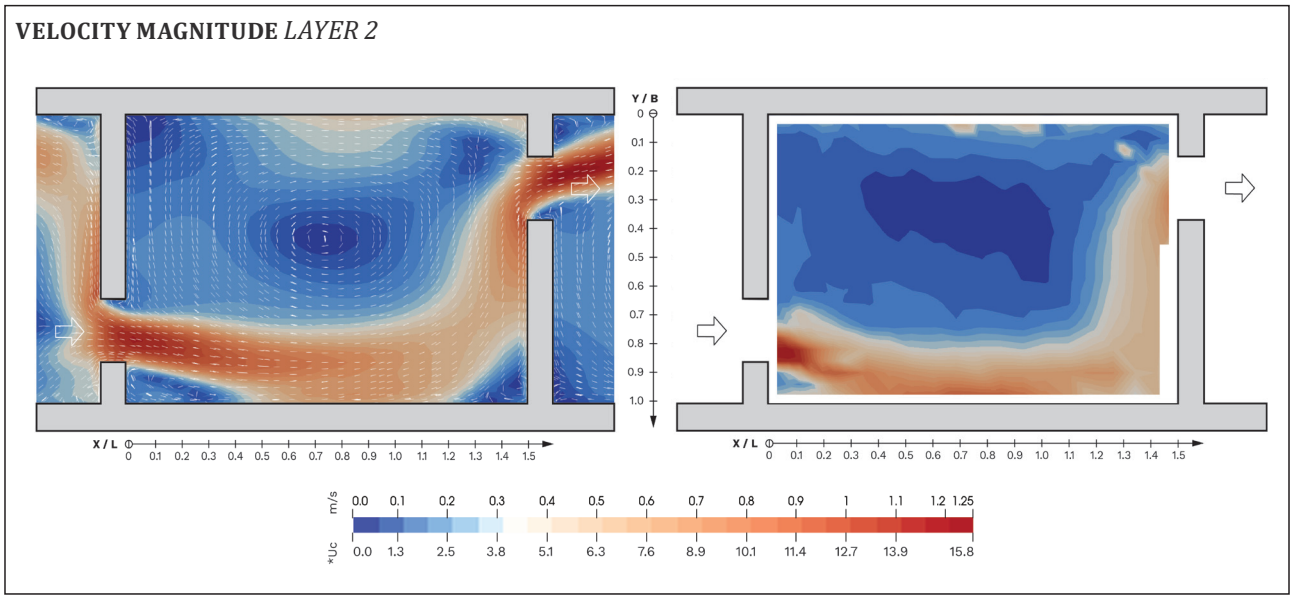

Figure 21: Velocity Magnitudes Layer 2 (V2)

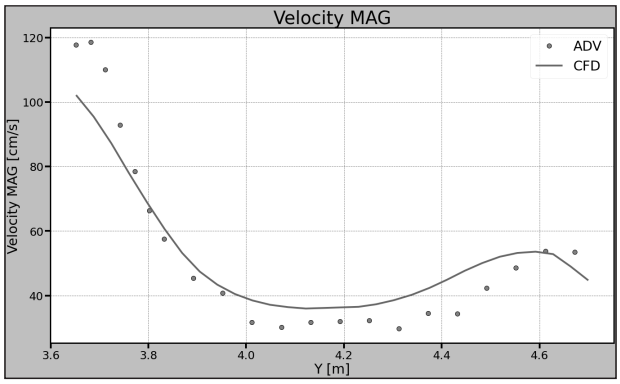

Figure 22: Velocity Magnitudes (1)

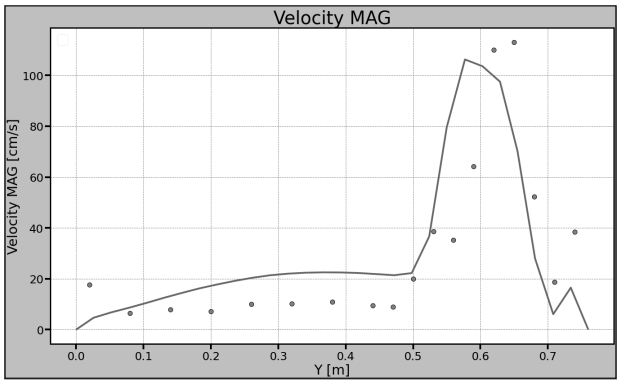

Figure 23: Velocity Magnitudes (2)

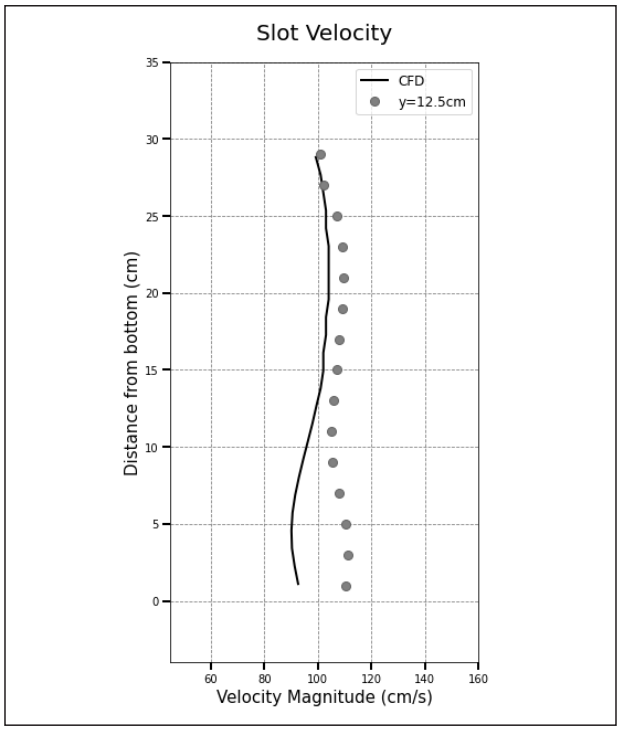

Figure 24: Velocity Magnitudes (3)

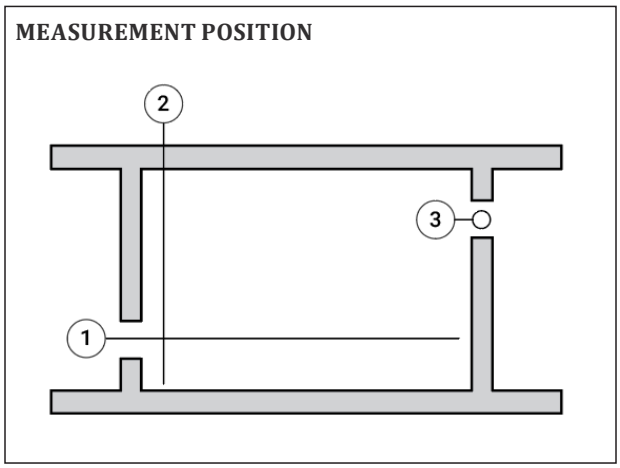

Figure 25: Validation Locations

05 RESULTS AND DISCUSSION

The measurement and simulation data so far produced a consistent picture of the flow inside of the PSF. Following the post-processing and validation of the collected data, the behaviour can now be shown, analysed and described. Due to the large amount of measurement data gathered for the investigation, figures will be reduced to the most relevant and discussed with the additional information in mind. An extensive collection of all the measurements results can then be found in the appendix. The main points of the discussion are the flow behaviour concerning the passability for fish, including zones of maximum velocities and recovery zones, as well as the turbulent behaviour as a potential influence on the migration path. Additionally, a change in geometry was introduced, the effects of which will also be targeted by the discussion.

The data visualization was done for a variety of separate plots, in most cases showing the velocity magnitude but later on also distinguishing between the three velocity components for a more detailed understanding of the flow behaviour. The plots also show a normalized scaling based on the average inflow velocity U_c, which for the first version of the PSF is 0.061 m/s and 0.079 m/s for the second one. Length scales are normalized as well, showing the width in a range from 0 to 1 and the length, in comparison to the width, from 0 to 1.5.

The following laboratory measurement results were first taken from the initial fishway geometry as described before. This first version having a slot width of 12.7 cm, which was then widened to 16.7 cm and the measurements were repeated on the second version. For version two the discharge was scaled accordingly, up to 42 l/s, to reach the same water levels as in version one, although some measurements were additionally done with the initial discharge of 33 l/s for calibration purposes.

POOL AND SLOT FISHWAY: VERSION 1
LABORATORY MEASUREMENTS

The following page shows a set of results from the second pool in flow direction, showing a plot from each of the three measurement depths alongside a vertical plane.

Figure 26 shows the velocity magnitude at the first layer within the second pool. From that, many of the essential flow characteristics can be determined. Primarily the main flow current running streamwise along the line of Y/B = 0.9, before turning at the end of the pool (X/L = 1.3–1.4) towards the following pool boundary. In blue, the large recirculation area can be seen with its low flow velocities, between Y/B = 0–0.8 and X/L = 0–1.2. Maximum velocities occur shortly after the slot outflow (Y/B = 0.85, X/L = 0.1), reaching approximately 1.24 m/s, or expressed in a dimensionless form as a multiple of the inflow velocity U_c: $20.7U_c$.

Since, at this point of the investigation, some reflection issues were not solved yet, velocity peaks along the streamwise wall (Y/B = 0) are likely due to measurement errors and could not be reproduced in the following measurements nor in the CFD. The second layer, slightly deeper, shows a similar behaviour as the first layer. Main currents follow a relatively focused path, leaving much space for fish to rest after pushing through the slot section. Maximum values peak at 1.13 m/s ($18.8U_c$). The third layer follows the same trend, maximum values at 1.11 m/s ($18.5U_c$) seem to decline over depth, which will later be analysed in more detail.

Finally, figure 29 shows a vertical view through the second slot along the line of approximately Y/B = 0.2. Due to geometrical restraints, velocities were only measured in the marked subsection of the flow. Here, the position of the critical area, including the highest velocities, can be identified within and after the slot. Peaks reaching up to 1.35 m/s ($22.5U_c$).

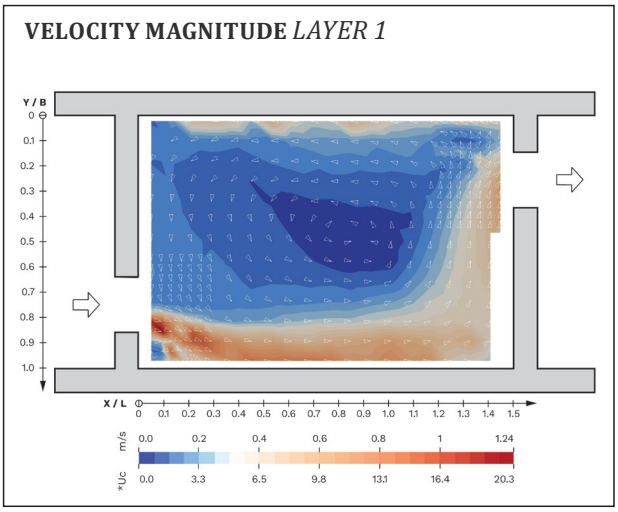

Figure 26: PSF Measurements V1, Layer 1

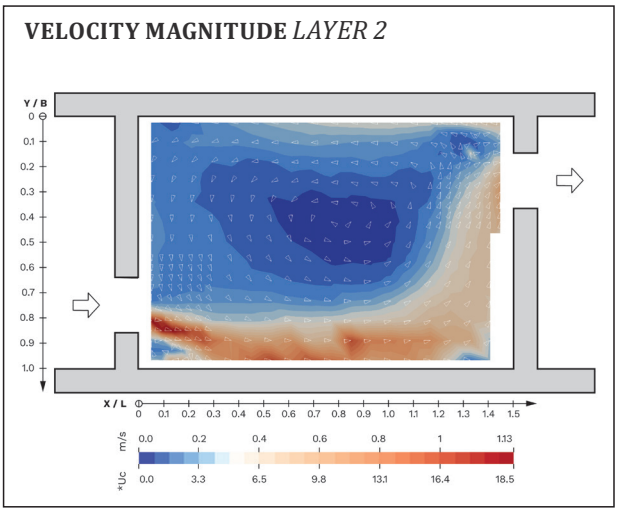

Figure 27: PSF Measurements V1, Layer 2

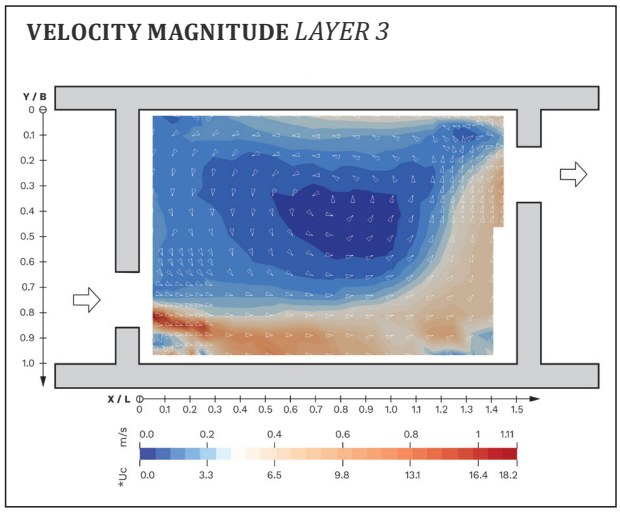

Figure 28: PSF Measurements V1, Layer 3

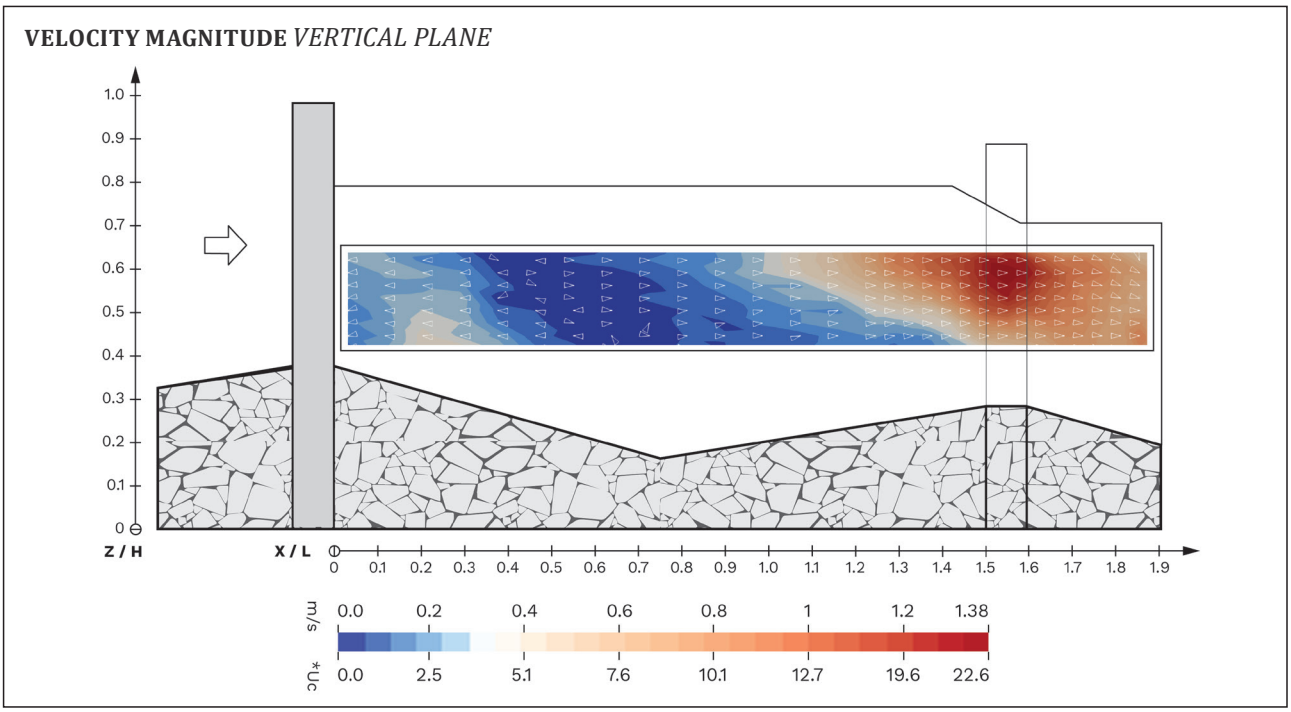

Figure 29: PSF Measurements V1, Vertical Plane

COMPUTATIONAL FLUID DYNAMICS

The results of the numerical simulations, in contrast to the laboratory measurements, span over the entire domain of the laboratory flume. Since measurements were only conducted at the second pool section, simulation results were cropped accordingly to display the same area. A lot of what has already been said about the flow behaviour, during the description of the laboratory measurement results, can equally be applied to the simulation results. This is especially true since the validation process concluded that both investigations share a matching proposition. For this reason, the following display of the results is kept to what the CFD data adds to the point measurements.

For the sake of keeping the presentation of results concise, only exemplary data plots are shown. A more detailed discussion is added in a subsequent chapter, addressing different aspects of the flow, and a comprehensive collection of the simulation results can be found in the appendix.

Figure 30 shows the velocity magnitudes as they were simulated by ANSYS Fluent, in the example of the second layer. The overall behaviour mirrors that of the measurements but is now shown over the entire domain without any geometrical measurement restrictions. This adds a view of the secondary recirculation zones in the two corners X/L = 0, Y/B = 1 and X/L = 1.5, Y/B = 1. Main velocity peaks can yet again be observed within and after the slot, in this case peaking at 1.18 m/s (19.3U_c) and notably the angle at which the stream enters the pool is well defined.

The vertical cross section through the second slot shows both the measurement pool, as well as the following pool section. Maximum velocities are almost exclusively centred around the pool boundary and fall off quickly towards the recirculation zones. The velocities along the slot depth are seemingly constant, with a pronounced horizontal development along the water surface, showing the turbulent collapse of the developing inflow water jet.

In addition to the velocity plots, the TKE could easily be exported without being subjected to measurement difficulties. It is still noted that the display of turbulent behaviour is connected to complex flow characteristics and therefore has to be treated with a critical eye. The most turbulent behaviour occurs, as expected, right after the pool boundary. Due to the difference in water level, a surface jet forms, which then enters the pool producing turbulences in the process. The remaining pool is devoid of any major turbulence, indicating an advantageous surrounding for fish to rest. Throughout the vertical cross section, turbulence distribution can be seen over the entire depth. In the slot sections, turbulences seem to occur mainly within the upper 2/3 of the depth, leaving a comparably calm section along the bottom. In addition to the aforementioned inflow TKE peak, another surface peak occurs when the main flow hits the boundary wall and is forced to redirect its path.

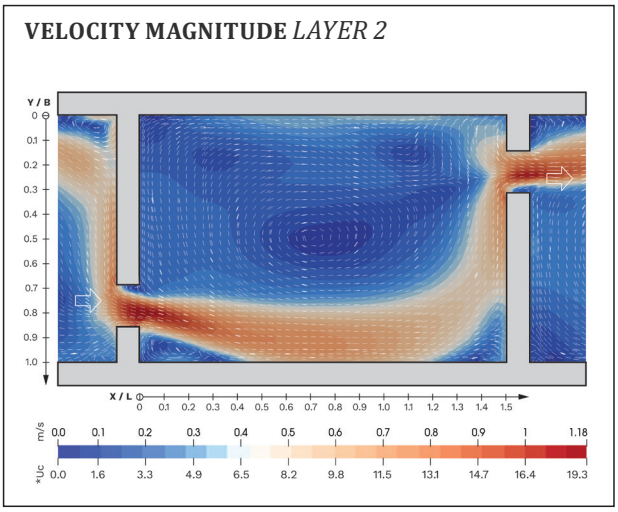

Figure 30: PSF CFD Version 1, Layer 2

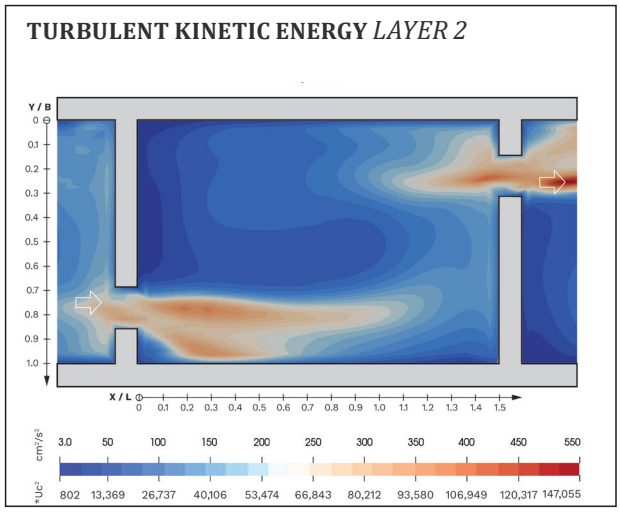

Figure 31: CFD Version 1, Layer 2 (TKE)

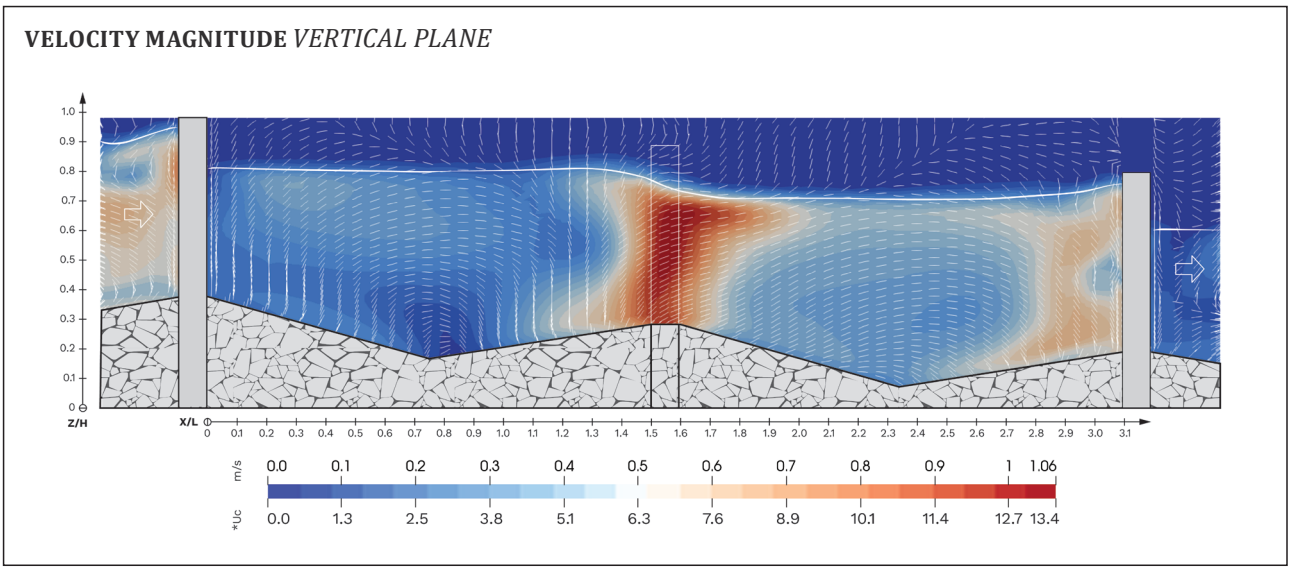

Figure 32: CFD Version 1, Vertical Plane

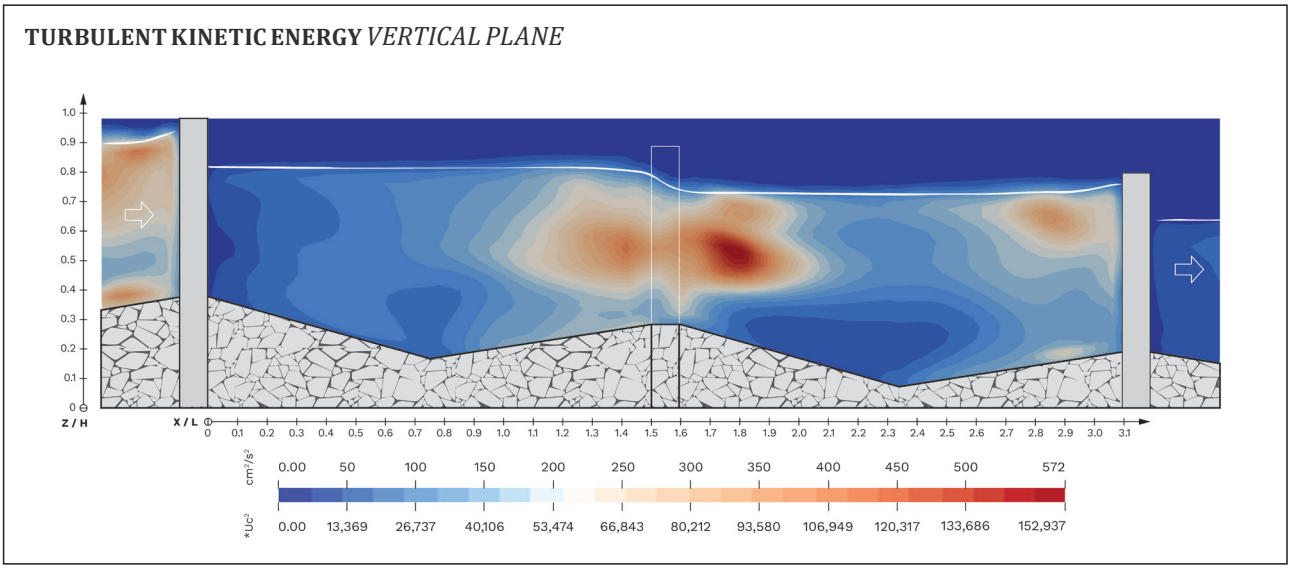

Figure 33: CFD Version 1, Vertical Plane (TKE)

POOL AND SLOT FISHWAY: VERSION 2
LABORATORY MEASUREMENTS

The second version of the fishway, with a discharge of 42 l/s and a slot width of 16.7 cm was measured at the same locations as the previous version. Only the wider slot allowed for a more detailed investigation of the pool boundary. Additionally, several measurement procedures were improved—flipping the probe orientation, decreasing the measurement frequency and increasing the measurement volume at critical sections, as well as a slight adjustment of the filter criteria (Correlation limit was lowered from 50% to 30% at critical spots). Thereby increasing the overall data quality, but especially producing better results around the slot sections. Measurements previous to those adjustments suffered under occasional reflection problems, which were significantly reduced. The average inflow velocity for version two was approximately 0.08 m/s.

The first layer (Figure 34) of the second version presents the flow pattern like previously discussed—the main current follows the wall at Y/B =1.0 in streamwise direction, bending at around X/L = 1.3 towards the following slot. The recirculation area is well defined and shows no recognizable flow disturbances. The maximum velocities are slightly lower (within the first layer), compared to the first version, although the discharge was increased by roughly a third. This, most likely, is due to the changed geometry in combination with a higher accuracy of the measurements, as previously discussed, at the critical slot outflow, avoiding unreasonable value spiking. Velocities peak at about 1.17 m/s (14.6U_c).

The second layer (Figure 35) repeats the same behaviour. Velocity spikes at the Y/B = 0 streamwise wall, indicating a slight pulse interference. The slot outflow at Y/B = 0.85, X/L = 0.1 on the other hand demonstrated a comparably high data quality. Maximum velocities reach 1.19 m/s (14.9U_c).

In the third layer (Figure 36), velocities peak at around 1.2 m/s (15.3U_c) at the pool inflow while the main outflow current seems to expand slightly between X/L = 1.2 and X/L = 1.5.

Vertical measurements of the second PSF version, after adjusting the procedure, produced a slightly different flow behaviour at the pool boundary. What previously looked like declining velocities towards the bottom, could not be reproduced during this step and further measurements were conducted to analyse the vertical behaviour. Maximum values along this plane reached up to 1.26 m/s (15.8U_c).

Due to the higher data quality, resulting from significantly reduced reflection problems, measurements of the TKE were possible, yet still influenced by noise. Figure 37 shows the TKE values at the first horizontal layer of the second fishway version.

Maximum turbulence occurs shortly after the slot outflow at (Y/B = 0.8, X/L = 0.2), corresponding to the maximum velocity location. Maximum TKE values of 1083 cm^2/s^2 were measured and the distribution follows a similar path as can be seen on the velocity plots. Similar to the CFD results, the turbulent slot outflow is focused at two parallel zones in close proximity. Measurements within the area marked with an ‘X’ were deemed insufficiently reliable due to wall reflections and had to be removed. It is worth mentioning, that data quality has a significantly higher impact on TKE values, since any error is squared during the calculation, compared to e.g. velocity components. Therefore, velocity measurements were possible, even at locations were TKE measurements were not.

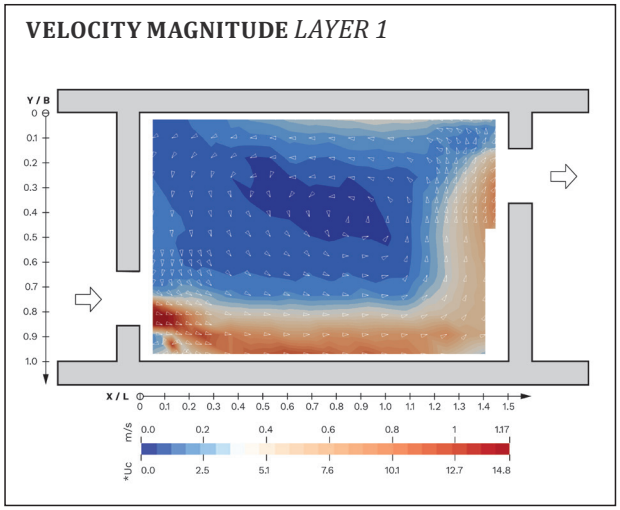

Figure 34: PSF Measurements V2, Layer 1

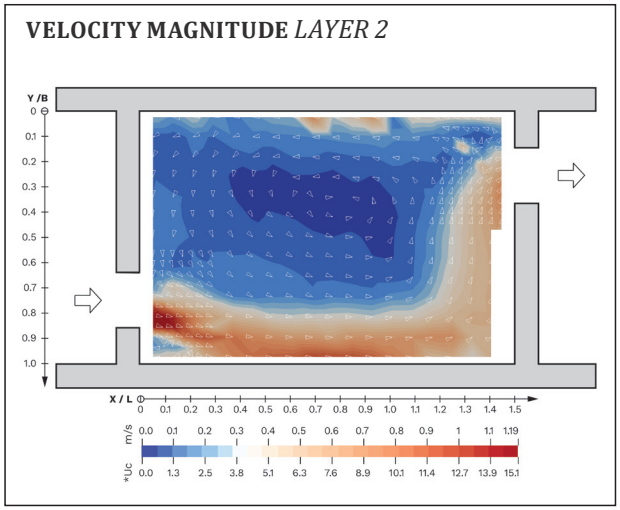

Figure 35: PSF Measurements V2, Layer 2

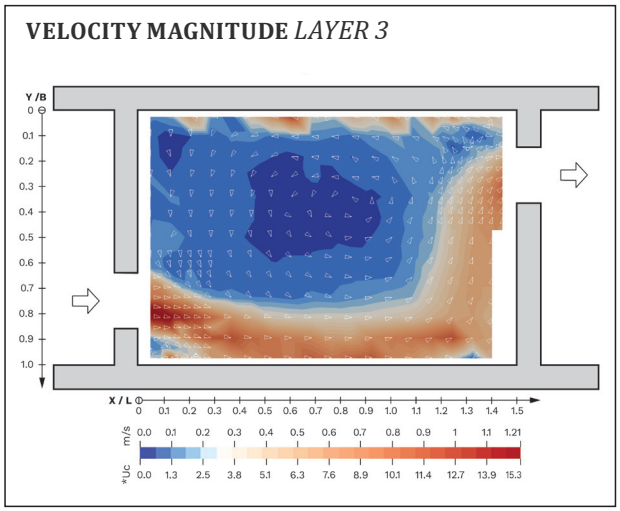

Figure 36: PSF Measurements V2, Layer 3

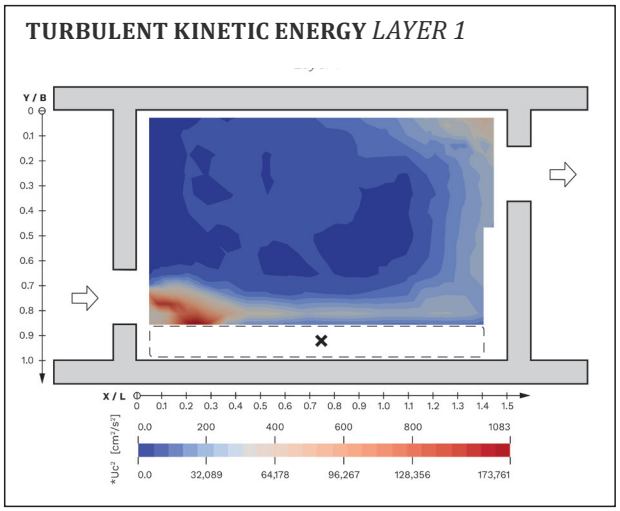

Figure 37: PSF (TKE) V2, Layer 1

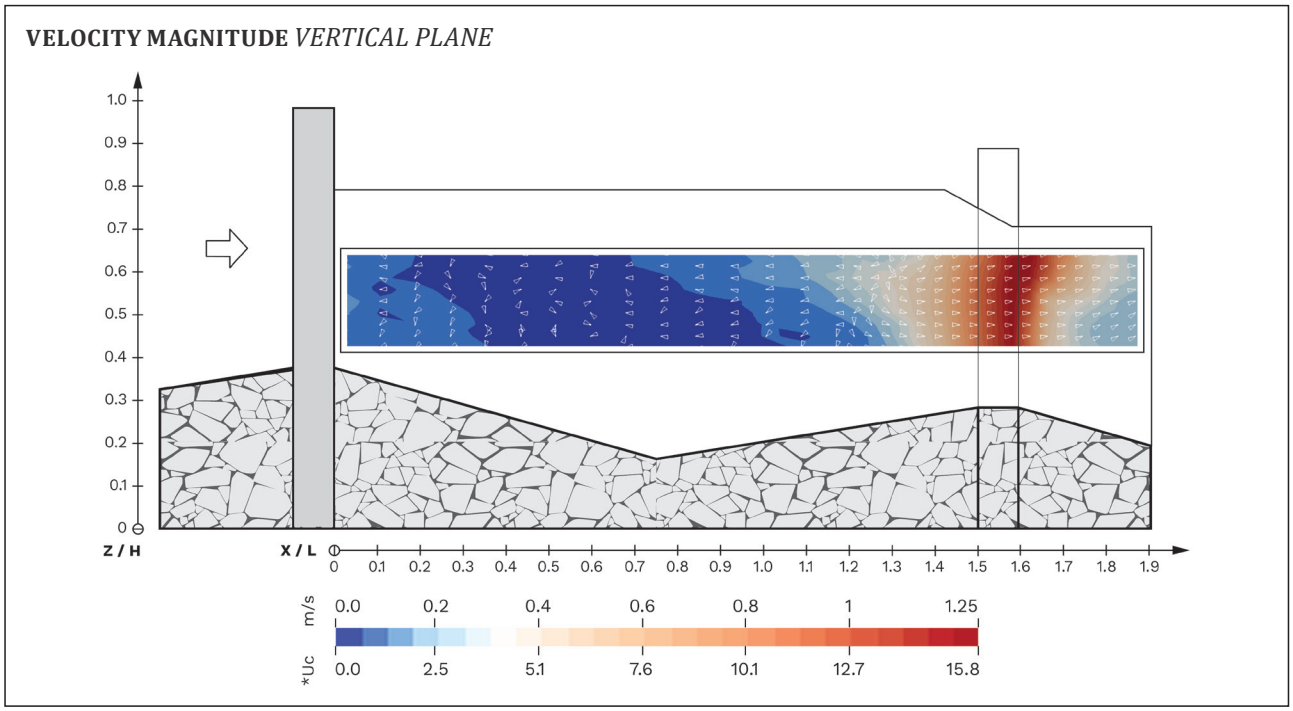

Figure 38: PSF Measurements V2, Vertical Plane

COMPUTATIONAL FLUID DYNAMICS

Results from the simulations incorporating the wider slot width of 16.7 cm provide a very similar picture as have already been shown in the previous chapter. The change in geometry, as well as the increased discharge of 42 l/s have brought some minor changes with them, but all together leaving the previous statements untouched. As a way of comparing the two fishway versions, differences in the contour plots and overall values will be discussed and exemplary results of the second simulation are shown on the following page. A comprehensive collection of simulation results can be found within the appendix.

Velocity magnitudes of Figure 39 are qualitatively almost identical to their predecessor, showing only a minor increase in the main flow width and a slightly more pronounced flow intensity after the slot inflow. Maximum velocities, in this case, rose in value from 1.18 m/s to 1.25 m/s , but at the same time decreased in their normalized flow velocity compared to the average inflow velocity from 19.3U_c to 15.8 U_c. The slight increase in flow velocity along the middle of the left boundary wall (Y/B = 0, X/L = 0.68), indicated in the laboratory measurements, could also be reproduced, further increasing the confidence in the simulation results.

Looking at the velocity magnitudes along the vertical plane (Figure 41), their distribution has changed moderately, assumingly due to a faint shift in the outflow specifics after the pool boundary. Qualitatively, results of the second version align with the laboratory measurements, showing consistently high-water velocities along the depth at X/L = 1.5–1.6. This could also be reproduced during vertical slot measurements.

TKE peaks increased by a rough 7 % as a result of the increased discharge. Distribution patterns although stayed constant, again showing the two parallel high-density zones after the slot and a focus in the upper regions, concerning the vertical plane.

VELOCITIES

Aside from the overall flow behaviour, maximum velocities play a significant role in the evaluation of a fishway. Zones of maximum velocities have already been indicated during the course of the documentation. They mainly occur in and shortly after the pool boundary and tend to be more pronounced in the upper section of the flow. Additional velocity peaks also occur at certain locations where the flow is redirected within a short distance, either meeting a boundary or close to the slot inflow. To get an overview of the velocity magnitudes, the following table summarizes the peaks throughout the measurements and simulations. Only the velocity vectors are considered and are shown as three different, but related values. First as a normalized value related to the average inflow velocity U_c, which is calculated by means of continuity, dividing discharge and flow area. Secondly, as the velocity vector measured in the laboratory flume or stemming from the numerical simulation. And finally, as an upscaled velocity, demonstrating the magnitude as it would occur in the life-sized fishway—scaled by a factor of 1.66. The cases are divided into version one (V1), with a discharge of 33 l/s and a slot width of 12.7 cm and version two (V2), with a discharge of 42 l/s and a slot width of 16.7 cm. Additionally, the cases are marked with an 'M' for measurement or 'S' for simulation, as well as their orientation, horizontal (h) or vertical (v).

Table 8: Velocities

Case	Norm. Vel. [-]	Velocity [m/s]	Vel. *1.66 [m/s]
V1M Layer1-h	20.3Uc1	1.24	2.06
V1M Layer 2-h	18.5Uc1	1.13	1.88
V1M Layer 3-h	18.2Uc1	1.11	1.84
V1M v	22.6Uc1	1.38	2.29
V2M Layer1-h	14.8Uc2	1.17	1.94
V2M Layer2-h	15.1Uc2	1.19	1.98
V2M Layer3-h	15.3Uc2	1.21	2.01
V2M v	15.8Uc2	1.25	2.08
V1S Layer1-h	18.5Uc1	1.13	1.88
V1S Layer 2-h	19.3Uc1	1.18	1.96
V1S Layer 3-h	19.8Uc1	1.21	2.01
V1M v	18.3Uc1	1.12	1.86
V2S Layer1-h	15.8Uc2	1.25	2.08
V2S Layer 2-h	15.8Uc2	1.25	2.08
V2S Layer 3-h	16.2Uc2	1.28	2.13
V2M v	13.4Uc2	1.06	1.76

V1: Version 1 ; V2: Version 2 ; M: Measurement ; S: Simulation
h: Horizontal ; v: Vertical ; Uc1: 0.06 m/s ; Uc2: 0.078 m/s

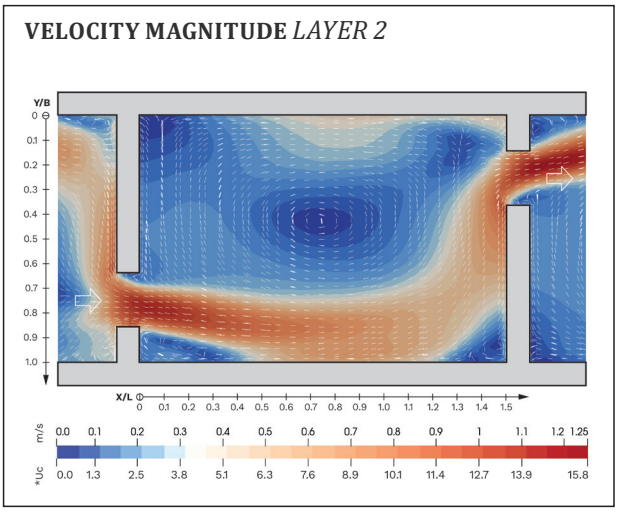

Figure 39: PSF CFD Version 2, Layer 2

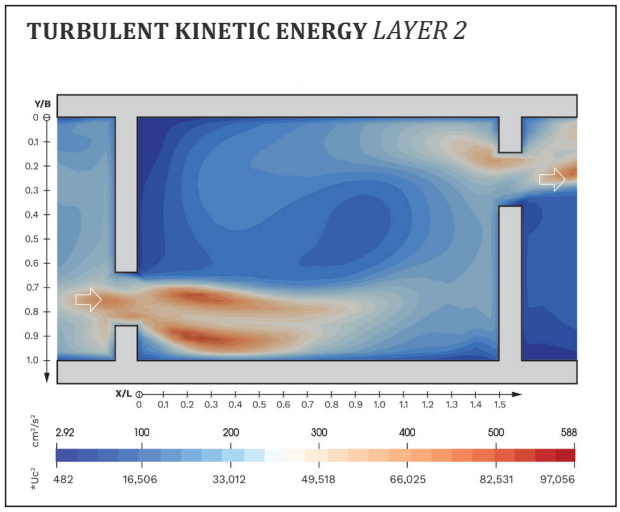

Figure 40: CFD Version 2, Layer 2 (TKE)

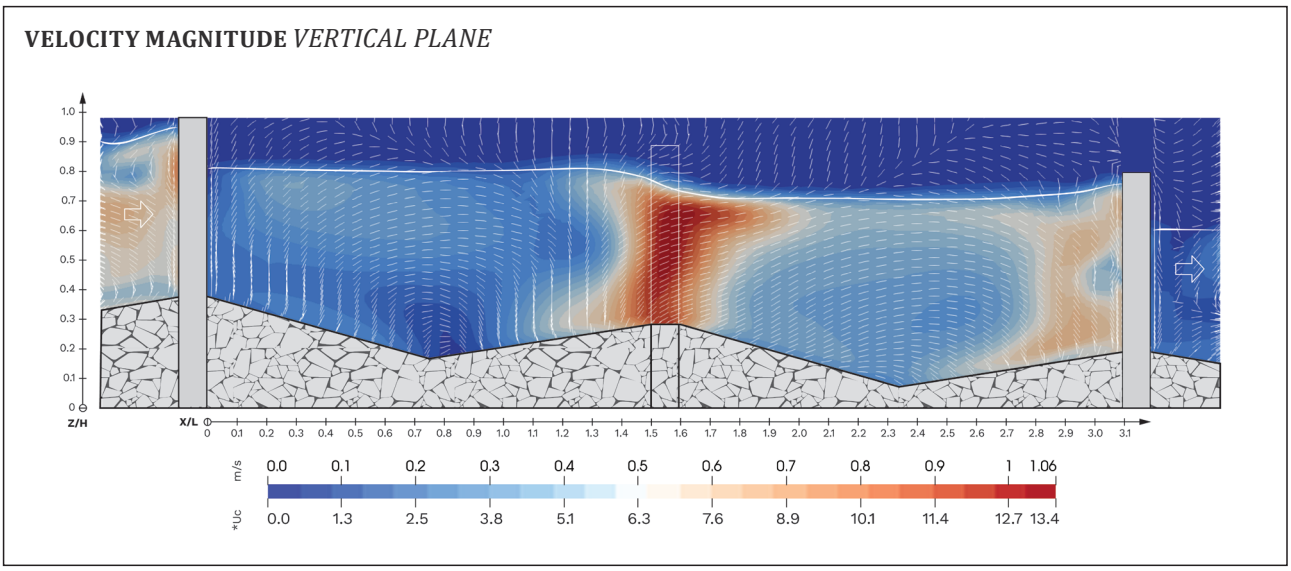

Figure 41: CFD Version 2, Vertical Plane

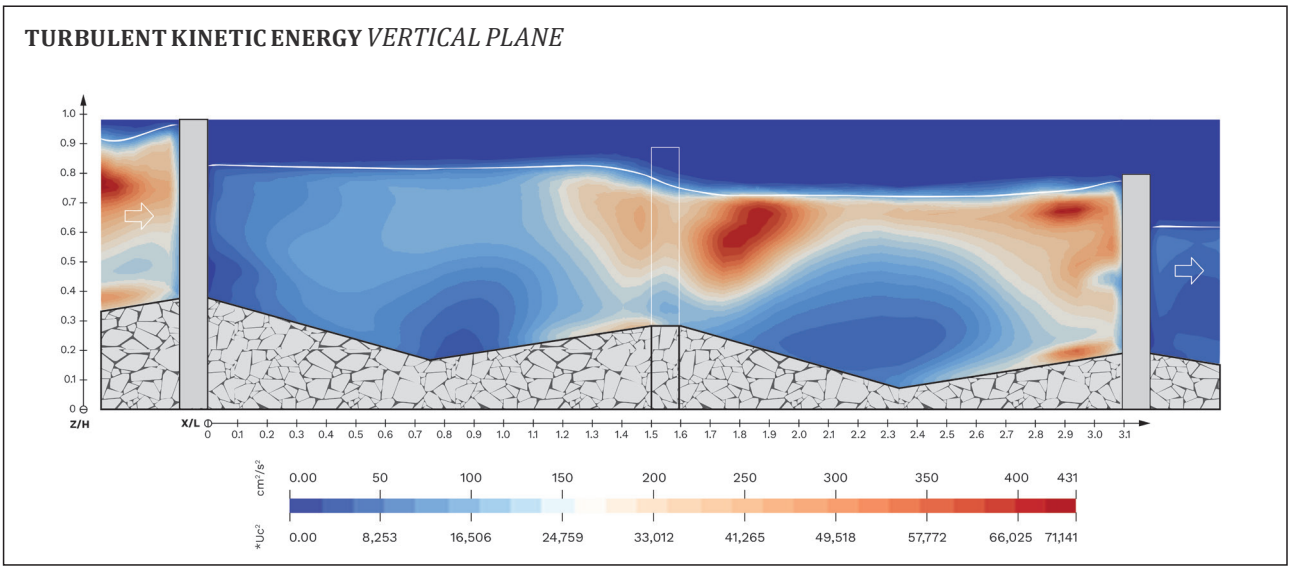

Figure 42: CFD Version 2, Vertical Plane (TKE)

TURBULENT KINETIC ENERGY

The TKE is a measure for the velocity fluctuations within a fluid volume. These fluctuations are a mean of quantifying small eddies and therefore also the amount of turbulence. Within a measurement the problem occurs, that fluctuations are not only produced by turbulence, but also by noise. Therefore, points with low quality or reflection interference often display artificially high turbulence. Such error readings have been carefully monitored and sections of high noise and reflections have been repeatably measured or excluded from the data sets. Additionally, the frequency of the measurements is related to how well fluctuation spikes can be monitored, as a lower frequency has a high probability of missing a velocity peak. On the other hand, high frequencies are prone to be affected by excessive noise. Therefore, settings have to be carefully balanced to fit the measurement situation.

The numerical simulation is free of such measurement contradictions but has, in its own right, challenging aspects to handle. Turbulent flow has proven to be a complex subject with many variables affecting its behaviour. Therefore, some real-life interactions might not be exactly matched by the simulation and demand for careful fine-tuning. Reality most probably lies somewhere in between the laboratory measurements and the CFD simulations and requires experienced judgement together with sufficient references. The figures on the following page show the distribution, as well as the values of the TKE simulation, utilizing ANSYS Fluent. Both PSF versions, with slot widths of 12.7 cm and 16.7 cm, are each represented by a plot of the first layer TKE values (Figure 43/44). Additionally, the vertical distribution is shown in Figure 46 accompanied by laboratory TKE measurements of the first layer (Version 2: slot width 16.7 cm) in Figure 45.

TKE distributions throughout the first version of the PSF (Figure 43) seem to be focused around the slots, trailing linearly along the path of the main-stream current (X/L = 0–1.0; Y/B = 0.7–1.0). This section also shows that TKE values occur in two parallel streams. This might be due to the directional shift of the main flow current, producing a jet that submerges along a focused line, creating a spiral like turbulence along the x-axis. The same behaviour can be observed at the following slot, with a more pronounced inflow turbulence (X/L = 1.2–1.5; Y/B = 0–0.3). The vertical view indicates that the higher TKE values seem to appear in the upper two thirds of the water body. This would match a visual assessment of the laboratory flume, where the inflow jet collapses right at its entry into the following pool. Note that this observation is purely anecdotal.

The vertical plot also indicates that the turbulence could be significantly lower close to the bottom, which would favour small fish and establish a flow behaviour that is advantageous for a wider range of fish species and other aquatic animals. Although further investigations must be conducted to confirm this behaviour, since its proximity to the bottom opposes a wide range of complexities.

Qualitatively, the TKE plots of the second PSF version match the first one, with only minor differences to detect, although notably the maximum values following the first slot increased by about 50 %, most likely due to the increased discharge.

Last but not least, the result of a TKE measurement on the first layer of the second PSF version is shown in Figure 45. Since much of what was measured previous to that had inadequate quality for displaying TKE values, TKE measurements were only done for reference purposes. The section labelled with an ‘X’ was masked out due to unavoidable reflections. The remaining data displayed maximum values at a similar position, compared to the CFD simulation, also indicating a split into two focused turbulence zones trailing along the x-axis, following the slot outflow.

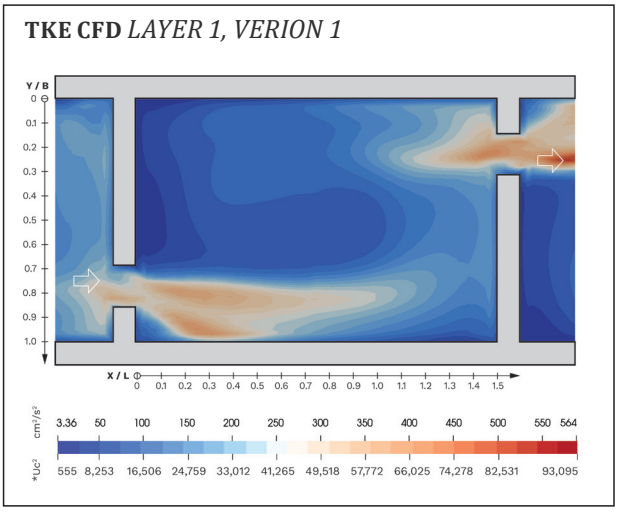

Figure 43: TKE CFD Version 1, Layer 1

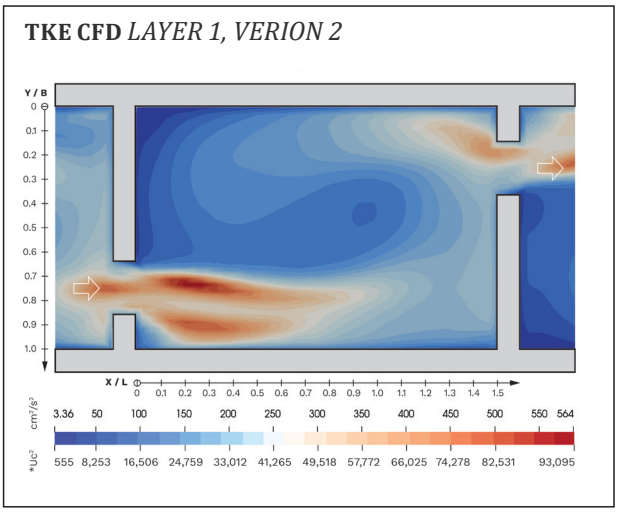

Figure 44: TKE CFD Version 2, Layer 1

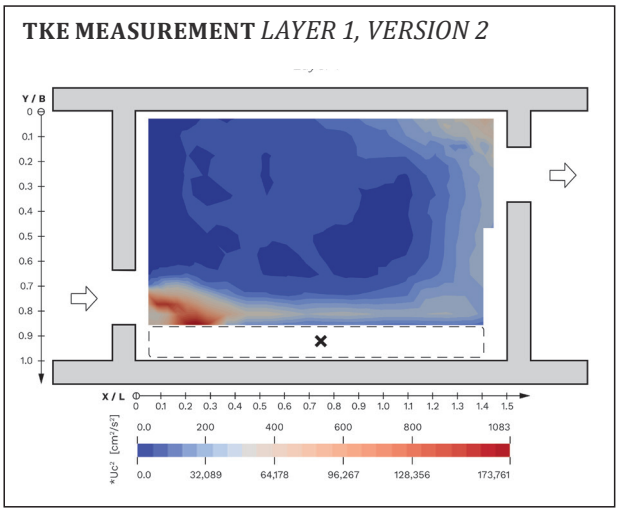

Figure 45: TKE Measurement Version 2, Layer 1

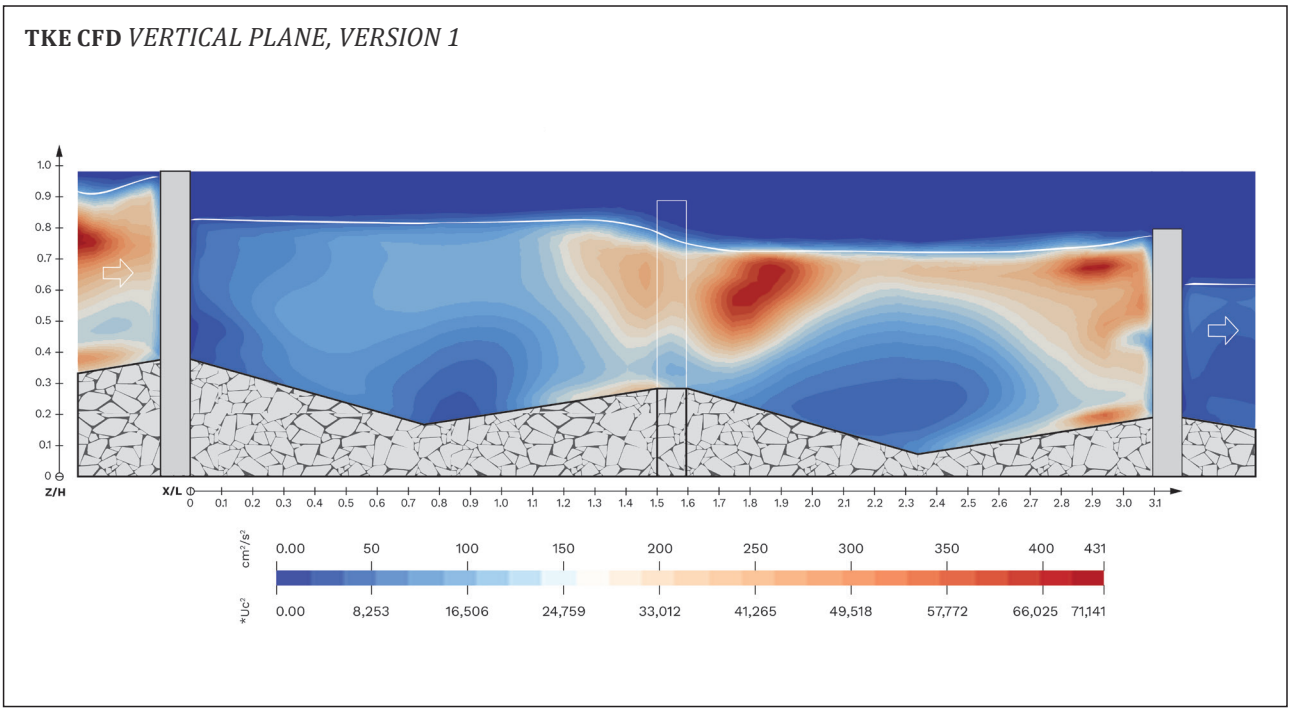

Figure 46: TKE Vertical Plane, Version 1

POOL BOUNDARIES

As a crucial point of the fishway, the pool boundaries require a higher degree of measurement data and although the entire domain was portrayed by the previous numerical simulation, the specific velocity behaviour along the depth of the slot is highlighted by additional measurements. The properties of the bottom material are thought to have a noticeable impact on the velocity gradient towards the bottom. That, and the impact of the potential difference between two pools in succession was analysed and described as follows.

To get a better view of the velocity distribution within the slots, the measurement probe had to be changed from the previously used ADV probe, to a system incorporating a Prandtl Tube. The new setup allowed for measurements close to the bottom and walls, without risking instrument damages and excessive reflection problems. The Prandtl Tube was calibrated, using ADV measurement data, concluding that the velocity magnitudes at equal locations differed only by under 0.1 m/s and were deemed as equally precise. Following this estimate, a series of slot measurements were conducted, evaluating the velocity distribution along the water depth at four locations along its width. Results of which can be seen on the following page.

The velocity measurements along the water depth, as seen in Figure 47, display the directional outflow jet with positive velocities at the right side of the third slot and negative values at the left (in streamwise direction). This is very much in line with the previously discussed result, showing the angled stream at the pool boundaries. Velocities also appear relatively constant over the entire depth, with only measurements at the 'Middle Left' jumping at certain points, most likely due to an uneven distribution of the velocity gradient from maximum values at the right to the negative values at the left.

Figure 48 then shows the relation of slot velocities to water level difference between the pools, represented by the relationship h_u/h_o, where higher numbers mean less of a water difference and vice versa. The measurements clearly show the tendency of increasing velocities with a falling h_u/h_o, meaning that the closer the water level between two successive pools is, the lower the slot velocities tend to be. Measurements were taken from the third slot at the 'Middle Right' where the main flow current is expected to occur. At this location, velocities also display a tendency to grow with depth, which in most other measurement cases has been the other way around.

Another point of interest was the overflow coefficient between the fishway pools. Rearranging the previously mentioned Poleni equation (see equation 25), as well as the water levels of two consecutive pools, the overflow coefficient μ_v ($\mu^*\alpha$) can be calculated as follows:

$$\mu_v = \frac{3Q}{2\,b\,\sqrt{2\,g}\;h^{3/2}} \quad [-] \qquad [25]$$

To collect a range of values, the overall potential difference between the uppermost- and the lowest water level was varied, producing a range of h_u/h_o ratios. Figure 49 shows the measured overflow coefficients in relationship to their respective h_u/h_o ratio. It shows that with a growing h_u/h_o ratio, the overflow coefficient declines and at the top end the values flatten out in a range between 0.5–0.6 [-].

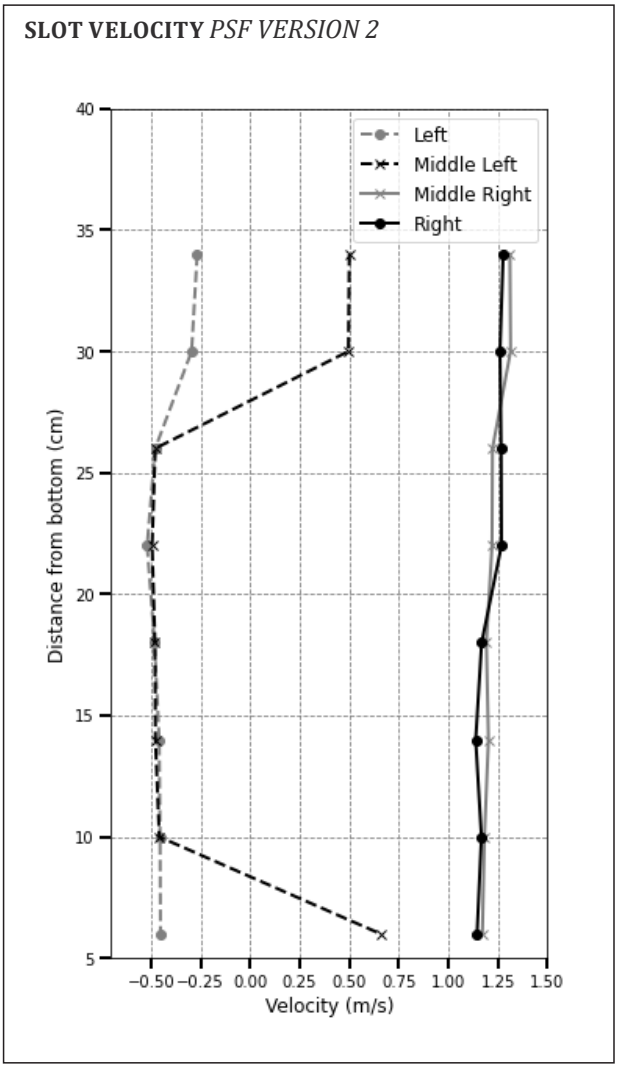

Figure 47: Slot Velocities PSF Version 2

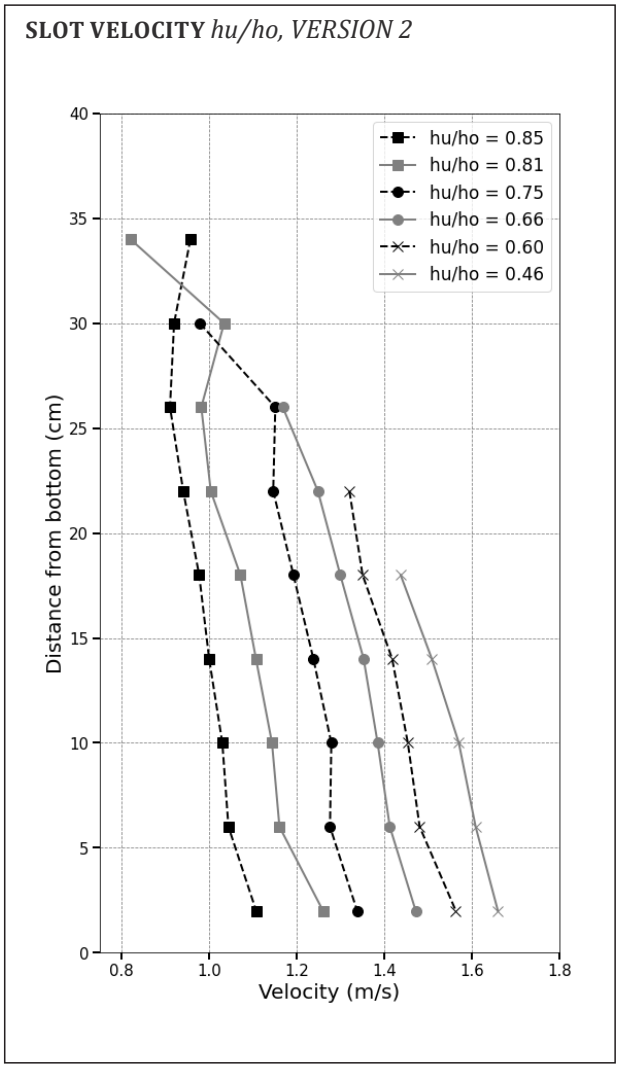

Figure 48: Slot Velocities hu/ho, Version 2

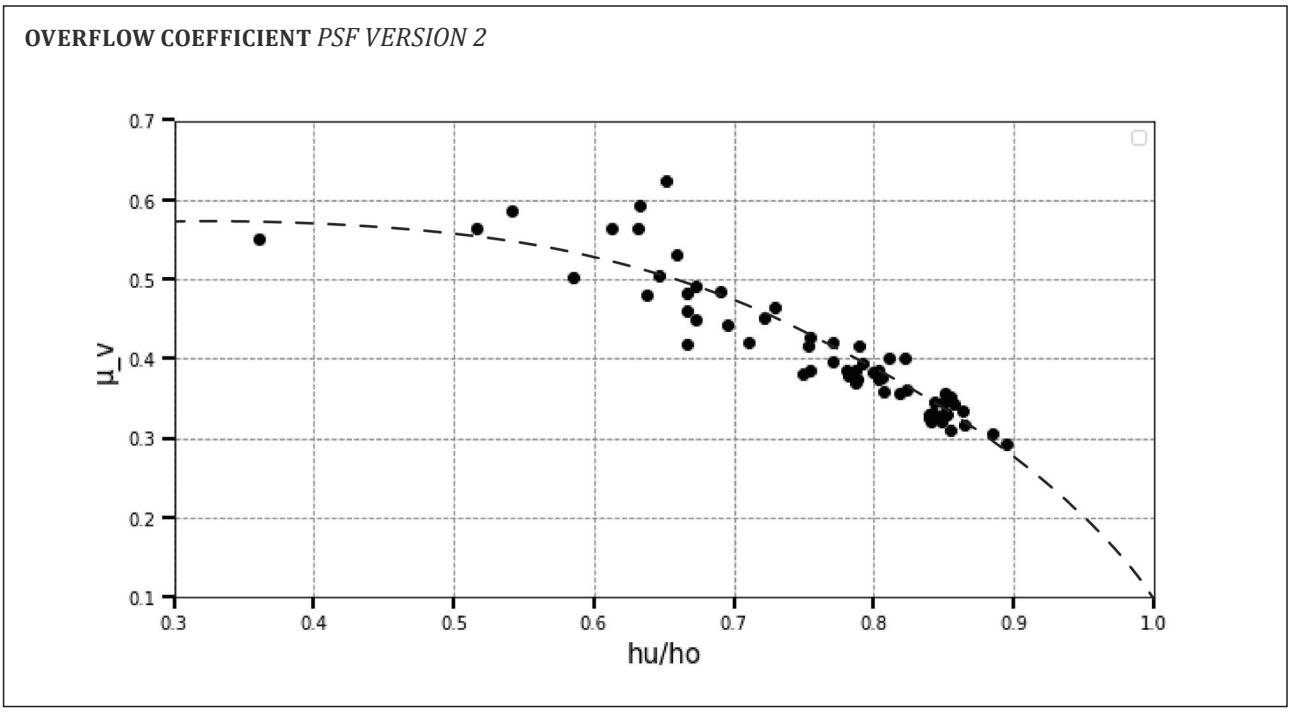

Figure 49: Overflow Coefficient Version 2

FLOW BEHAVIOUR

Velocity distribution and the overall flow behaviour play a major role in the effectiveness of any fishway. If velocities are too high, smaller or weaker fish cannot ascend, too low and the entrance cannot be detected by passing fish. Furthermore, a wide range of fish species introduces the contradiction that the size-defining fish enforce a larger geometry, which subsequently leads to higher flow velocities, making it harder for smaller fish to make use of the fishway. The goal of modifying the vertical-slot fishway is to establish a flow condition that is advantageous for fish ascend, in a way that swim paths only cross critical areas for a short amount of time and are followed by a recovery zone, both large and calm enough for all types of fish to regain their strength to continue. The type of flow that occurs due to the simplified design can be seen on the exemplary CFD plots, on the following page.

The main flow path (Figure 50 (4)) is well defined on the orographic right side, following the wall until it is redirected in an almost 90° angle towards the following slot by the separating wall. The in- and outflow (2)(5) occurs at an angle towards the closest wall due to the alternating position of the slots. This allows for fish to enter the slot section from the recovery zone (3) in a way that they are not directly subjected by the main current during their approach. Following the same theoretical swim-path, fish are met with the next recovery zone right after the slot, since the main flow is approaching, not from the centre of the pool, but almost from the adjacent corner. The main flow separation happens at the outflow approach (5), where a fraction of the main current is guided back along the orographic left wall. Because of that, a recirculation area (3) is formed around the centre of the pool, during this thesis regularly addressed as the recovery zone. Spanning over most of the length and about two thirds of the width, it is large enough for fish to recover their strength after expending their burst speed, overcoming the slot area. Two additional flow separations occur at the corners passed by the main flow current (2)(6). Those are hardly relevant for this type of PSF but depending on the slot type, can grow to be a comparably large recirculation zone, as the flow path of the main current changes. This can often be observed with conventional vertical-slot fishways, where the hook like elements at the slots guide the flow further to the centre of the pool. This general behaviour of the flow could consistently be observed over the entirety of the measurements and simulations. The depth was observed to have only minor effects on the flow, primarily on the maximum velocities, as can be seen on the previously shown vertical cross section (Figure 41).

The maximum velocities inside and right after the slot at X/L = 1.5–1.6 span from the surface to the bottom, showing only minor deviations in the process. Although the exact behaviour close to the bottom is governed by complex interactions of the flow with the bed material, possibly resulting in velocity variation less smooth than what is shown in the numerical simulation. The recovery zone displays another minor separation in depth, forming a zone at the bottom, within the basin, with minimum flow velocities. This area could be beneficial for very small fish, moving close to the bottom, where they can find conditions most suitable for recovery.

Dividing the flow into its spatial velocity components facilitates the evaluation process and highlights certain behaviours.

First of all, the velocity component in x-direction (U_x) shows a high velocity trail following the acceleration within the slot (X/L = 0–1.0; Y/B = 0.8). Then followed by a redirection towards the following slot and another acceleration towards the next pool at the slot around X/L = 1.5; Y/B = 0.2. The recirculation zone, on the other hand, shows only minor velocities in x-direction. Figure 54 additionally shows the U_x distribution across the vertical plane. Here, the first pool between X/L = 0–1.5 displays the calm recirculation area, while the second pool (X/L = 1.6–3.1) shows a vertical cut of the main flow current. In their ascend, fish theoretically only cross the main current between X/L = 1.4–1.8 and are therefore only shortly subjected to high flow velocities.

FLOW PATH *PSF VERSION 2*

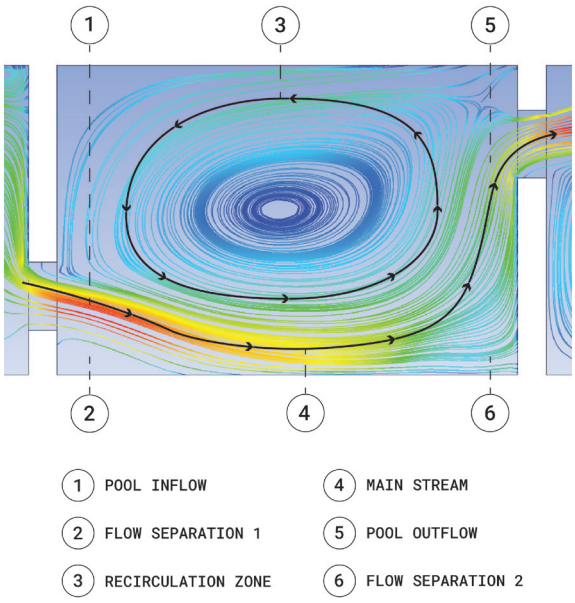

Figure 50: Flow Path CFD Version 2

VELOCITIES Wz *LAYER1, VERSION 2*

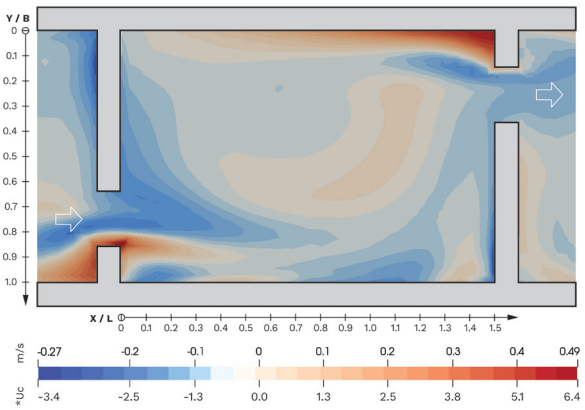

Figure 53: Velocities Wz CFD

VELOCITIES Ux *LAYER1, VERSION 2*

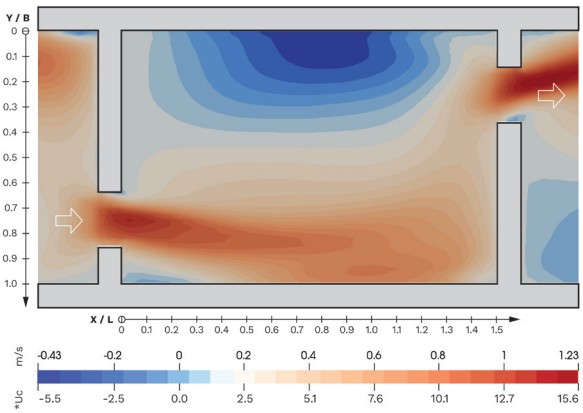

Figure 51: Velocities Ux CFD

VELOCITIES Vy *LAYER1, VERSION 2*

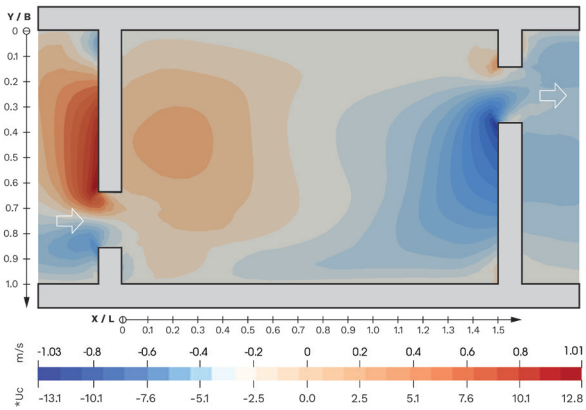

Figure 52: Velocities Vy CFD

VELOCITIES Ux *VERTICAL PLANE VERSION 2*

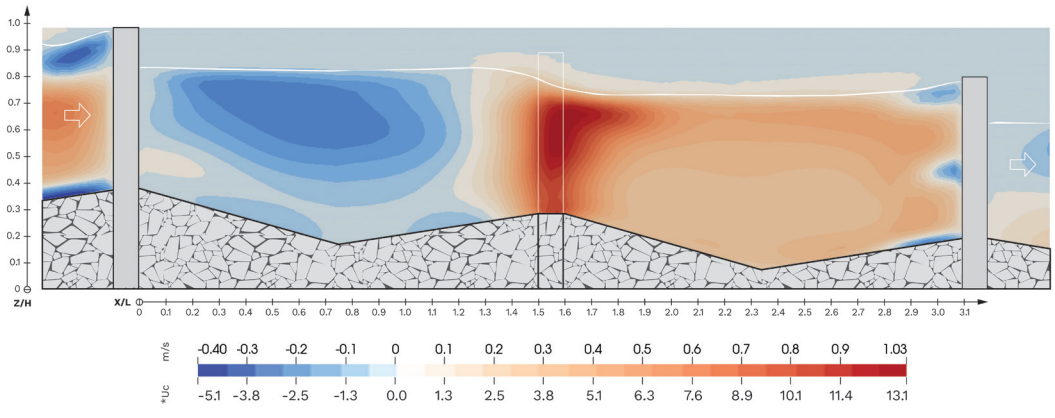

Figure 54: Ux Vertical Plane Version 2

Figure 53: Velocities Wz CFD

A similar observation can be made for the velocity component in y-direction (Figure 52). While the U_x velocities are roughly mirrored along the y-axis at about Y/B = 0.5, the V_y velocities split the pool spanwise at about X/L = 0.75, creating two opposite streams. One approach flow towards the pool boundary from X/L = 0.8–1.5 and the recirculation backflow from X/L = 0–0.8. Along the following pool, this behaviour is then mirrored, alternating from pool to pool according to the slot position. Both the slot approach flow, as well as the recirculation flow are well defined, peaking in their magnitude where the flow bends into the slot. Otherwise, the V_y velocities show no apparent potential for disturbing the fish migration.

Vertically there isn't an extensive flow condition affecting the PSF's functionality (Figure 53). A slight heaving of the flow occurs (X/L = 0.9–1.35) as it approaches the slot, which is shortly after redirected towards the bottom (X/L = 1.35–2.1) as the water level changes from one pool to the other, following the bottom shape. Then, as the current meets the spanwise boundary, some vertical flow can be observed. Generally, the flow follows the geometry of the bottom gravel bed and is primarily shaped by the two-dimensional flow along the x-y plane.

Between the two versions of the fishway only quantitative differences were measured while the qualitative flow behaviour stayed constant, repeating the characteristics previously discussed.

FINAL CONCLUSION

The data produced during the course of this thesis, on two versions of a PSF, paint a recurrent and reproducible picture of its behaviour. Flow patterns repeat throughout both laboratory measurements and CFD simulations and seemingly confirm the initial hypothesis of an advantageous flow-pattern for fish migration. Main flow currents are focused close to the boundaries, allowing for only a minimal disturbance at the pool boundaries where fish must cross the slot section to reach the following upstream pool. A large amount of the pool volume is occupied by the recirculation zone, providing low flow velocities for recovery purposes. This zone, aside from its rotational characteristic, is in large parts basically unaffected by the mainstream current and is neither crossed, nor split by it.

Maximum velocity magnitudes in and after the slot sections reach extreme values at around 2.10 m/s (upscaled), with noticeably lower values in close proximity. While keeping the water levels constant, an increase of the slot width by roughly 30 % (31.5 %) from 12.7 cm to 16.7 cm caused an approximate increase in discharge of equally 30 % (27.3 %) from 33 l/s to 42 l/s. Notably, maximum velocities did not rise as significantly with an average plus of under 10 % within the sample of maximum values.

Evaluating the results of the TKE turned out to be the most challenging aspect of the investigation. Although valuable insights were gathered from their distribution and behaviour. Showing a focused appearance right after the slot, where the incoming water jet meets the following pool volume. Additionally, a reduction in turbulent intensity towards the bottom of the slot was indicated by the CFD data. This, if confirmed by additional studies, would provide a flow section within the slot for smaller/ weaker fish to migrate, further solidifying the PSFs effectiveness.

Comparing CFD data to laboratory measurements showed that the flow behaviour in both cases matched considerably well. Many of the detailed flow characteristics, indicated by the measurements, could be reproduced using simulation software. And although this sample size is nowhere enough to prove a repeatably sound way of designing a fishway via CFD applications, it implies its potential.
With additional fine tuning and a set of sensitivity analyses, design options could be evaluated in a relatively short amount of time—testing the impact of e.g. discharge, slot-width and bed inclination on the overall system.

Overall, the PSF, as it was presented during this thesis, showed a high potential for an advantageous flow behaviour concerning fish migration. The data provided can hopefully support future evaluations and play its part in the improvement of the ecological situation within the lotic system.

06 REFERENCES

AG-FAH (2012): Arbeitsgruppe Fischaufstiegshilfen: "Leitfaden zum Bau von Fischaufstiegshilfen (FAHs)", BMLFUW (Hrsg.): Bundesministerium für Land- und Forstwirtschaft, Umwelt und Wasserwirtschaft. Marxergasse 2, 1030 Wien.

ANSYS (2018): "ANSYS Fluent User's Guide 19.2", ANSYS, Inc. (https://www.ansys.com/)

CLOUGH, S. C. und A. W. H. TURNPENNY (2001): "Swimming Speeds in Fish: Phase 1. Southampton.", Fawley Aquatic Research Laboratories Ltd, Marine & Freshwater Biology Unit (AG-FAH 2012: s14)

DWA (2014): "Merkblatt DWA-M 509 – Fischaufstiegsanlagen und fischpassierbare Bauwerke – Gestaltung, Bemessung, Qualitätssicherung.", Deutsche Vereinigung für Wasserwirtschaft, Abwasser und Abfall e.V.

HASLWANTER M. (2020): "Messungen im Labor zur Optimierung technischer Schlitzpässe.", Graz University of Technology, Institute of Hydraulic Engineering and Water Resource Management)

IMAN H. HAMEED AND ALI N. HILO (2020): "Numerical Analysis on the Effect of Slot Width on the Design of Vertical Slot Fishways.", IOP Publishing Ltd

JASON M. DUNGUAY AND R.W. JAY LACEY (2016): "Numerical study of an innovative fish ladder design for perched culverts.", NRC Research Press

JÄGER, P., V. GFRERER und N. BAYRHAMMER (2010): "Morphometrische Vermessung von Fischen zur Ermittlung des Phänotyps.", Österreichs Fischerei 63(Heft 1): 14-28.

JENS, G., O. BORN, R. HOHLSTEIN, M. KÄMMMEREIT, R. KLUPP, P. LABATZKI, G. MAU, K. SEIFERT und P. WONDRAK (1997): "Fischwanderhilfen: Notwendigkeit, Gestaltung, Rechtsgrundlagen.", Offenbach am Main, Verband Deutscher Fischereiverwaltungsbeamter und Fischereiwissenschaftler e.V.: 114.

JUNGWIRTH, M. und B. PELIKAN (1989): "Zur Problematik von Fischaufstiegshilfen.", (AG-FAHG 2012: s15)

KEVIN BRIAN MULLIGAN, BRETT TOWLER, ALEX HARO AND DAVID P. AHLFELD (2016): "A computational fluid dynamics modeling study of guide walls for downstream fish passage.", Elsevier

MENTER, F. R. (1993): "Zonal Two Equation k-ω Turbulence Models for Aerodynamic Flows", AIAA Paper 93-2906.

MENTER F.R. (1994): "Two-Equation Eddy-Viscosity Turbulence Models for Engineering Applications.", NASA Ames Research Centre, California 94035

NORTEK MANUALS (2018): "The Comprehensive Manual for Velocimeters.", NORTEK (https://www.nortekgroup.com/)

NORTHCOTE, T. G. (1978): "Migratory strategies and production in freshwater fishes. Ecology of Freshwater Fish Production.", S. D. GERKING. Oxford-London-Edinburgh-Melbourne, Blackwell Scientific Publications: 326-359.

PARSHEH, MEHRAN, SOTIROPOULOS, FOTIS, PORTÉ-AGEL, FERNANDO (2010): "Estimation of Power Spectra of Acoustic-Doppler Velocimetry Data Contaminated with Intermittent Spikes", Journal of Hydraulic Engineering

PATANKAR, S. V. AND SPALDING, D.B. (1972): "A calculation procedure for heat, mass and momentum transfer in three-dimensional parabolic flows", Int. J. of Heat and Mass Transfer, Volume 15, Issue 10, October 1972, Pages 1787-1806.

PAVLOV D. S. (1989): "Structures assisting the migrations of non-salmonid fish: USSR. Rome", FAO: 97.

POPE S. B. (2000): "Turbulent Flows.", Cambridge University Press

SEIDL G. (2018): "Technische Beckenpässe - Eine funktionale Variante zu den Vorgaben des Leitfadens.", WASSERWIRTSCHAFT Wasserbausympo-sium Graz 2018: Seiten 175 bis 181.

STROBL T., ZUNIC F. (2006): "Wasserbau: aktuelle Grundlagen - Neue Entwicklungen", Springer. Berlin: 604 Seiten.

WARD, J. V. (1989): "The 4-dimensional nature of lotic ecosystems.", Journal of the North American Benthological Society 8(1): 2-8.

WOSCHITZ G. AND GÜNTER P. (2013): "Fischökologische Zustandserhebung der Mur im Stadtgebiet von Graz", Amt der Steiermärkischen Landesregierung Abteilung 15, Referat Gewässeraufsicht und Gewässerschutz

ZITEK, A., G. HAIDVOGL, M. JUNGWIRTH, P. PAVLAS und S. SCHMUTZ (2007): "Ein ökologisch-strategischer Leitfaden zur Wiederherstellung der Durchgängigkeit von Fließgewässern für die Fischfauna in Österreich.", AP 5 des MIRR Projektes - A Model based Instrument for River Restoration. Wien, Institut für Hydrobiologie und Gewässermanagement, BOKU: 139.

07 LIST OF FIGURES

08 LIST OF TABLES

09 ACRONYMS

PSF	Pool and slot Fishway
CFD	Computational Fluid Dynamics
ADV	Acoustic Doppler Velocimeter
Vx, u, ux	Velocity in x-direction
Vy, v, uy	Velocity in y-direction
Vz, w, uz	Velocity in z-direction
***Uc**	Ratio of measured velocity to inlet velocity
TKE	Turbulent Kinetic Energy
SNR	Signal to Noise Ratio
RMS	Root Mean Square
V1	Fishway Version 1 (Slot Width 12.7 cm)
V2	Fishway Version 1 (Slot Width 16.7 cm)
BMNT	Austrian Federal Ministry for Agriculture, Regions and Tourism (Bundesministerium - Nachhaltigkeit und Tourismus)
RANS	Reynolds Averaged Navier-Stokes (Equation)
VOF	Volume of Fluid
SST	Shear Stress Transport
SIMPLE	Semi-Implicit Method for Pressure-Linked Equations

10 APPENDIX

MEASUREMENTS LAYER 1

1 / 2

Laboratory flume: Version 1

Slot-width: 12.7 cm
Discharge: 33 l/s

VELOCITY MAGNITUDE

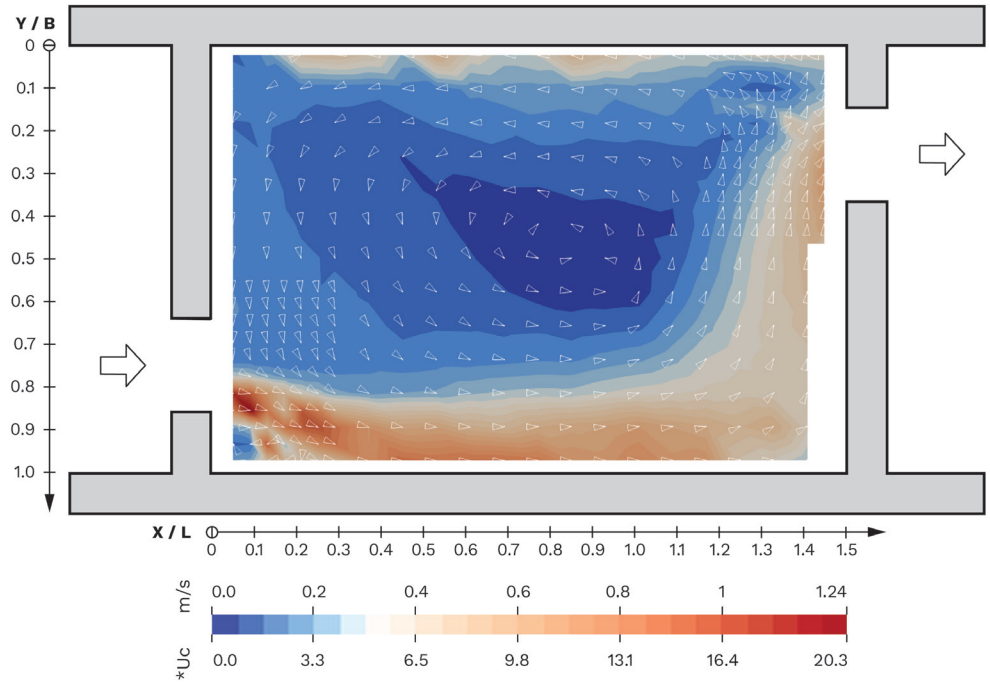

VELOCITY U_X

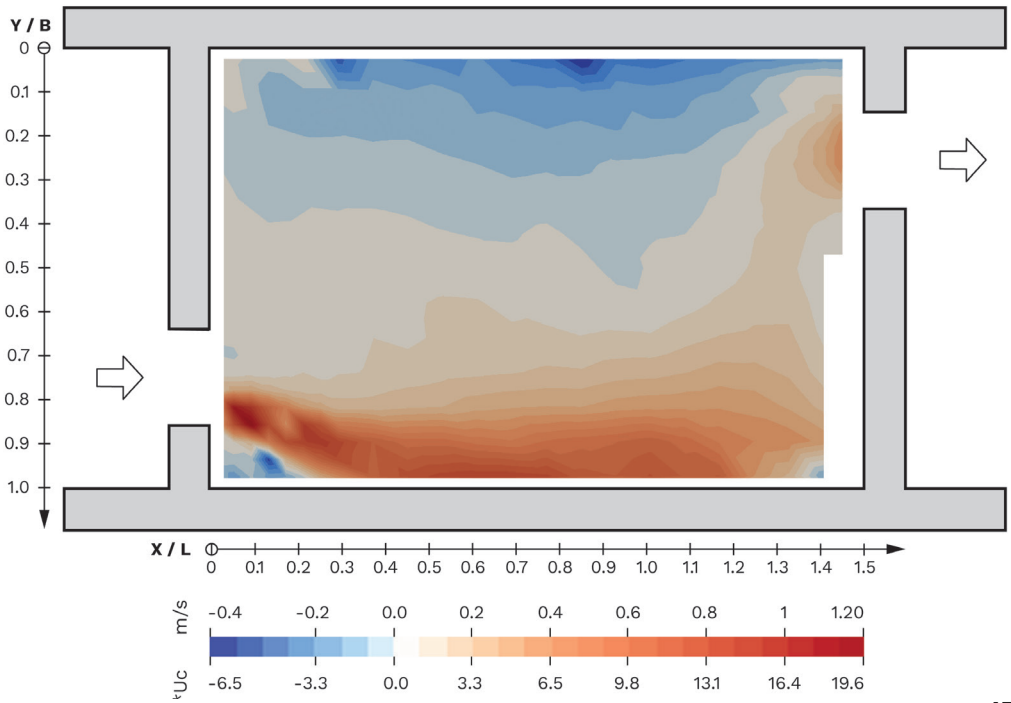

MEASUREMENTS LAYER 1

Laboratory flume: Version 1

Slot-width: 12.7 cm
Discharge: 33 l/s

VELOCITY V_Y

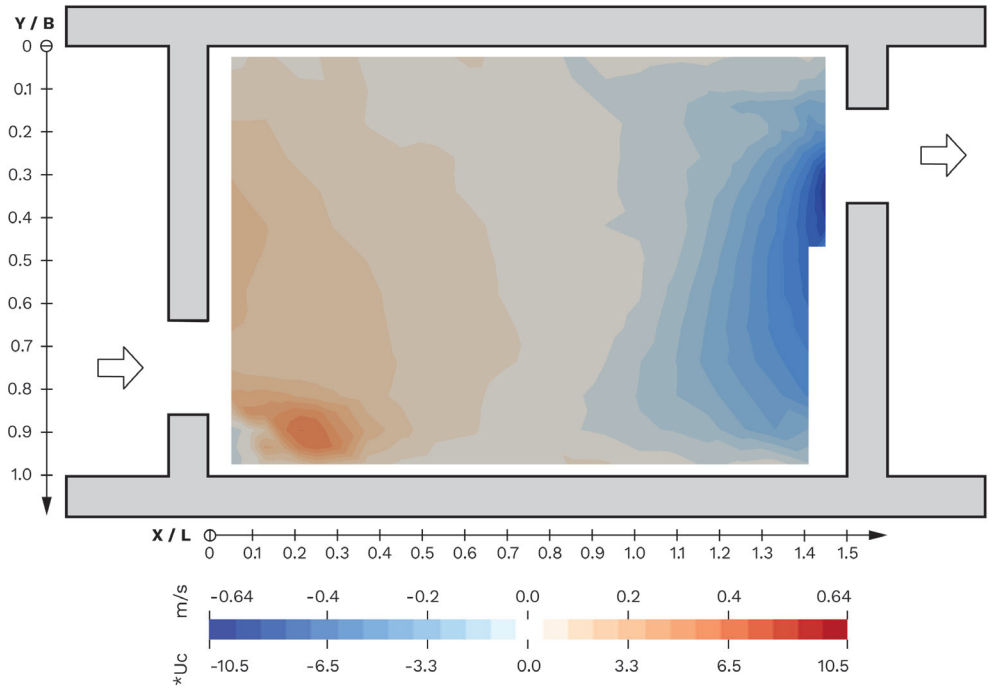

VELOCITY W_Z

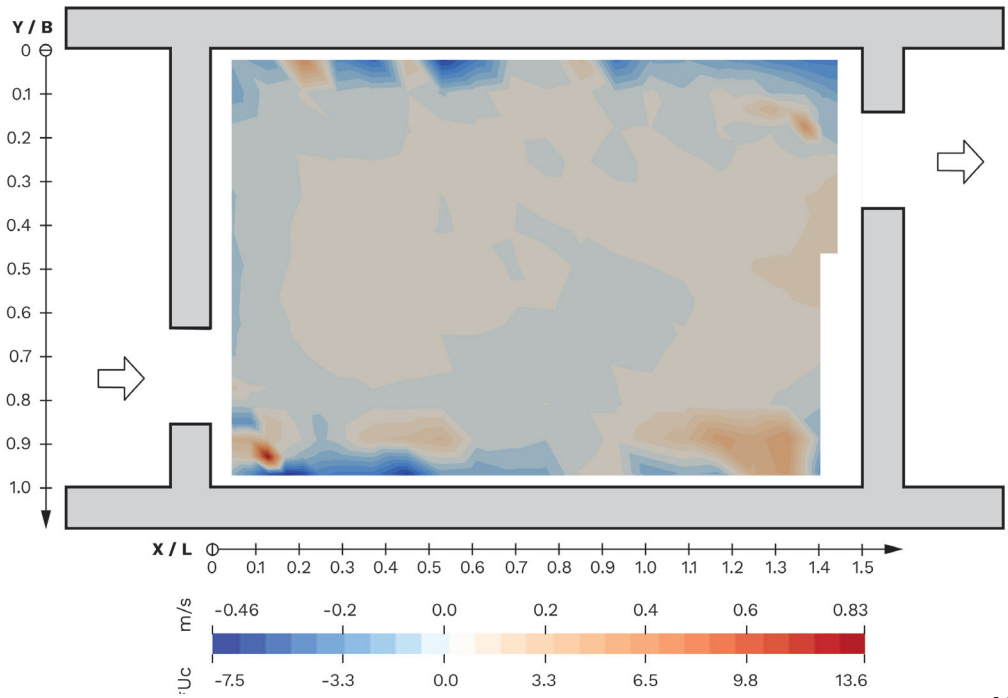

MEASUREMENTS LAYER 2

Laboratory flume: Version 1

Slot-width: 12.7 cm
Discharge: 33 l/s

VELOCITY MAGNITUDE

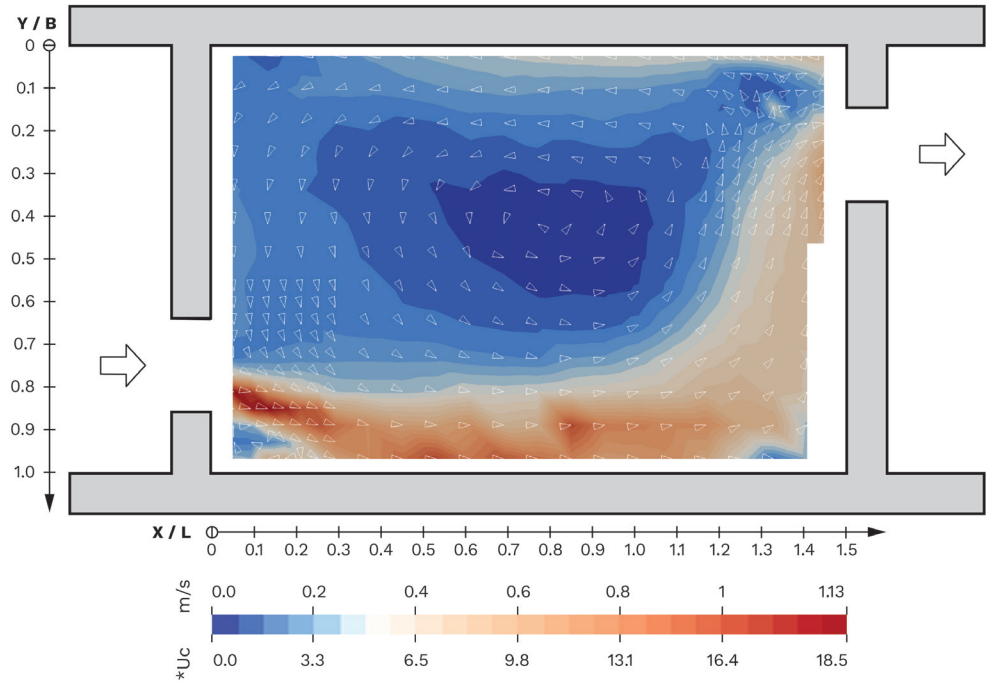

VELOCITY U_X

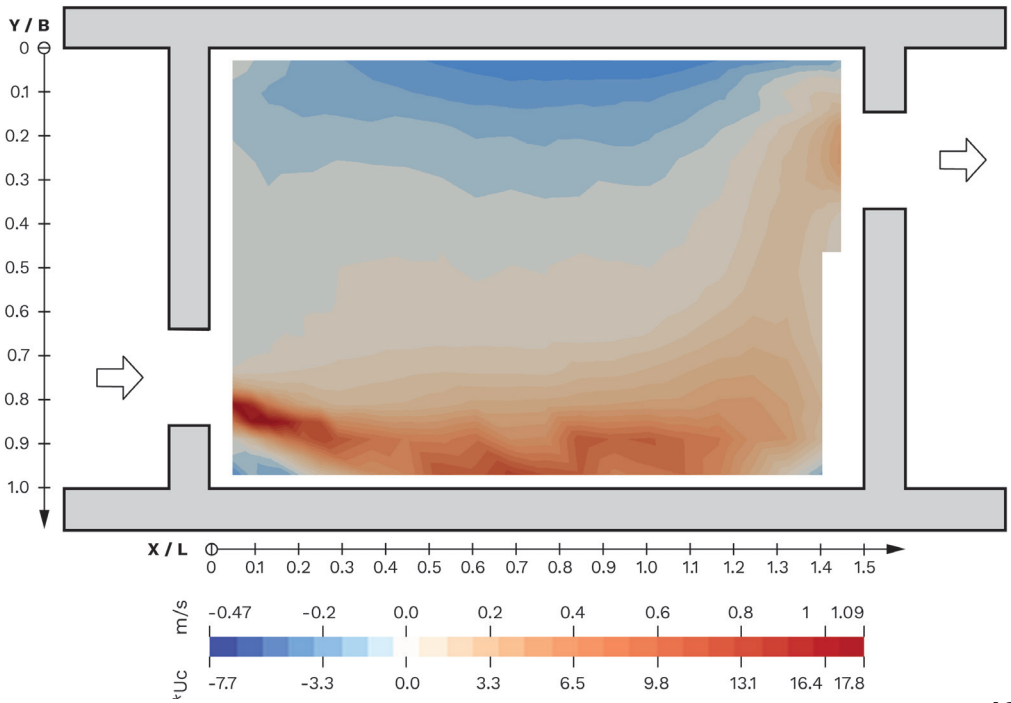

MEASUREMENTS LAYER 2

Laboratory flume: Version 1

Slot-width: 12.7 cm
Discharge: 33 l/s

VELOCITY V_Y

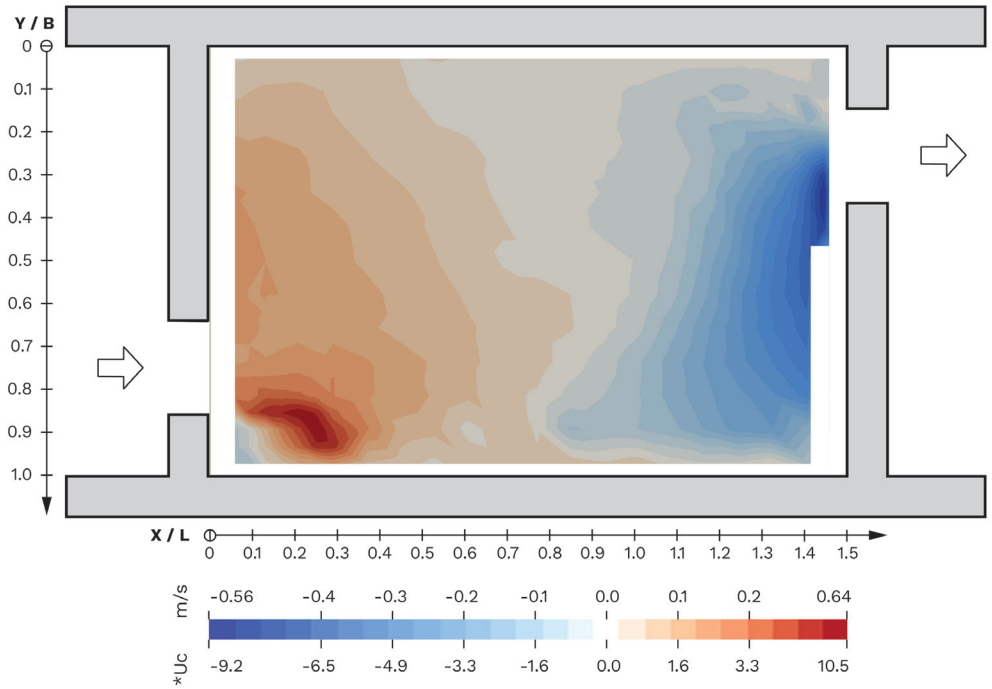

VELOCITY W_Z

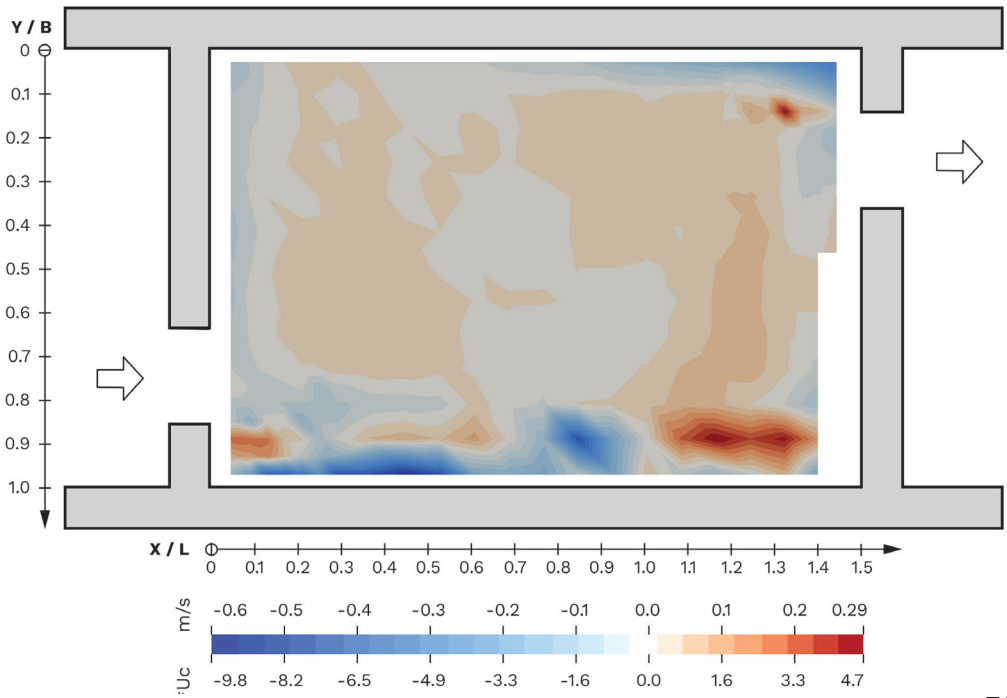

MEASUREMENTS LAYER 3

Laboratory flume: Version 1

Slot-width: 12.7 cm
Discharge: 33 l/s

VELOCITY MAGNITUDE

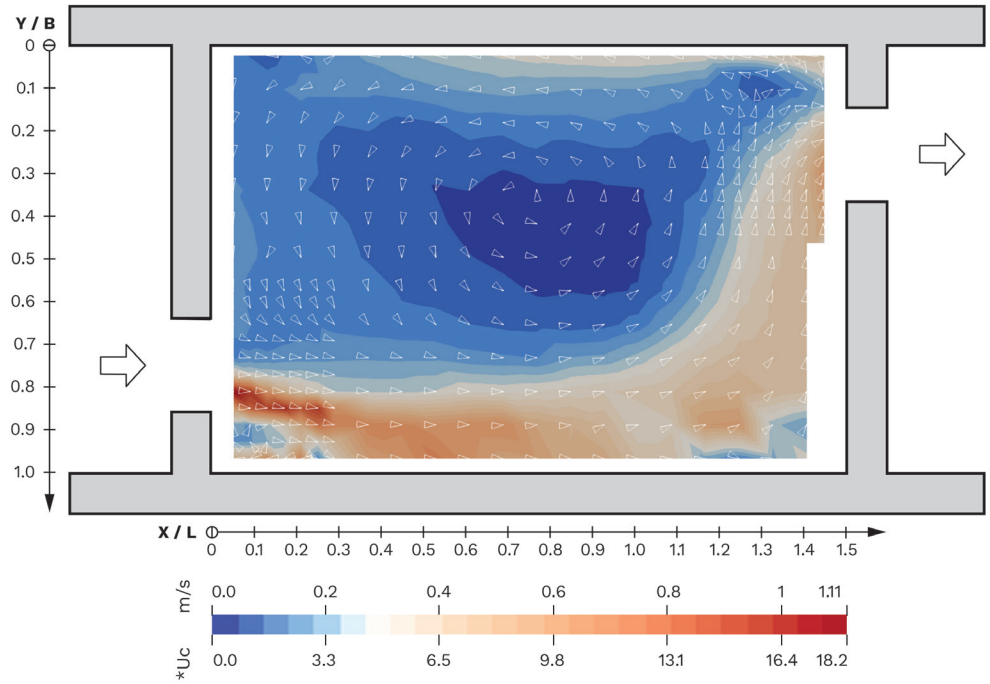

VELOCITY U_X

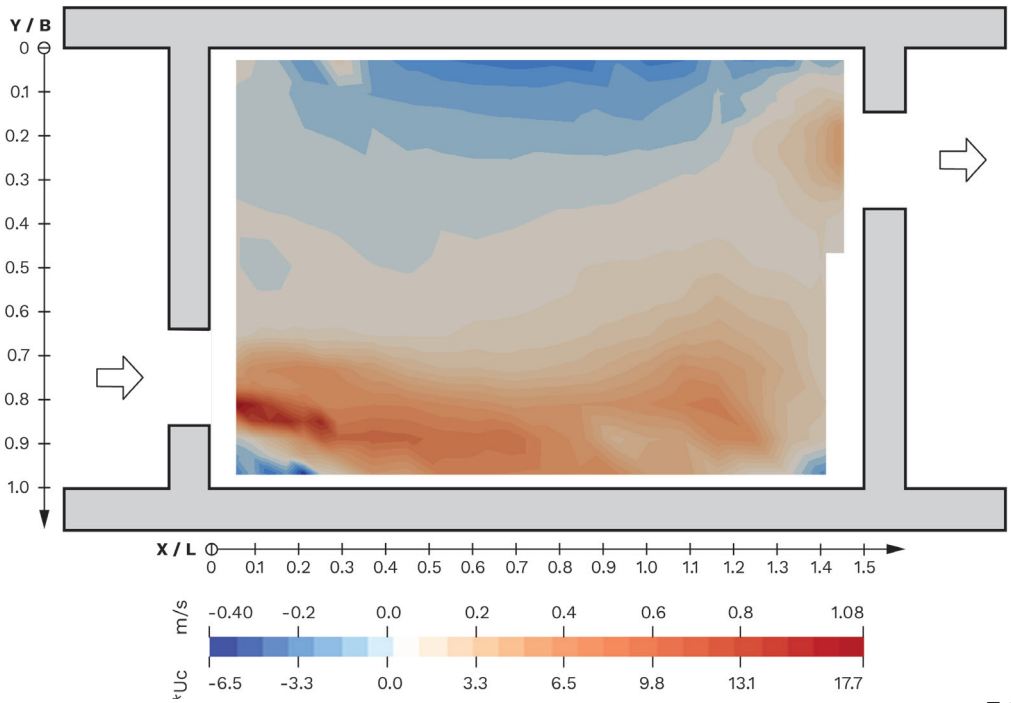

MEASUREMENTS LAYER 3

Laboratory flume: Version 1

Slot-width: 12.7 cm
Discharge: 33 l/s

VELOCITY V_Y

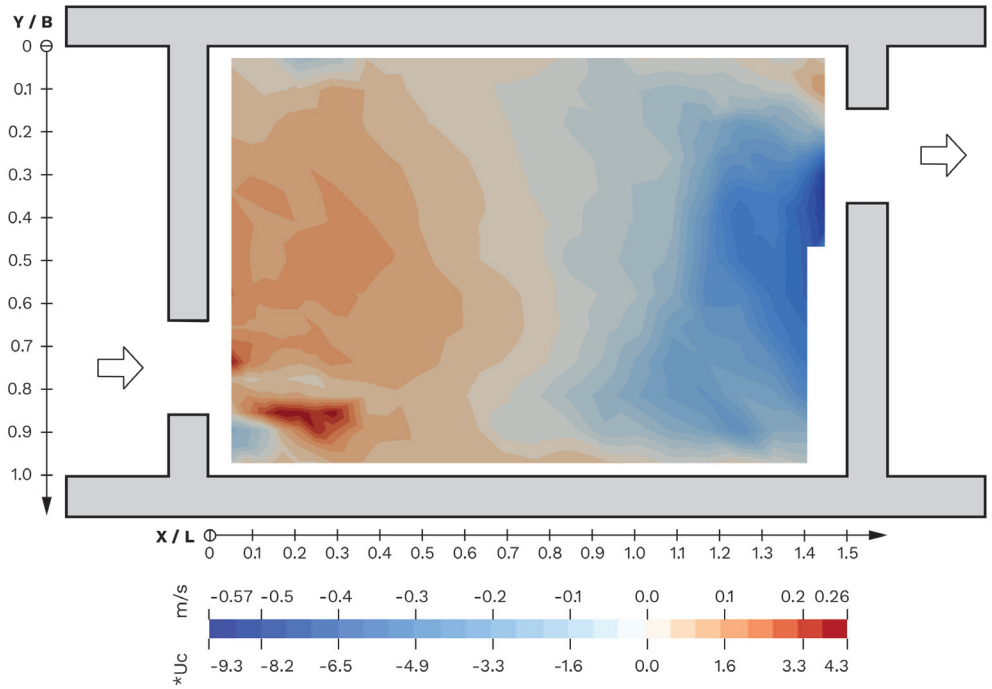

VELOCITY W_Z

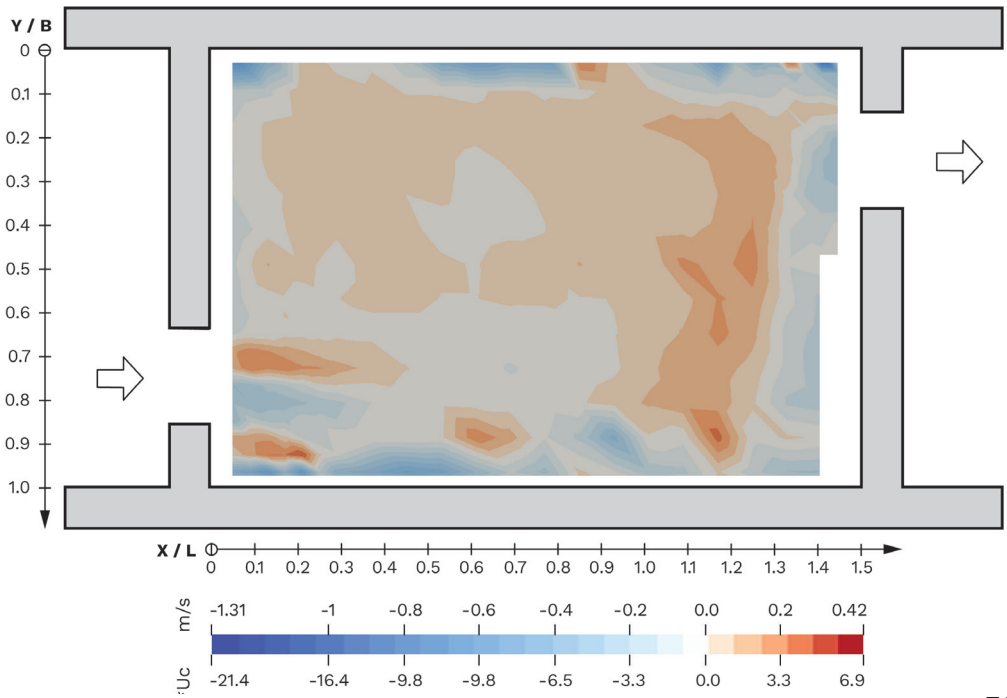

MEASUREMENTS VERTICAL

1 / 1

Laboratory flume: Version 1

Slot-width: 12.7 cm
Discharge: 33 l/s

VELOCITY MAGNITUDE

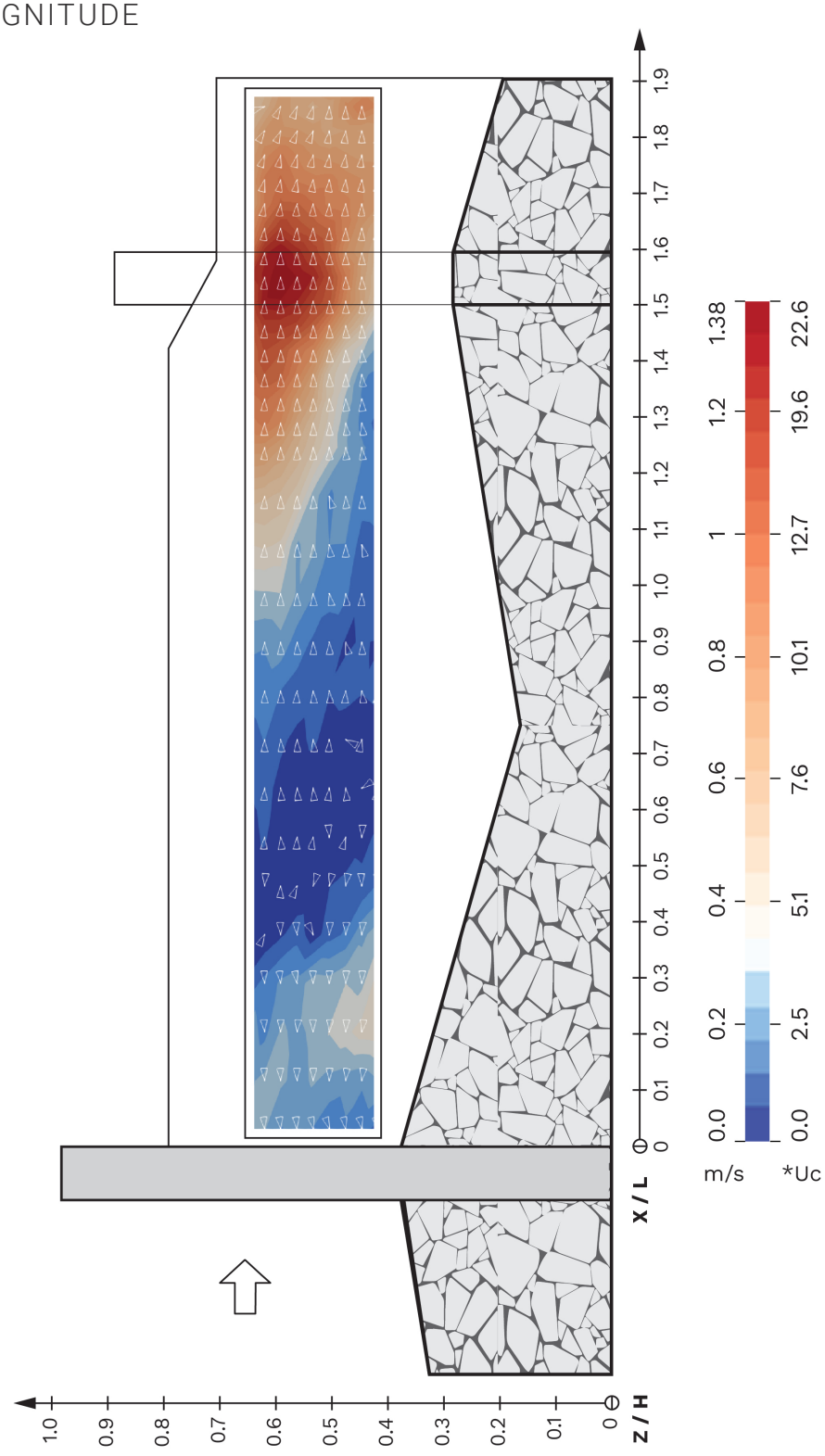

MEASUREMENTS VERTICAL

Laboratory flume: Version 2

Slot-width: 16.7 cm
Discharge: 42 l/s

VELOCITY MAGNITUDE

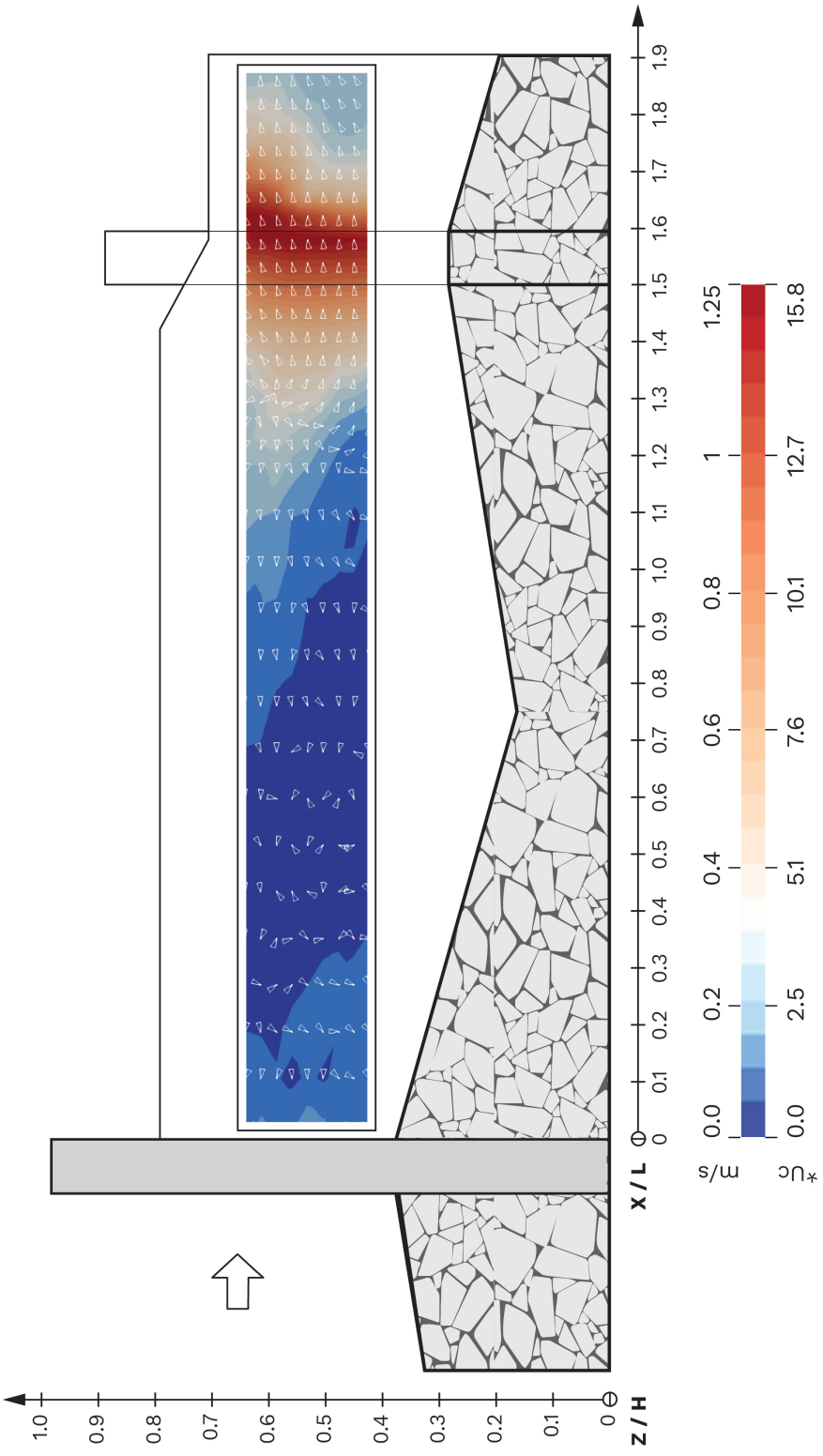

MEASUREMENTS LAYER 1

1 / 3

Laboratory flume: Version 2

Slot-width: 16.7 cm
Discharge: 42 l/s

VELOCITY MAGNITUDE

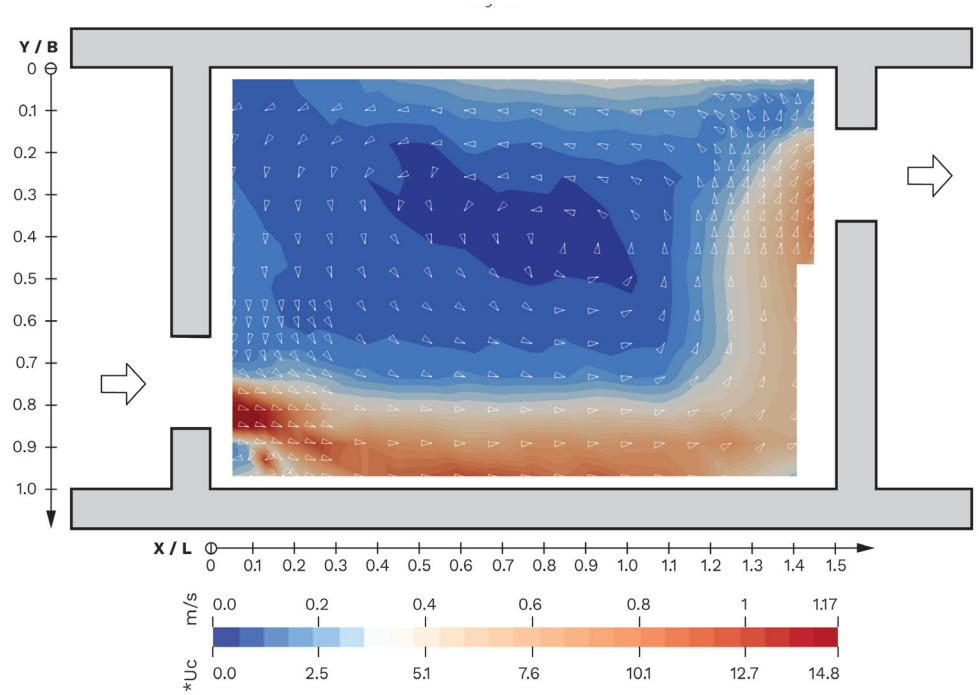

TURBULENT KINETIC ENERGY (TKE)

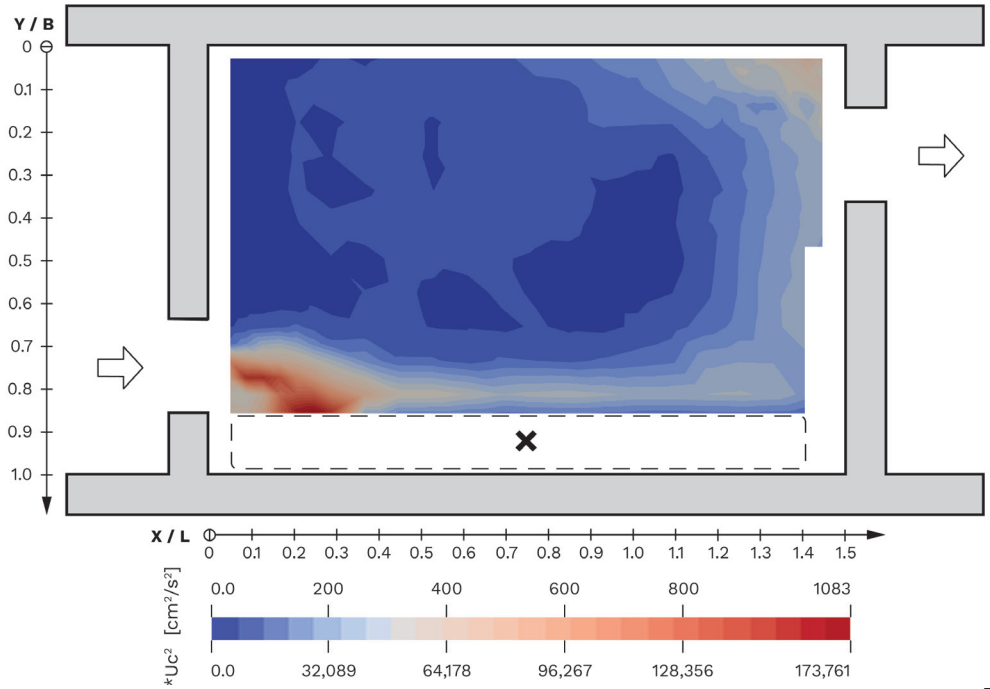

MEASUREMENTS LAYER 1

2 / 3

Laboratory flume: Version 2

Slot-width: 16.7 cm
Discharge: 42 l/s

VELOCITY U_X

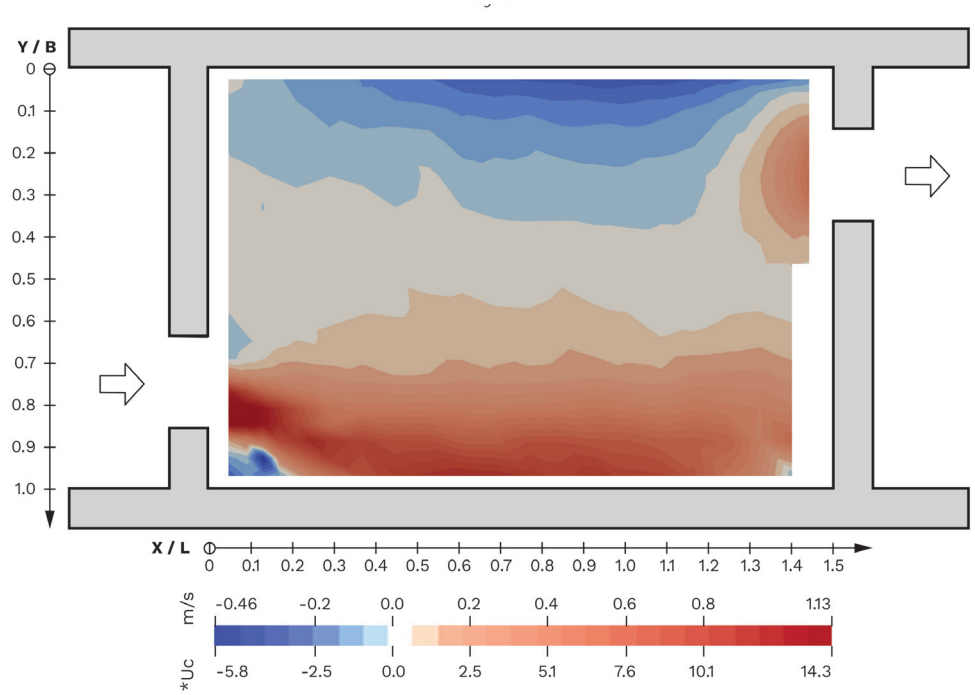

VELOCITY V_Y

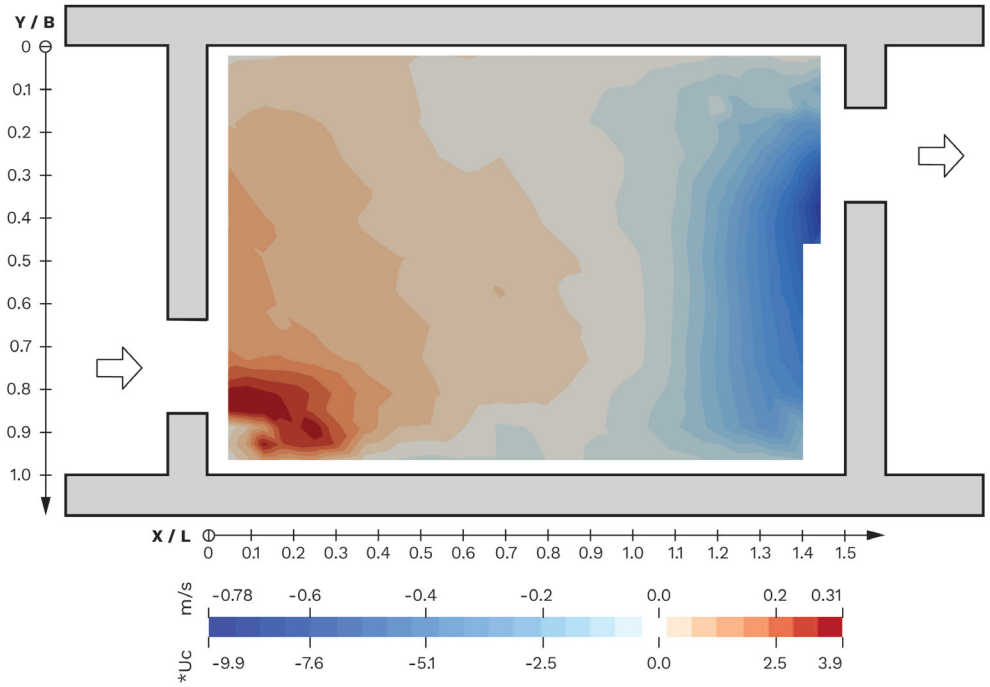

MEASUREMENTS LAYER 1

Laboratory flume: Version 2

Slot-width: 16.7 cm
Discharge: 42 l/s

VELOCITY W_Z

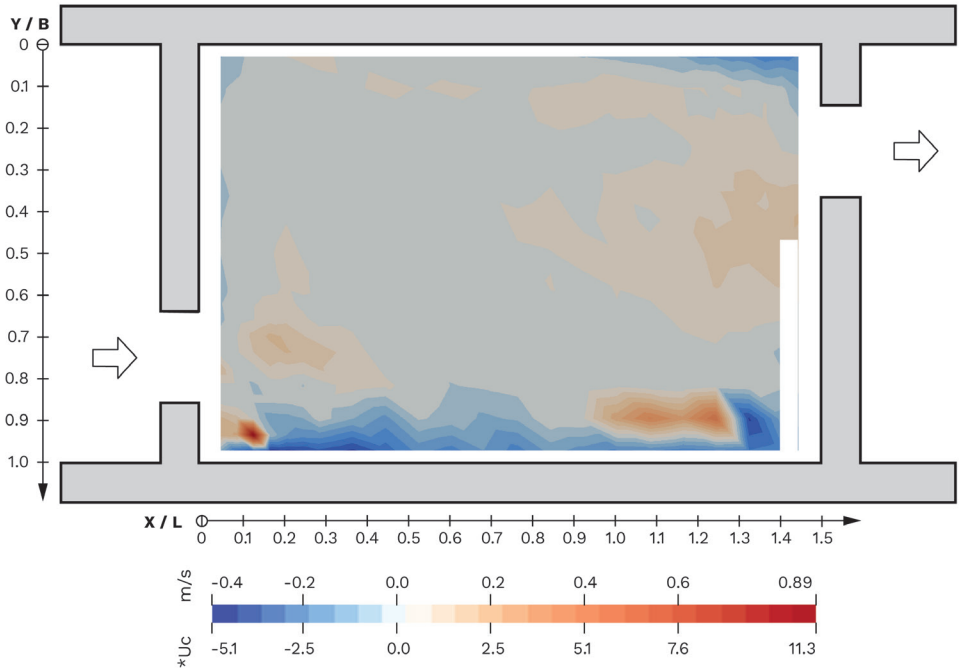

MEASUREMENTS LAYER 2

Laboratory flume: Version 2

Slot-width: 16.7 cm
Discharge: 42 l/s

VELOCITY MAGNITUDE

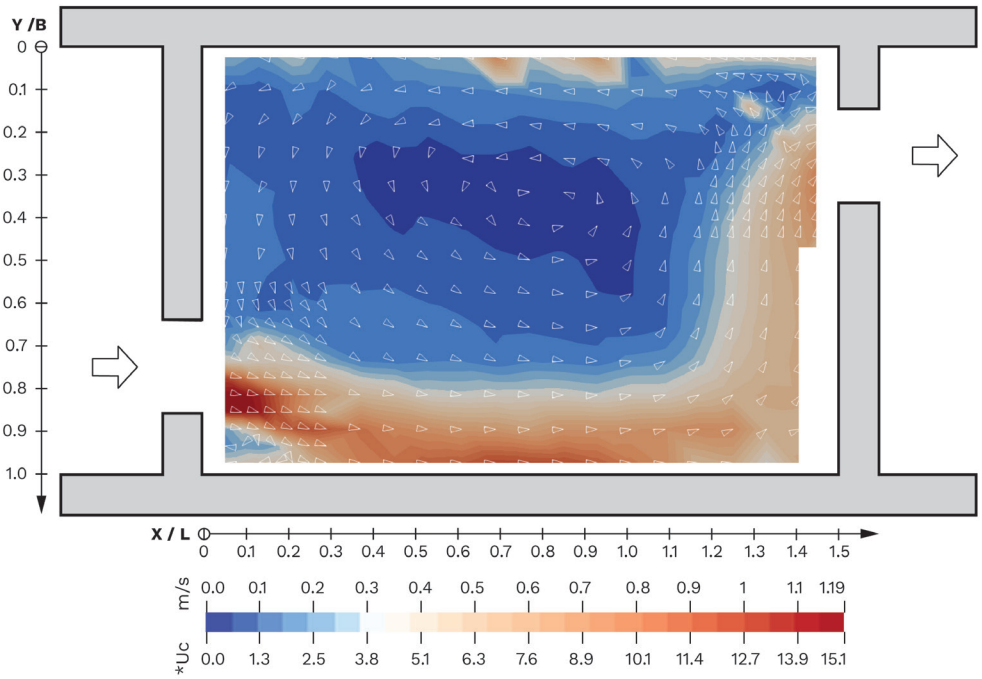

VELOCITY U_X

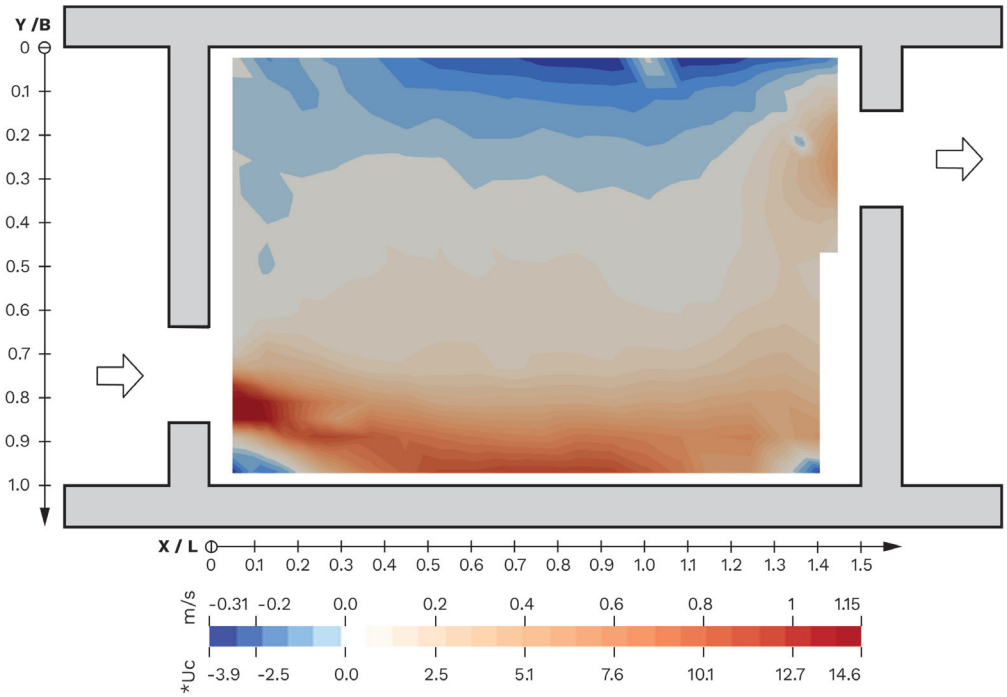

MEASUREMENTS LAYER 2

2 / 2

Laboratory flume: Version 2

Slot-width: 16.7 cm
Discharge: 42 l/s

VELOCITY V_Y

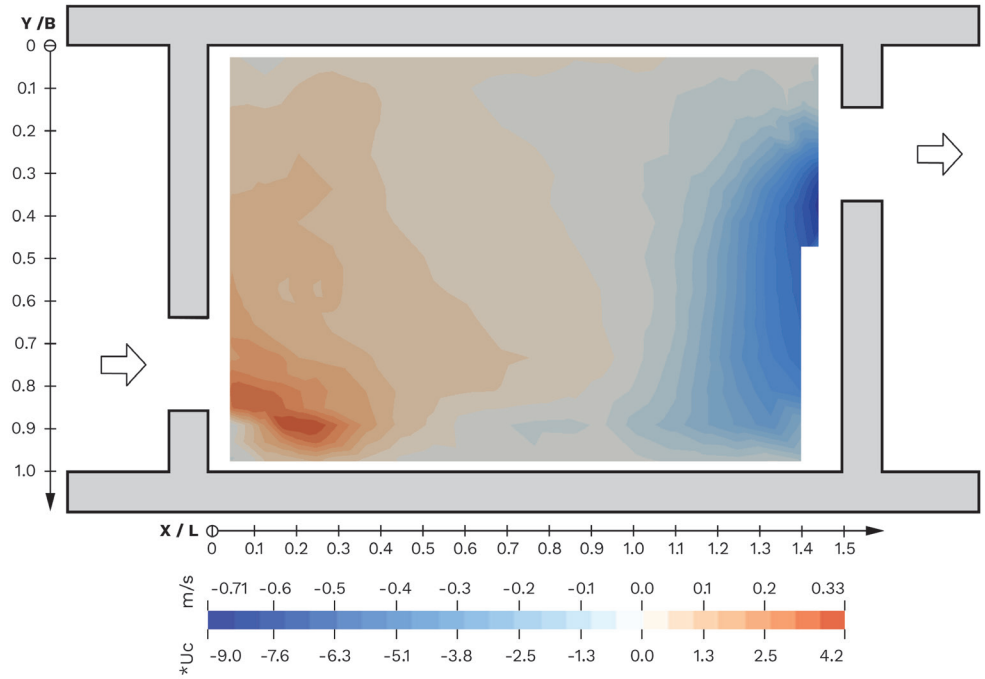

VELOCITY W_Z

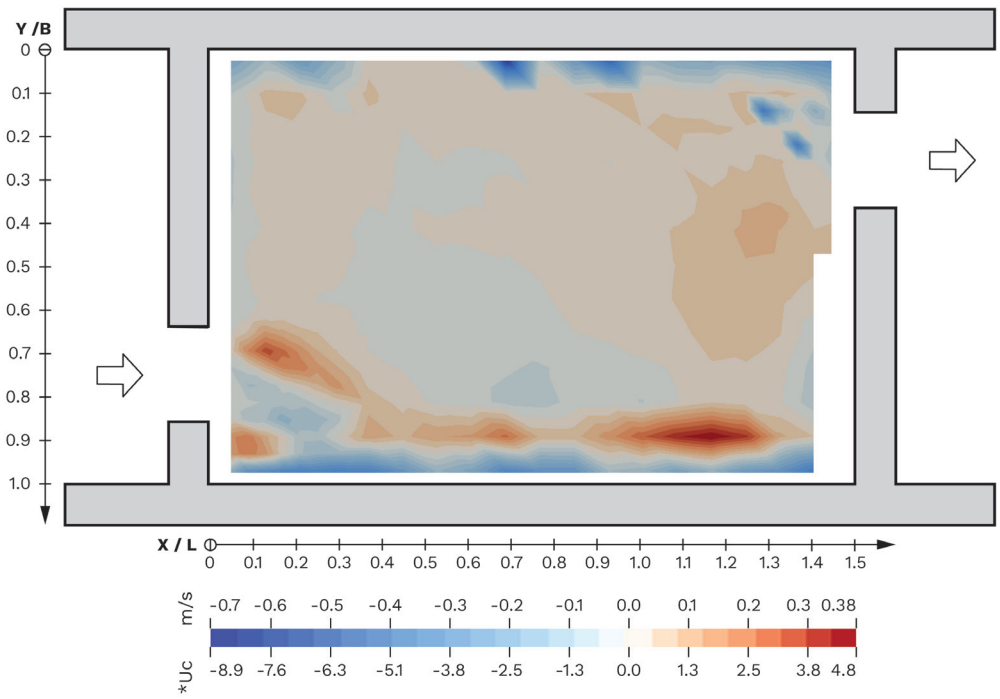

MEASUREMENTS LAYER 3

Laboratory flume: Version 2

Slot-width: 16.7 cm
Discharge: 42 l/s

VELOCITY MAGNITUDE

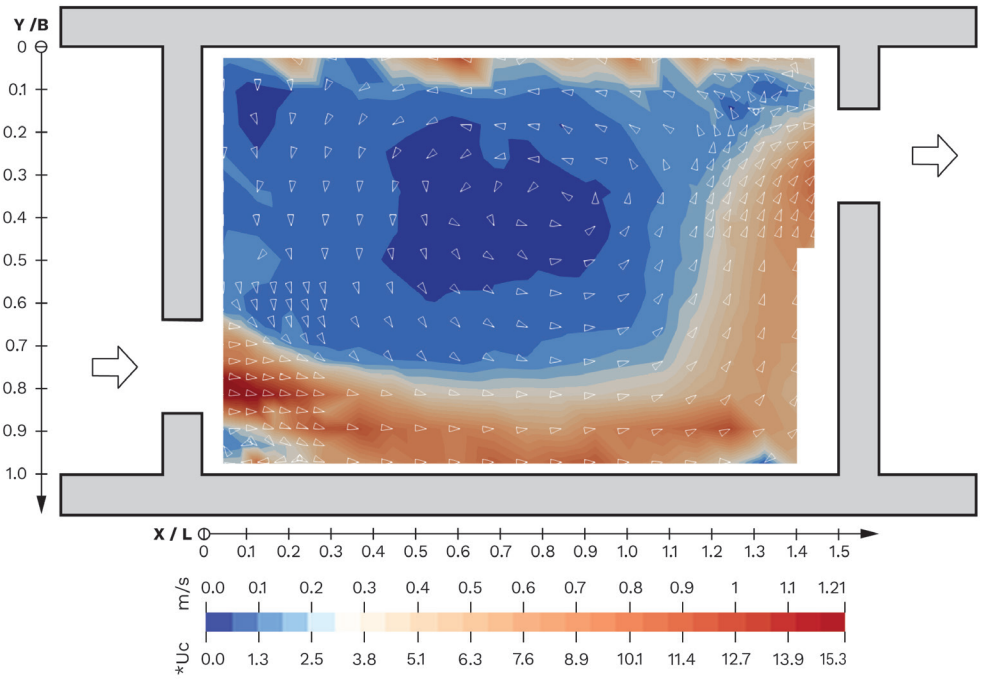

VELOCITY U_X

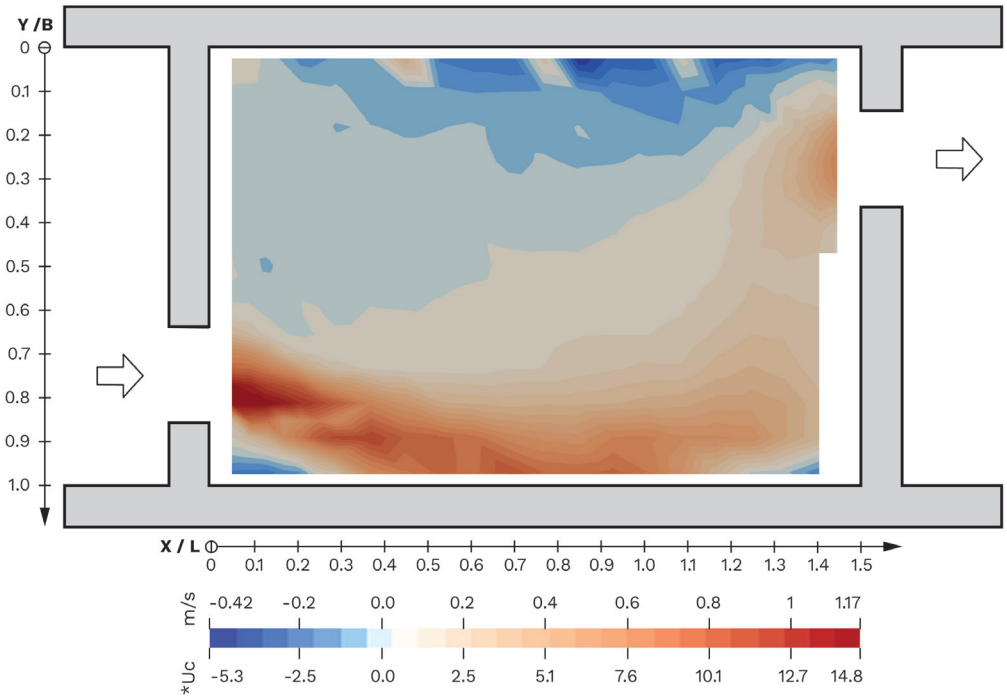

MEASUREMENTS LAYER 2

Laboratory flume: Version 2

Slot-width: 16.7 cm
Discharge: 42 l/s

VELOCITY V_Y

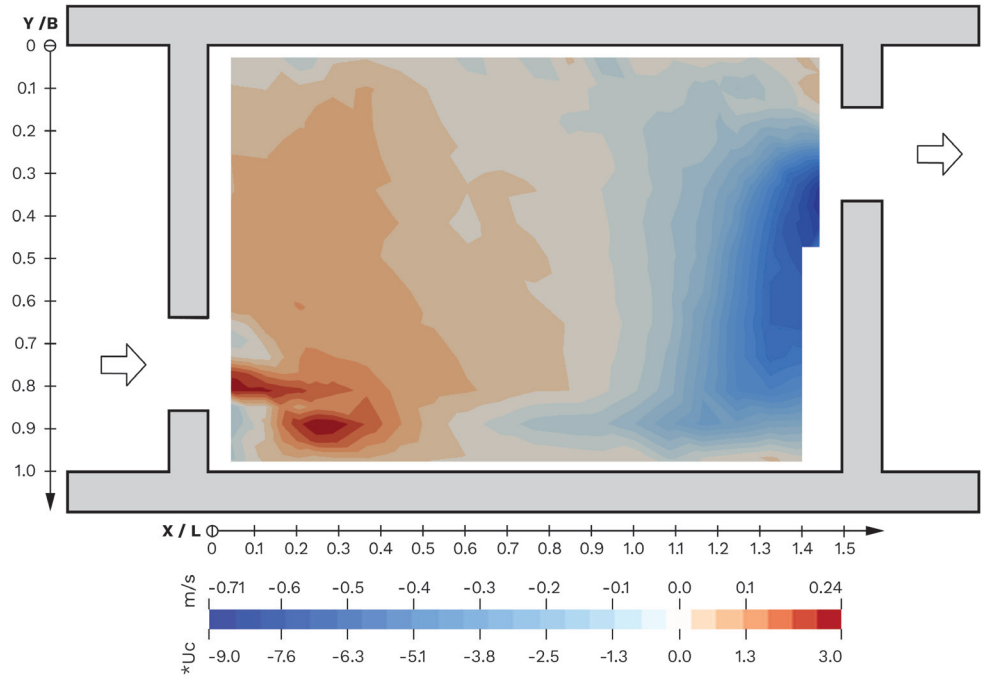

VELOCITY W_Z

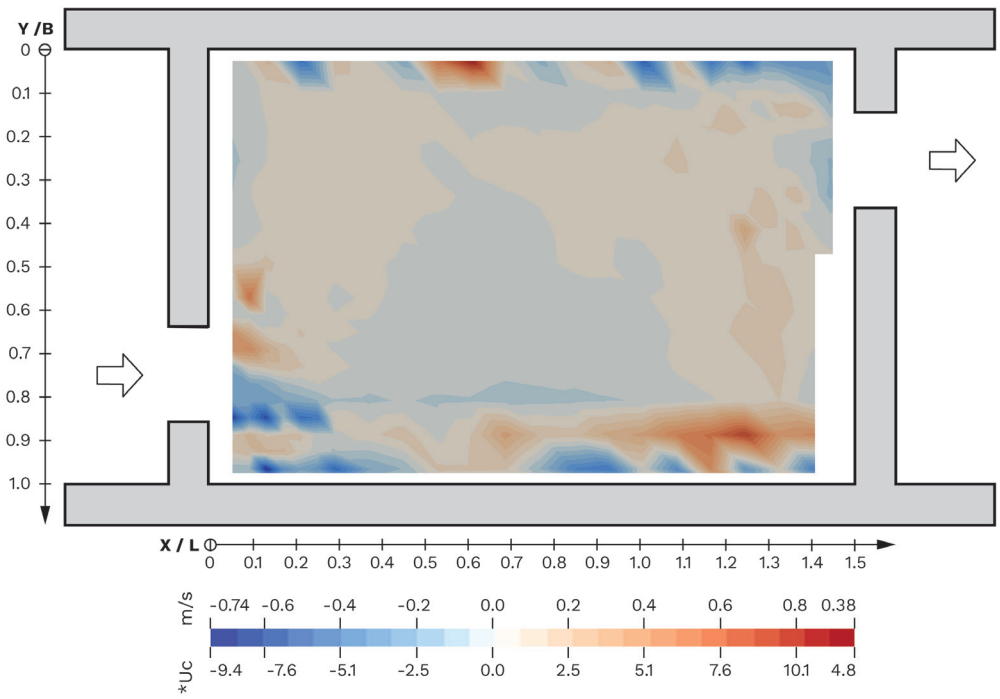

CFD LAYER 1

Laboratory flume: Version 1

Slot-width: 12.7 cm
Discharge: 33 l/s

VELOCITY MAGNITUDE

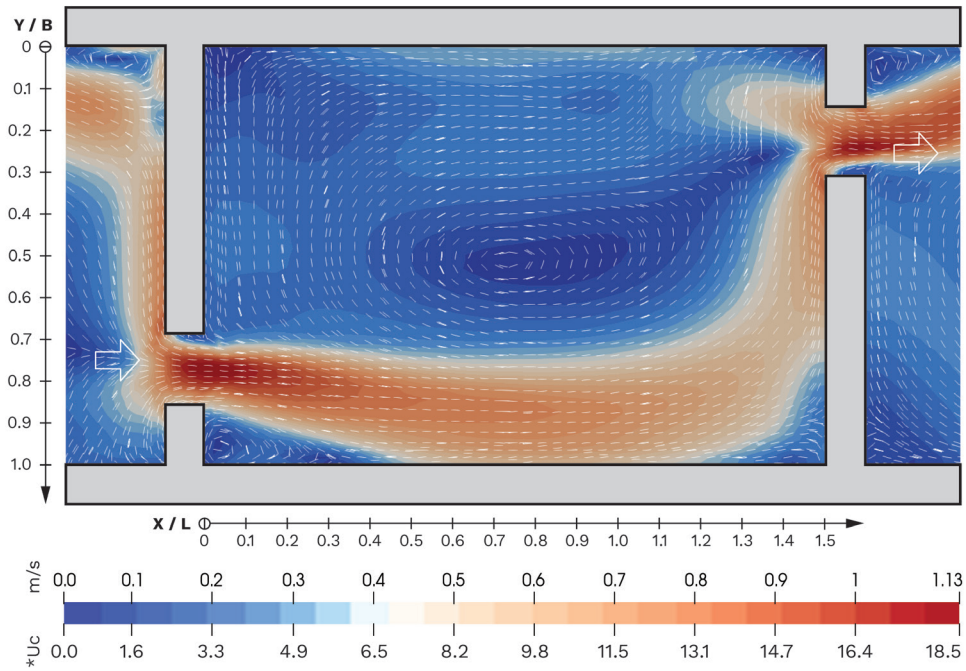

TURBULENT KINETIC ENERGY (TKE)

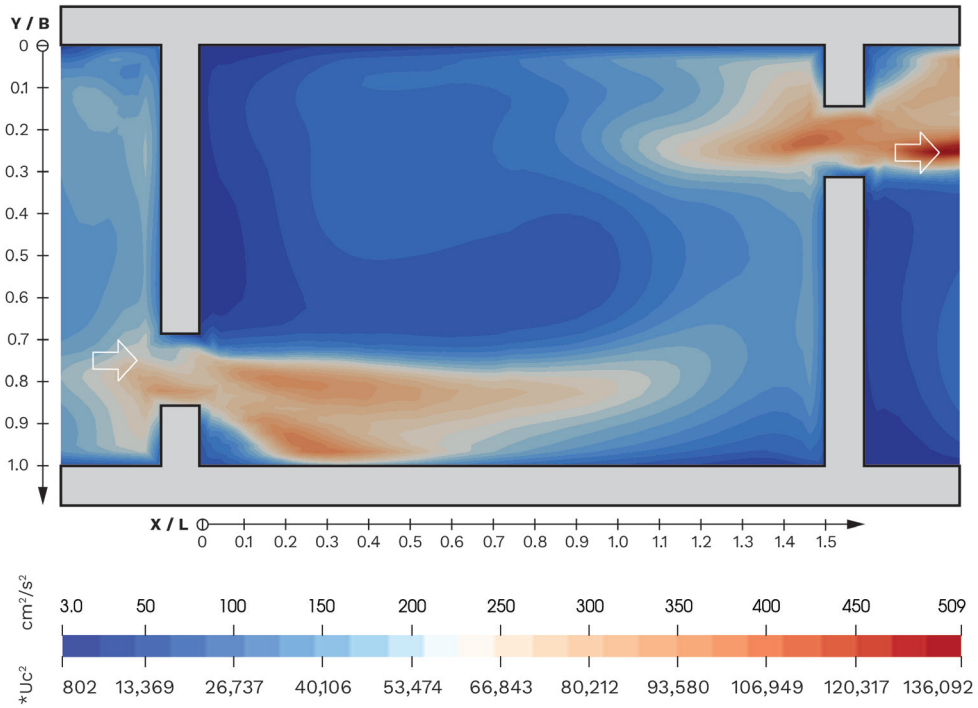

CFD LAYER 1

Laboratory flume: Version 1

Slot-width: 12.7 cm
Discharge: 33 l/s

VELOCITY U_X

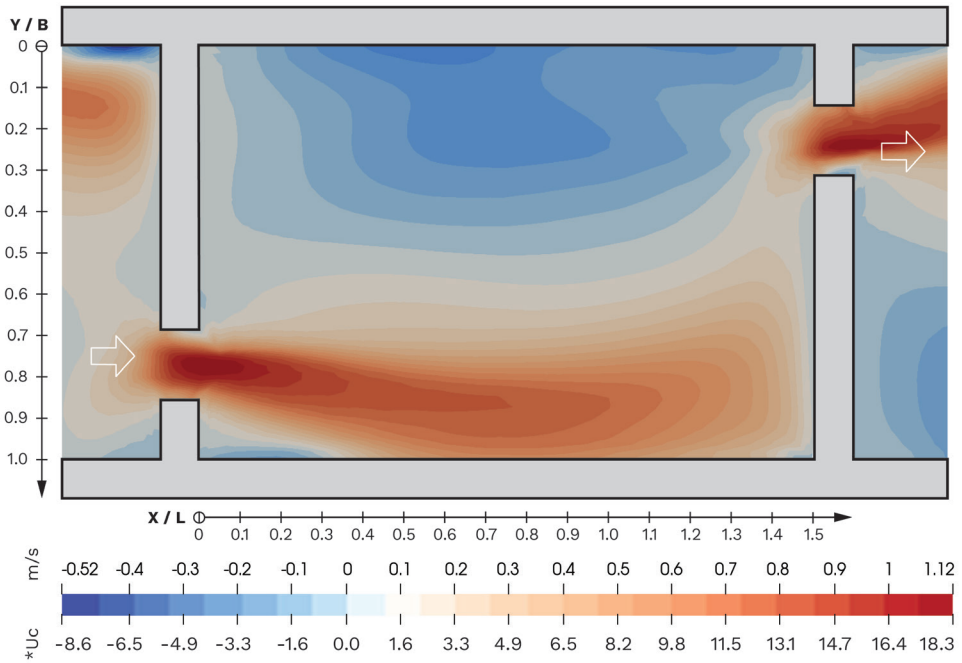

VELOCITY V_Y

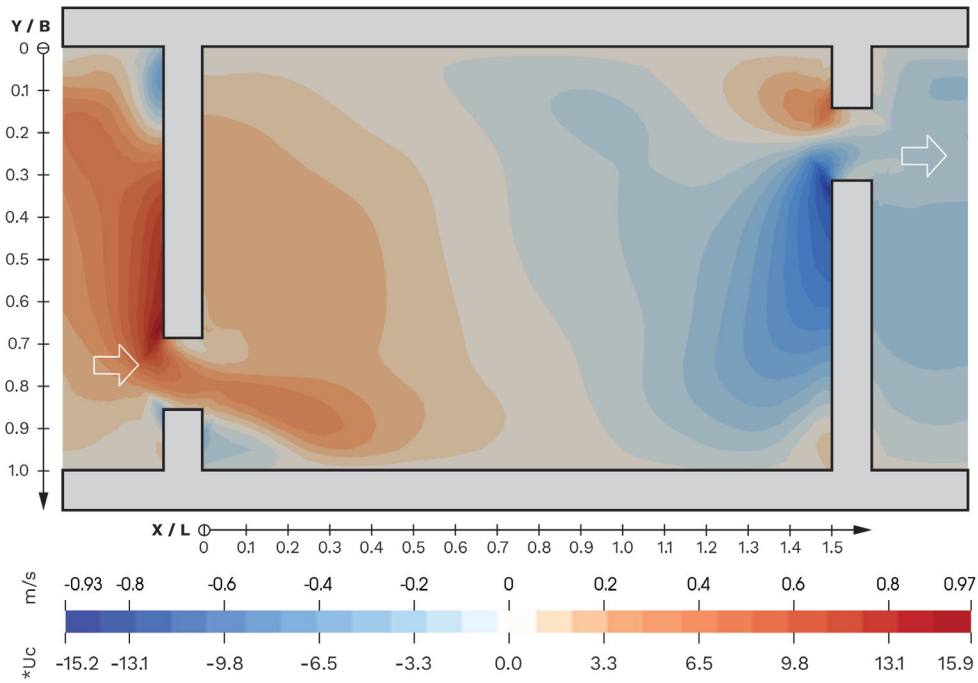

CFD LAYER 1

Laboratory flume: Version 1

Slot-width: 12.7 cm
Discharge: 33 l/s

VELOCITY W_Z

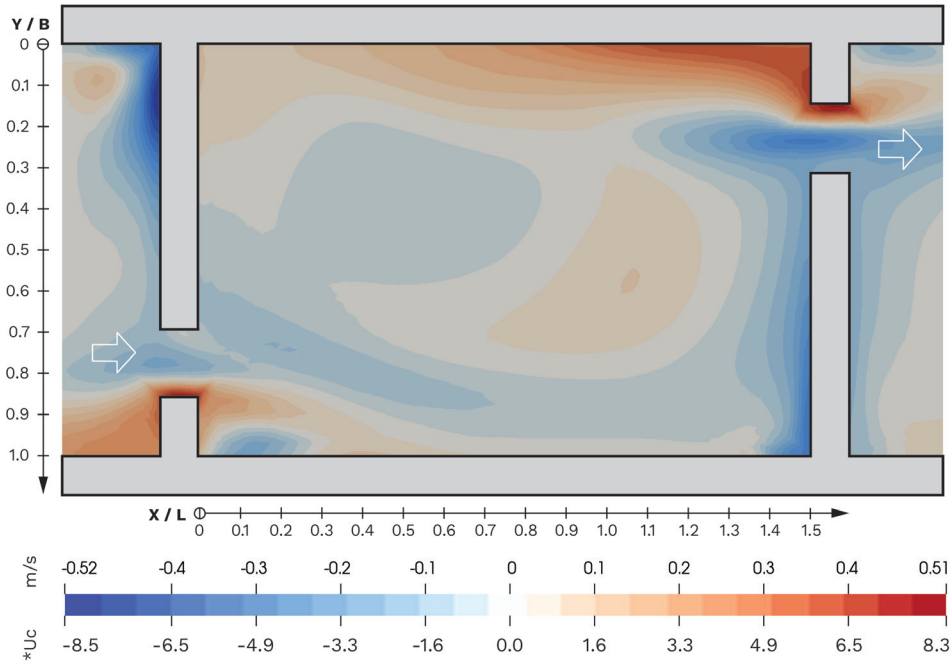

CFD LAYER 2

Laboratory flume: Version 1

Slot-width: 12.7 cm
Discharge: 33 l/s

VELOCITY MAGNITUDE

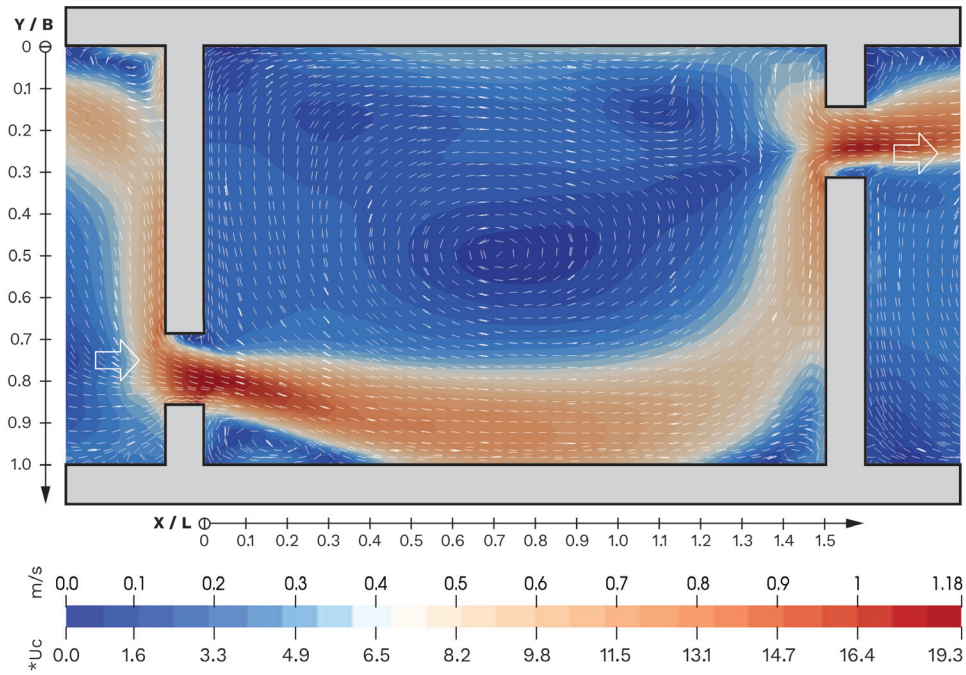

TURBULENT KINETIC ENERGY (TKE)

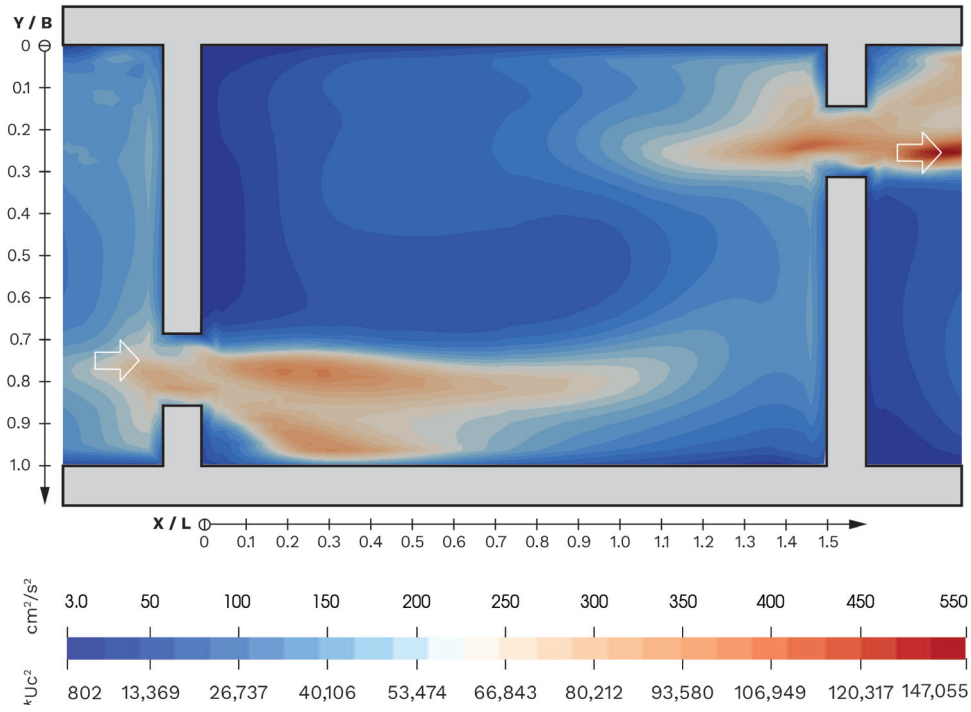

CFD LAYER 2

Laboratory flume: Version 1

Slot-width: 12.7 cm
Discharge: 33 l/s

VELOCITY U_X

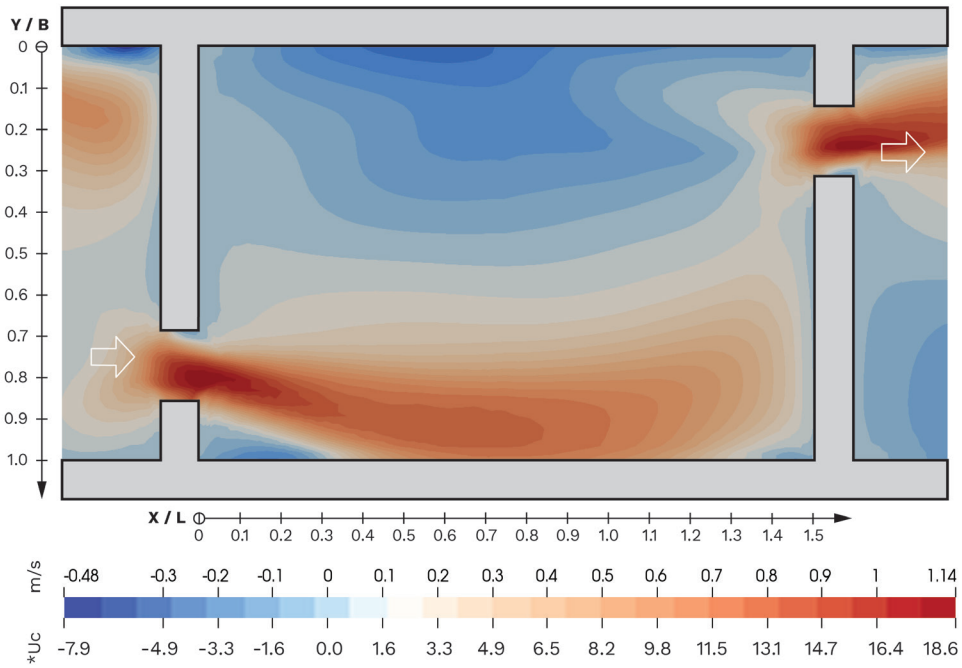

VELOCITY V_Y

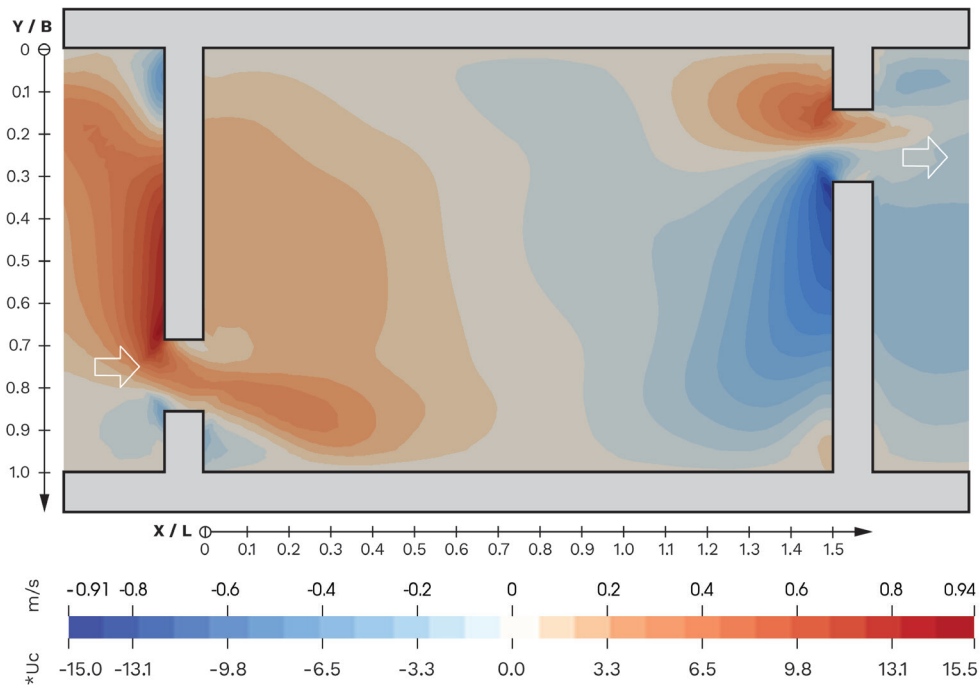

CFD LAYER 2

Laboratory flume: Version 1

Slot-width: 12.7 cm
Discharge: 33 l/s

VELOCITY W_Z

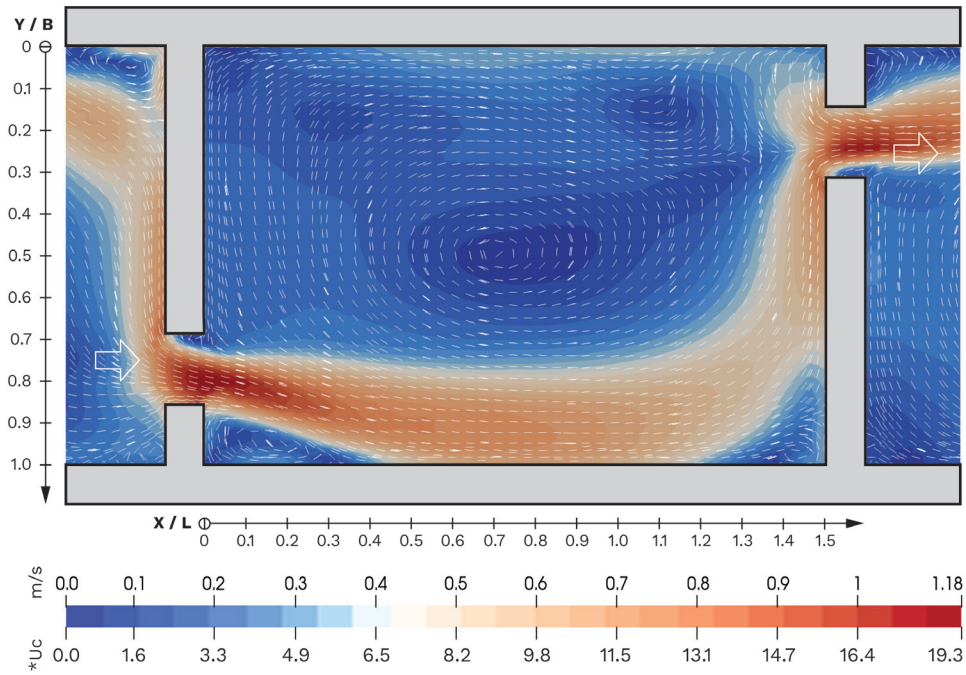

CFD LAYER 3

1 / 3

Laboratory flume: Version 1

Slot-width: 12.7 cm
Discharge: 33 l/s

VELOCITY MAGNITUDE

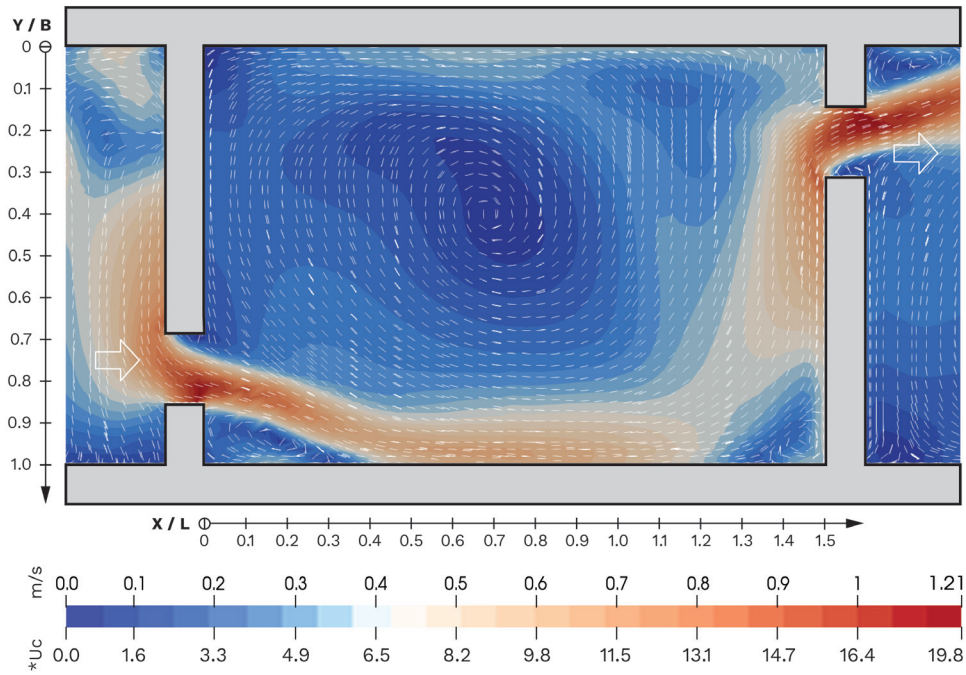

TURBULENT KINETIC ENERGY (TKE)

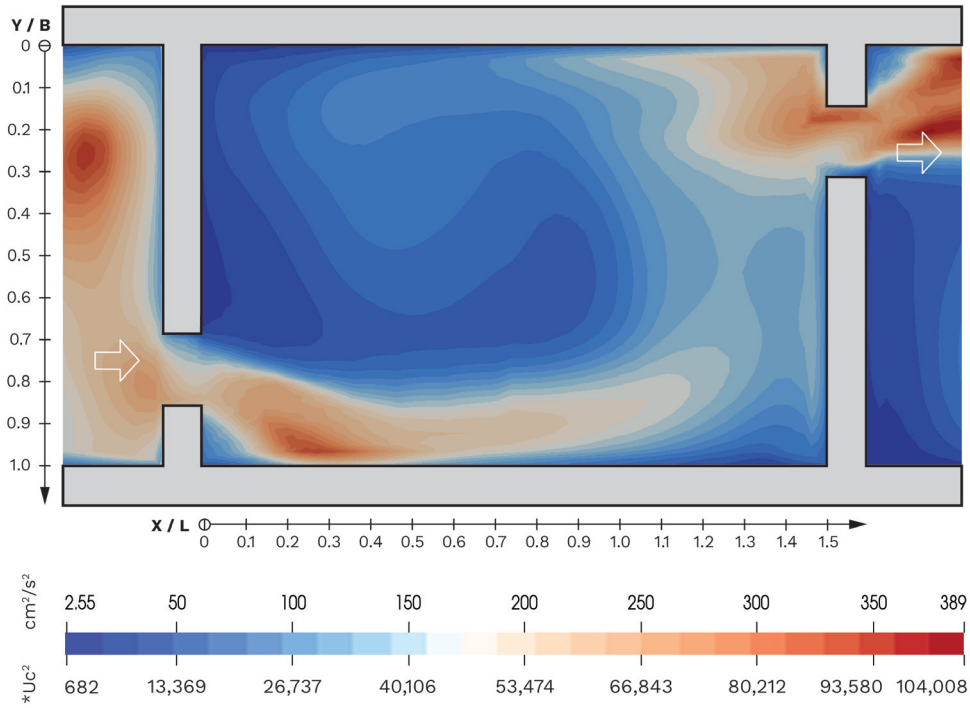

CFD LAYER 3

2 / 3

Laboratory flume: Version 1

Slot-width: 12.7 cm
Discharge: 33 l/s

VELOCITY U_X

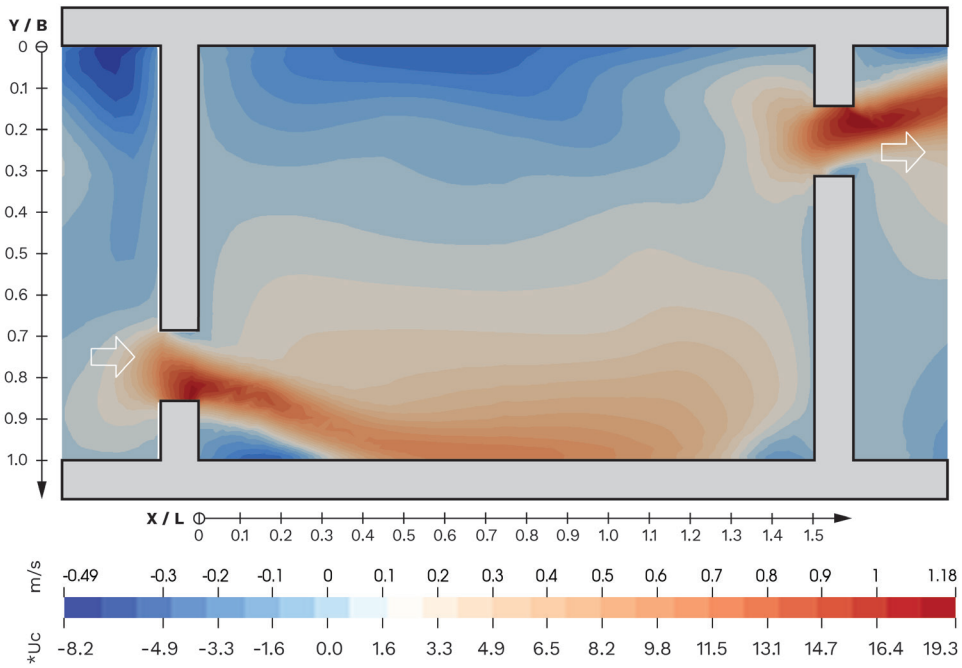

VELOCITY V_Y

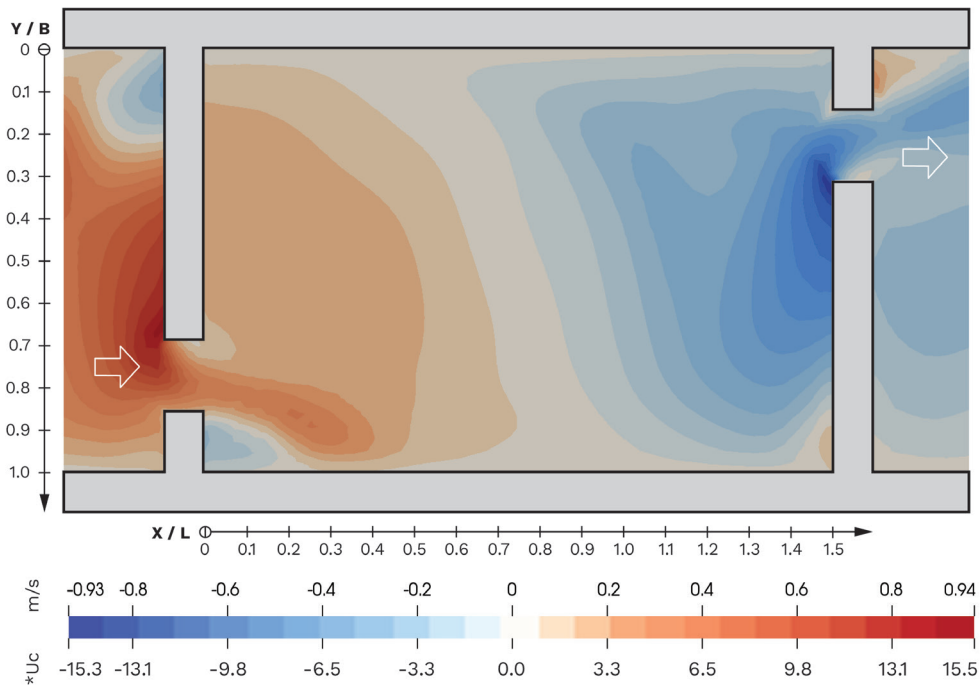

CFD LAYER 3

3 / 3

Laboratory flume: Version 1

Slot-width: 12.7 cm
Discharge: 33 l/s

VELOCITY W_Z

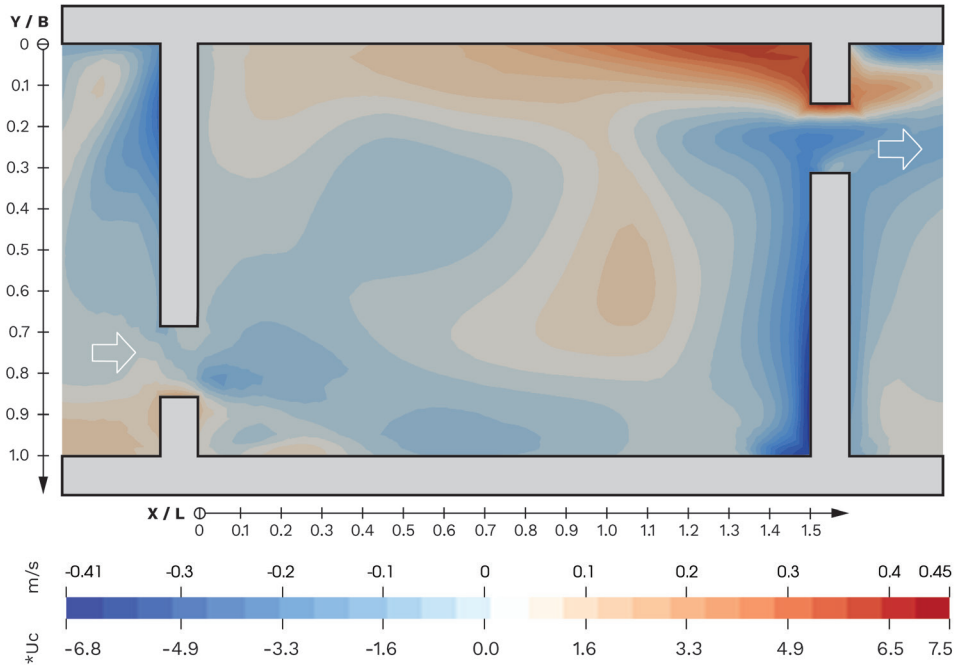

CFD VERTICAL

Laboratory flume: Version 1

Slot-width: 12.7 cm
Discharge: 33 l/s

VELOCITY MAGNITUDE

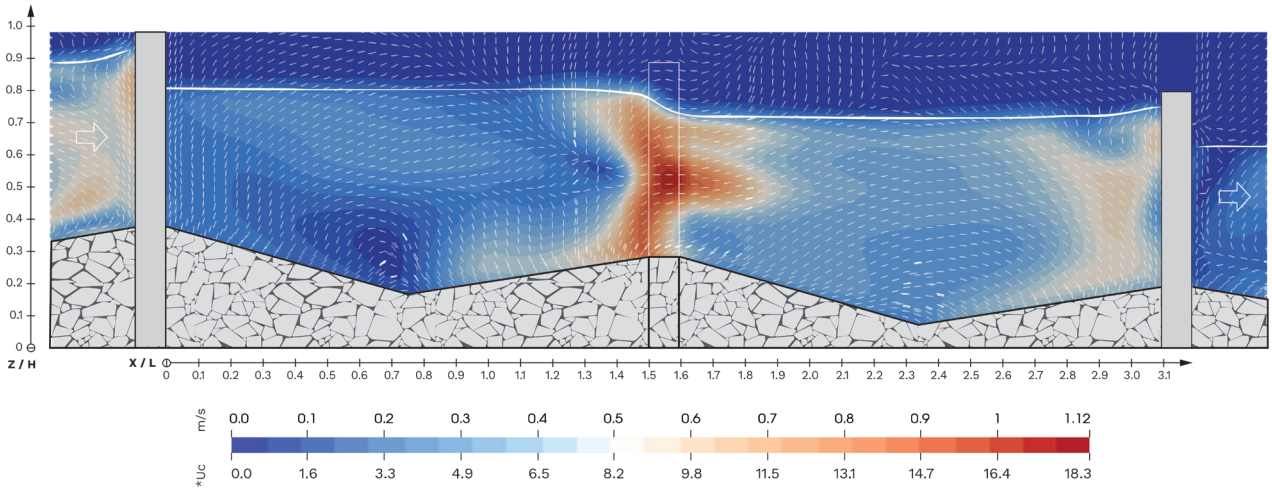

TURBULENT KINETIC ENERGY (TKE)

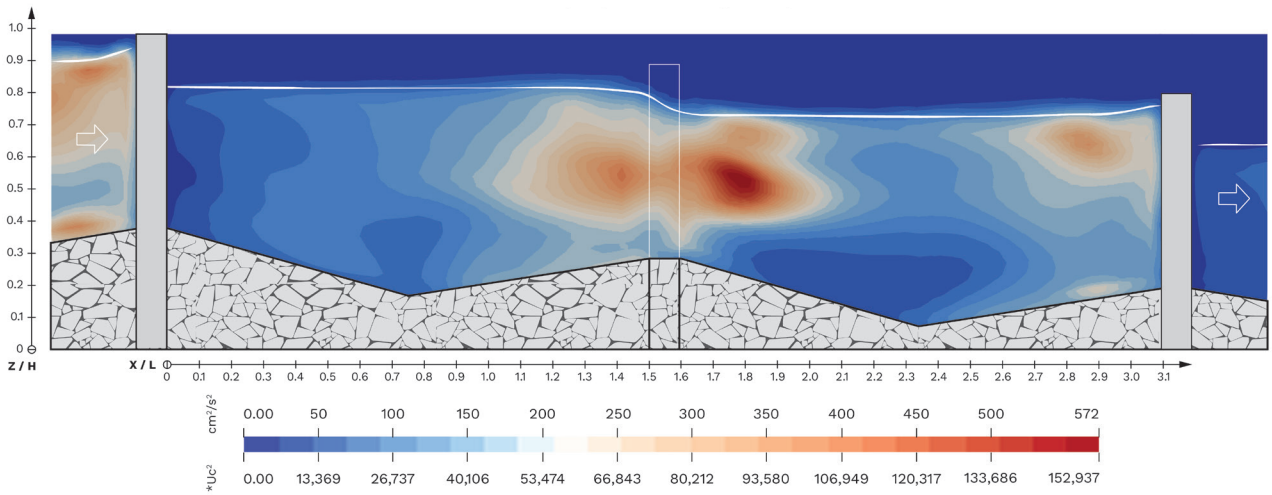

CFD VERTICAL

Laboratory flume: Version 1

VELOCITY U_X

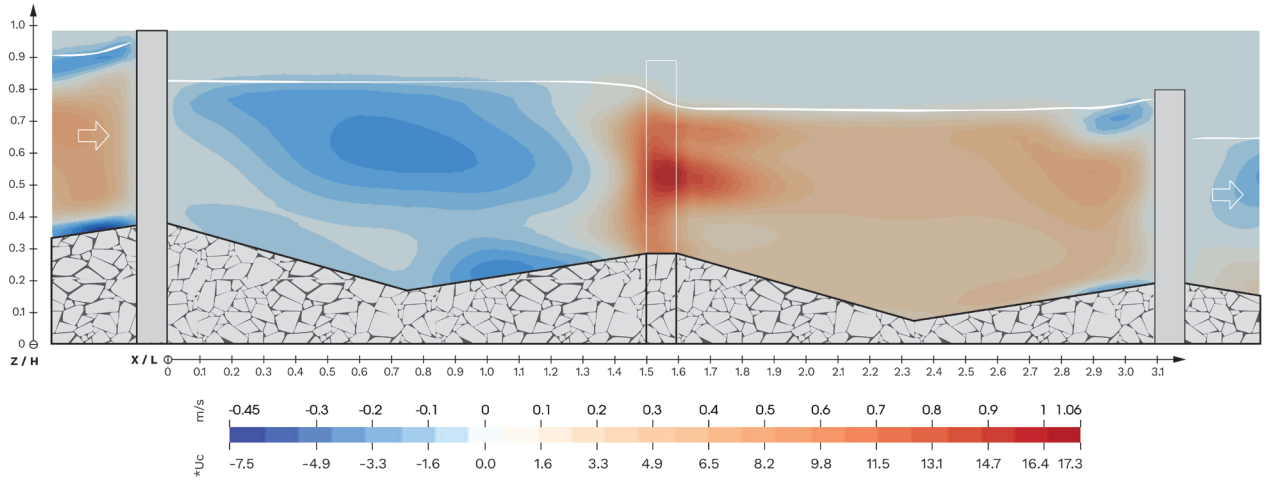

VELOCITY Y_V

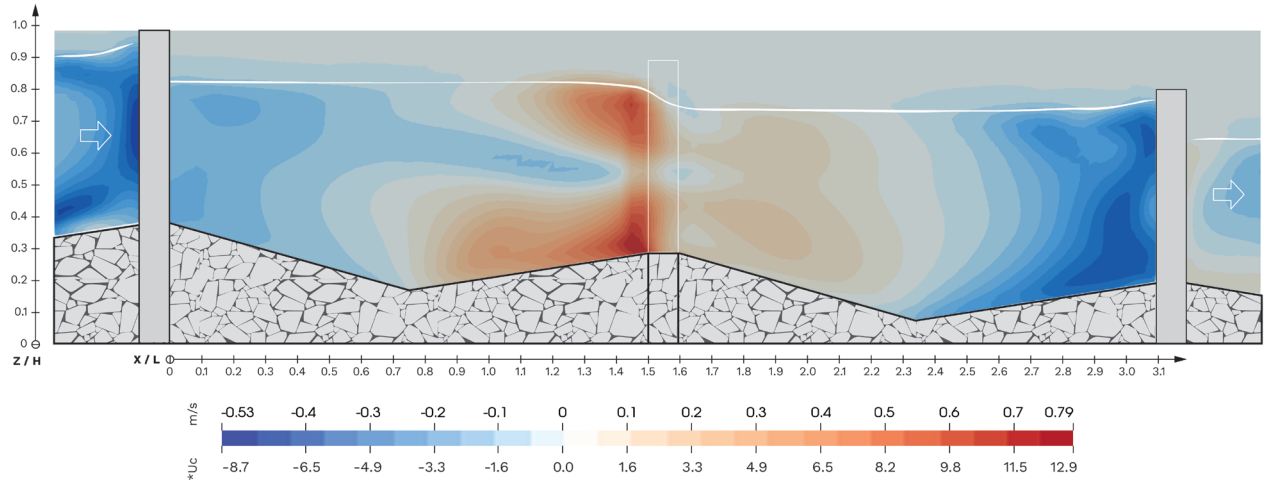

VELOCITY W_Z

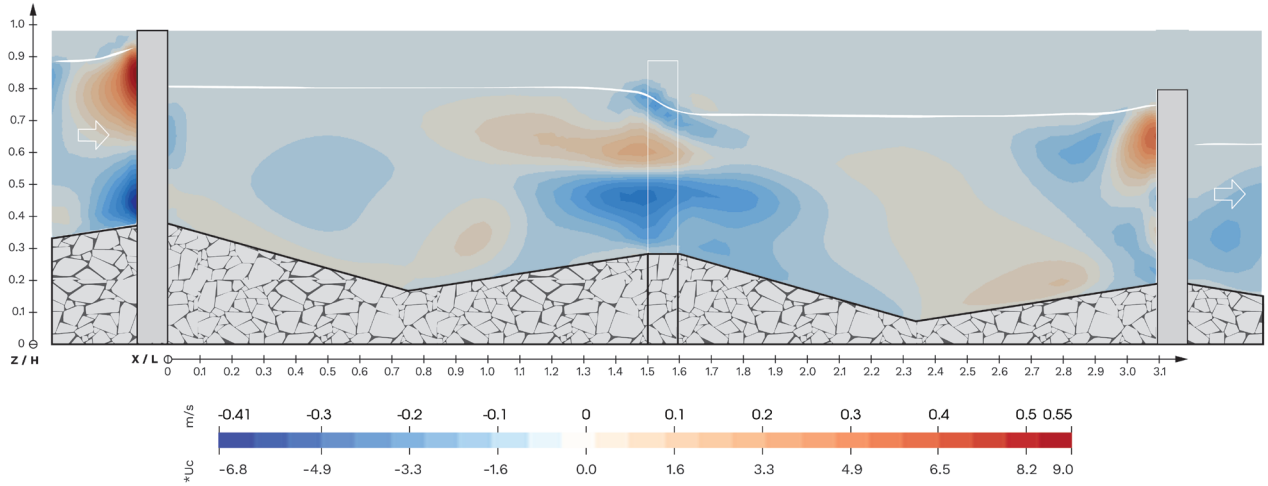

CFD LAYER 1

Laboratory flume: Version 2

Slot-width: 16.7 cm
Discharge: 42 l/s

VELOCITY MAGNITUDE

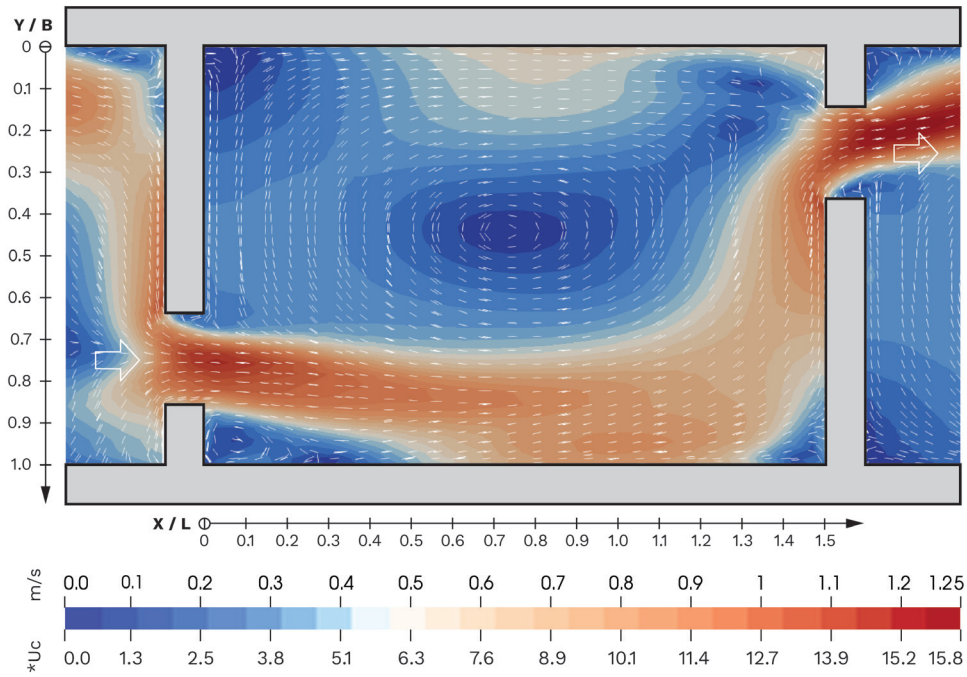

TURBULENT KINETIC ENERGY (TKE)

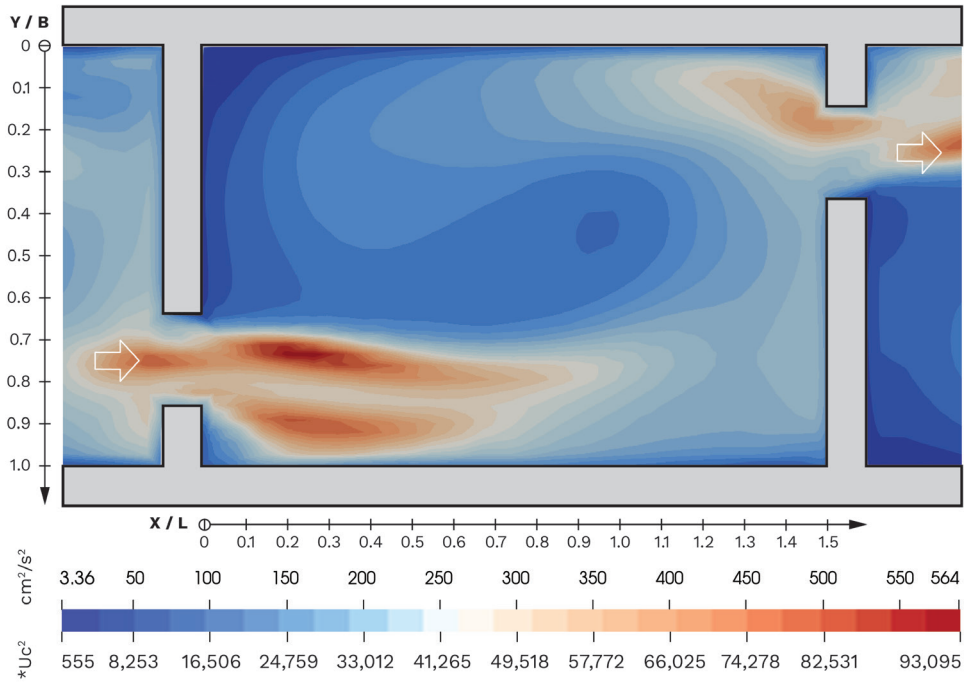

CFD LAYER 1

Laboratory flume: Version 2

Slot-width: 16.7 cm
Discharge: 42 l/s

VELOCITY U_X

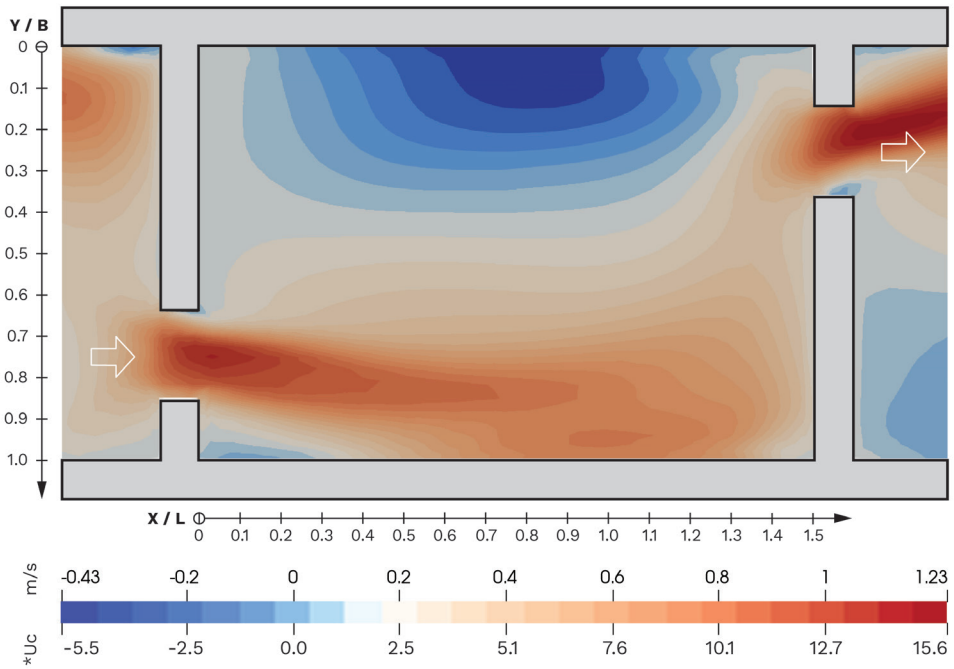

VELOCITY V_Y

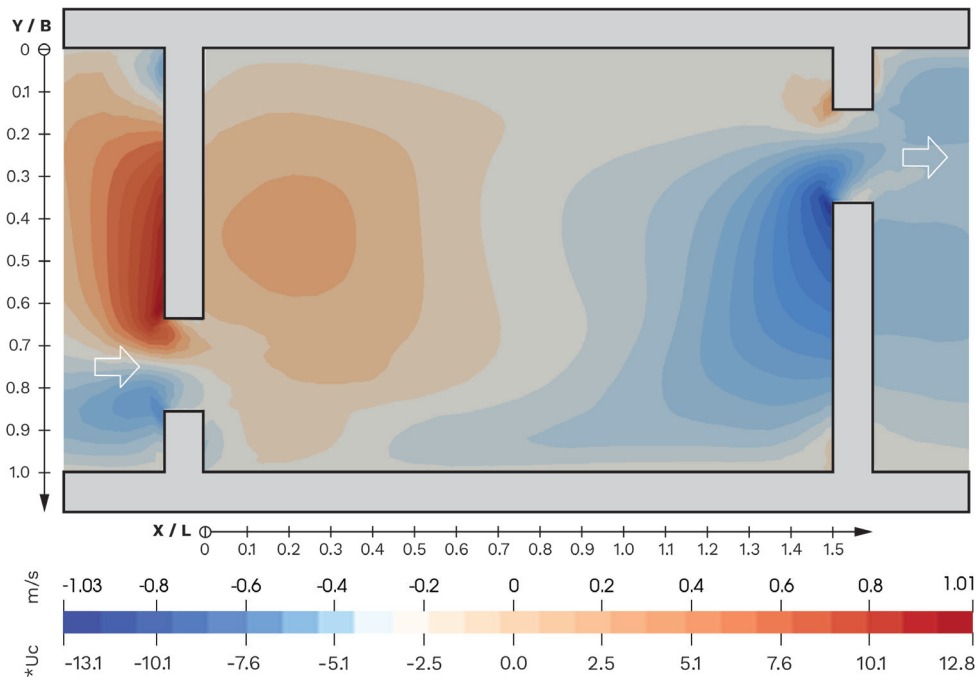

CFD LAYER 1

Laboratory flume: Version 2

Slot-width: 16.7 cm
Discharge: 42 l/s

VELOCITY W_Z

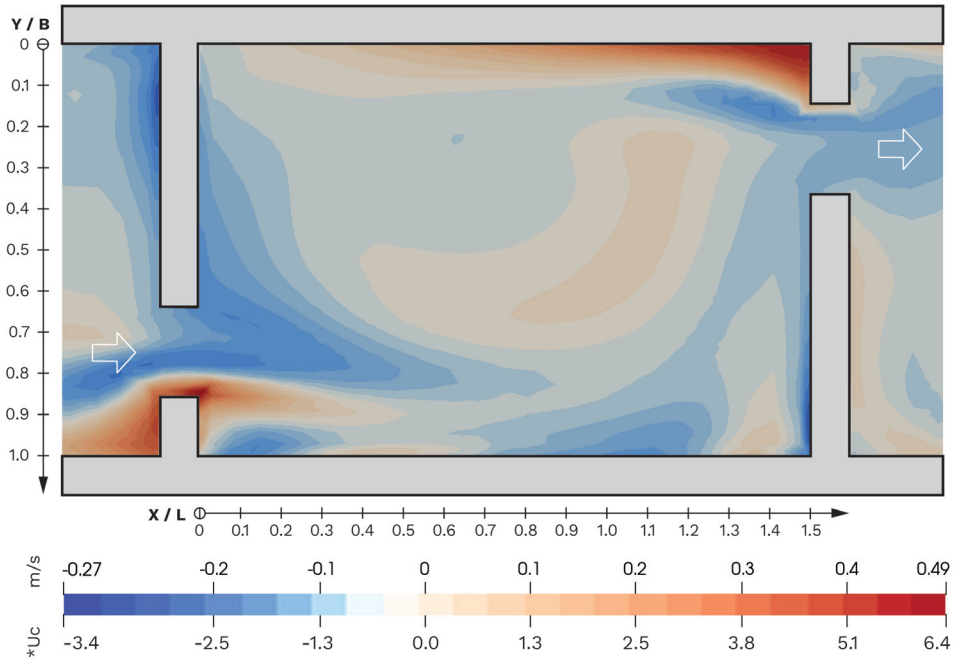

CFD LAYER 2

Laboratory flume: Version 2

Slot-width: 16.7 cm
Discharge: 42 l/s

VELOCITY MAGNITUDE

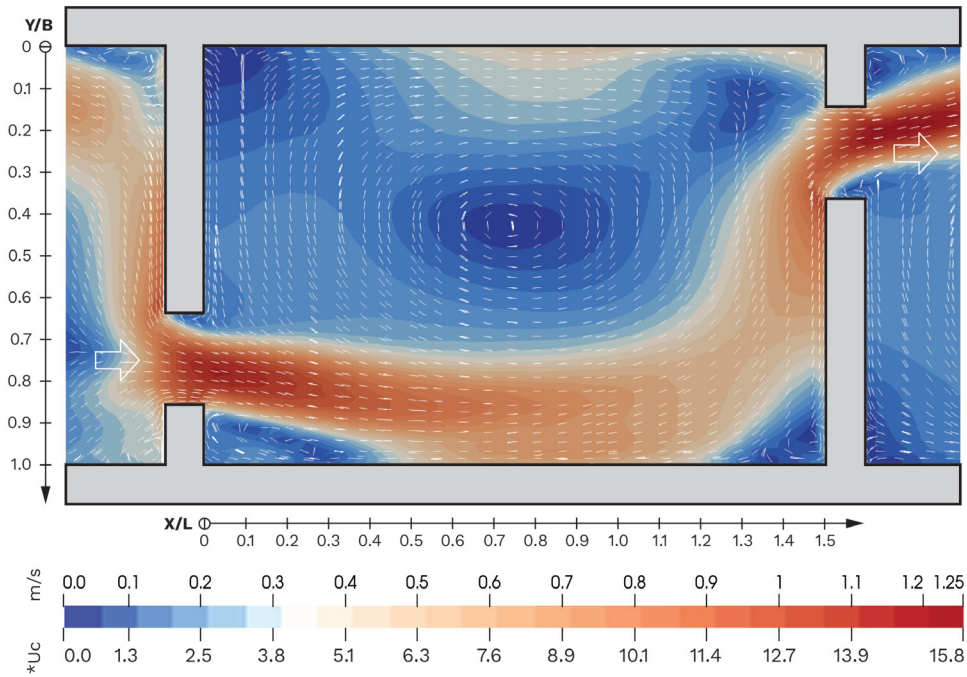

TURBULENT KINETIC ENERGY (TKE)

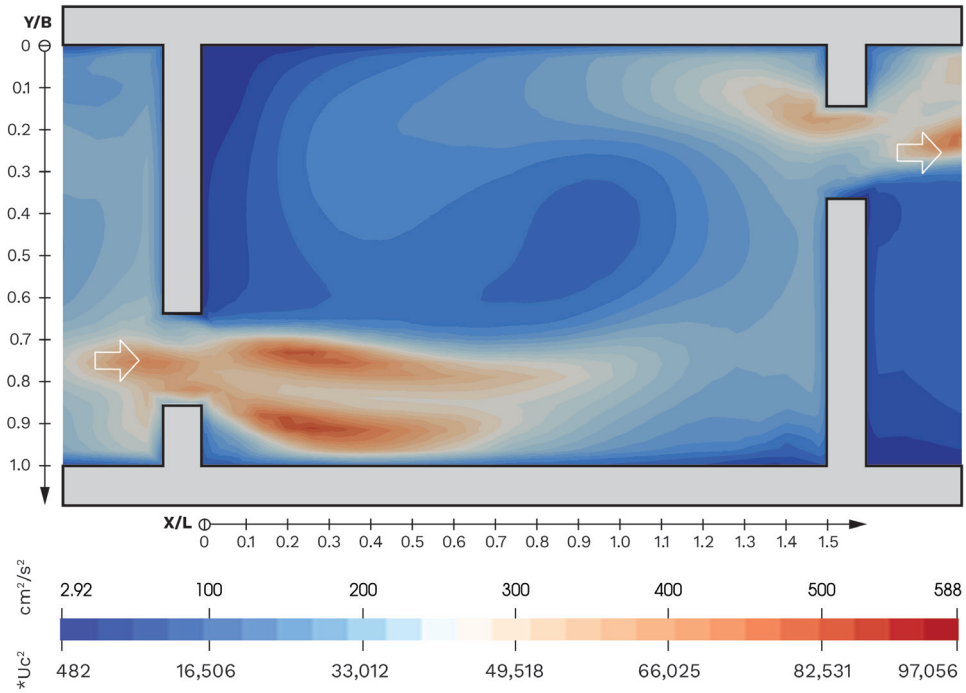

CFD LAYER 2

Laboratory flume: Version 2

Slot-width: 16.7 cm
Discharge: 42 l/s

VELOCITY U_X

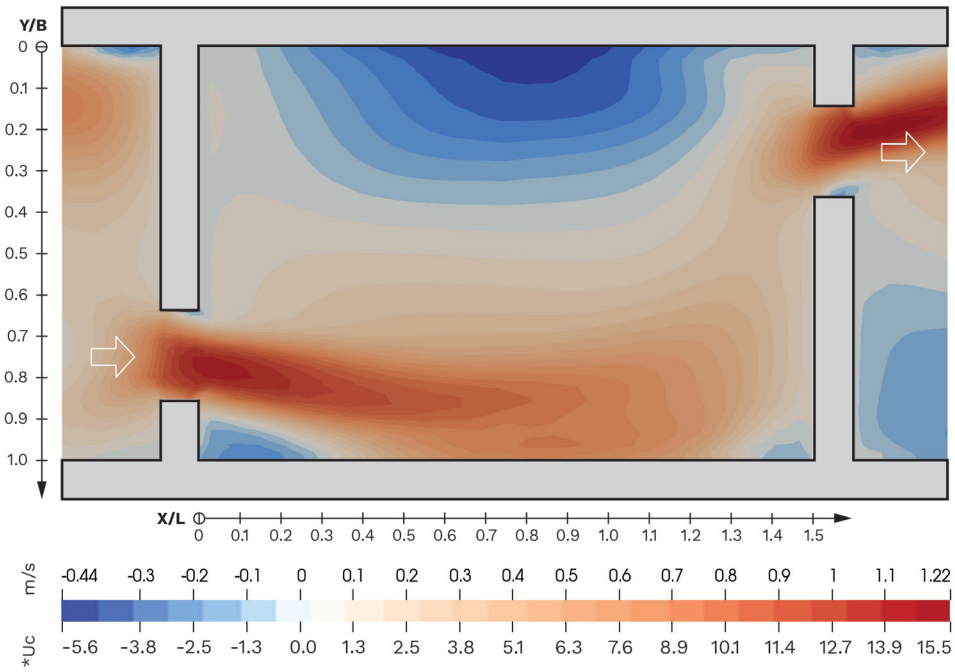

VELOCITY V_Y

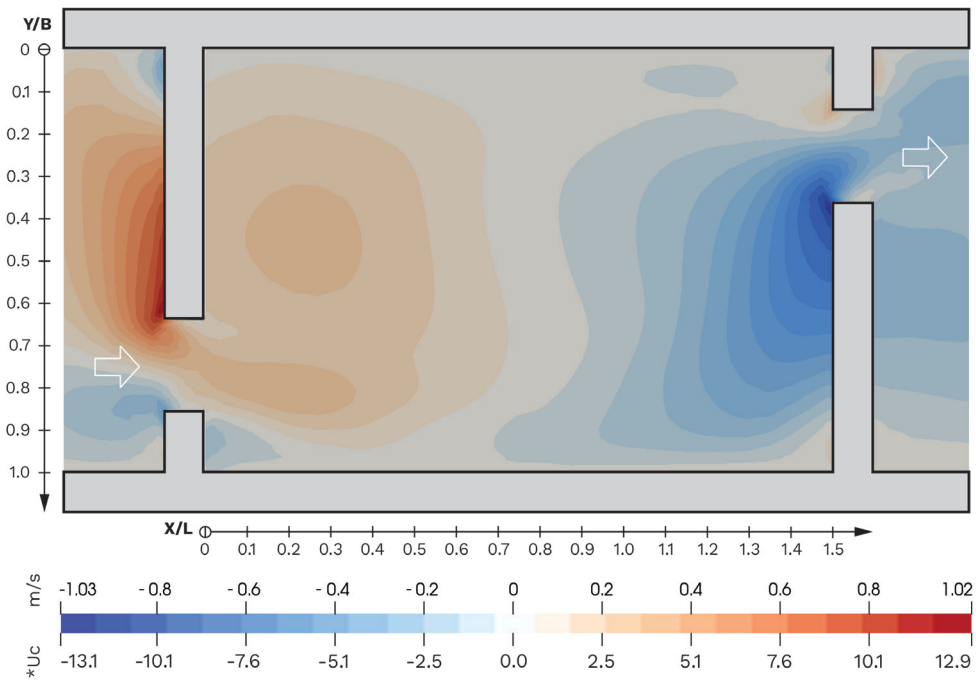

CFD LAYER 2

Laboratory flume: Version 2

Slot-width: 16.7 cm
Discharge: 42 l/s

VELOCITY W_Z

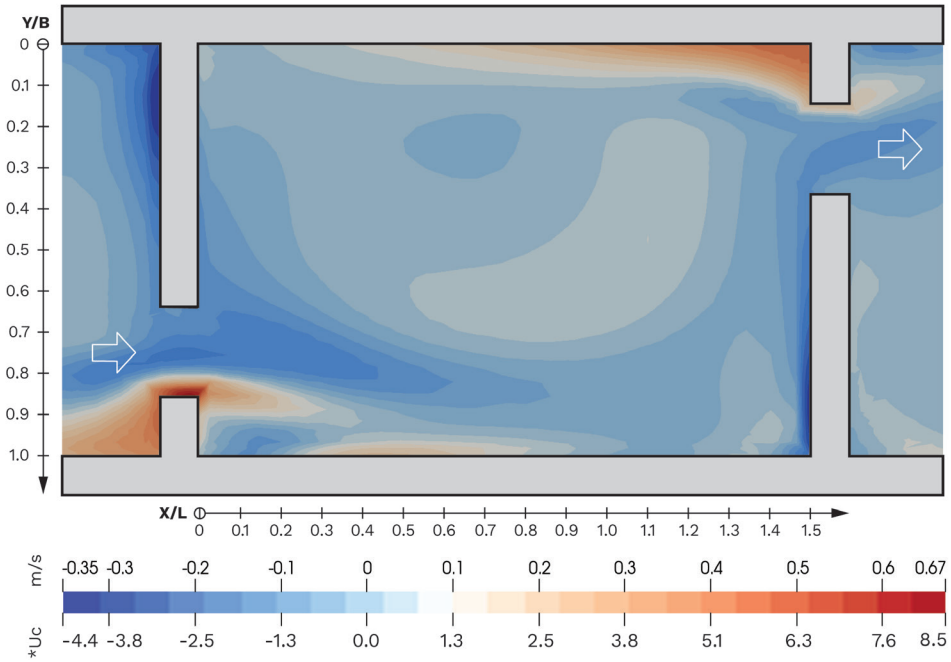

CFD LAYER 3

Laboratory flume: Version 2

Slot-width: 16.7 cm
Discharge: 42 l/s

VELOCITY MAGNITUDE

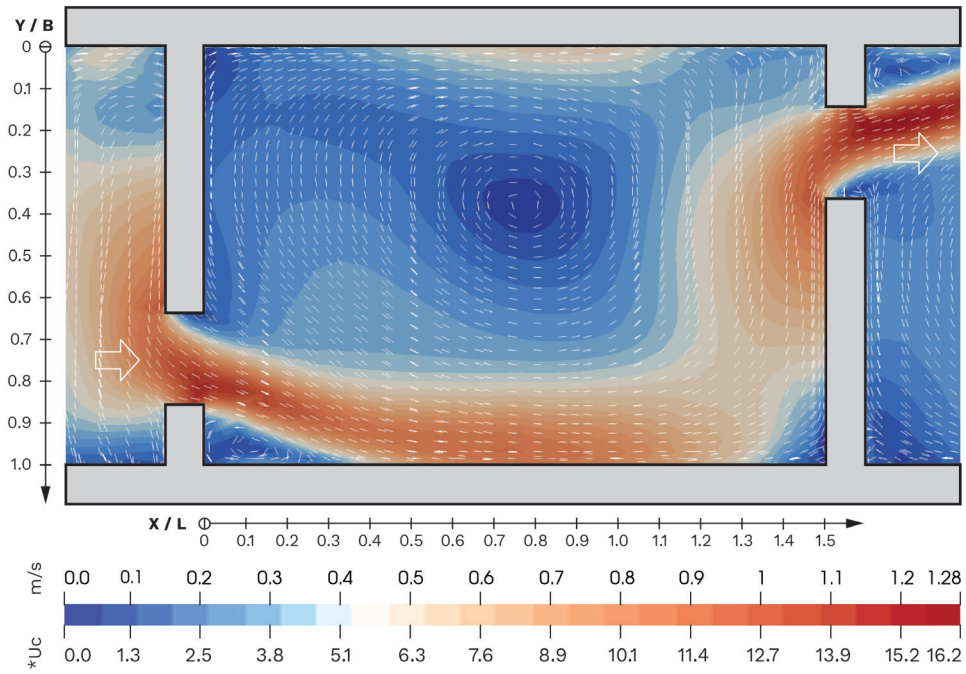

TURBULENT KINETIC ENERGY (TKE)

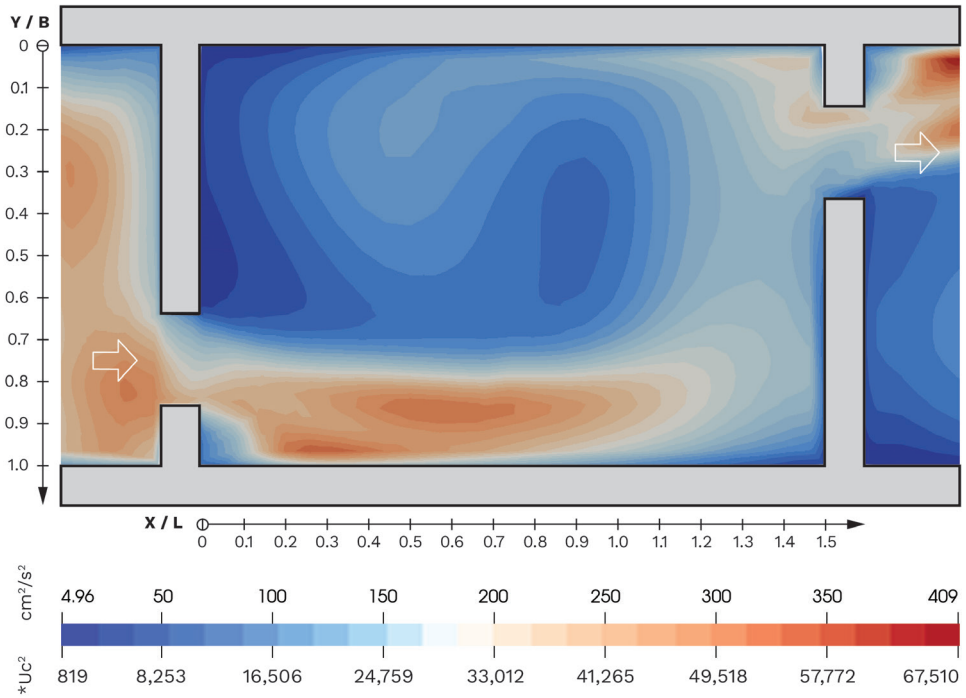

CFD LAYER 3

Laboratory flume: Version 2

Slot-width: 16.7 cm
Discharge: 42 l/s

VELOCITY U_X

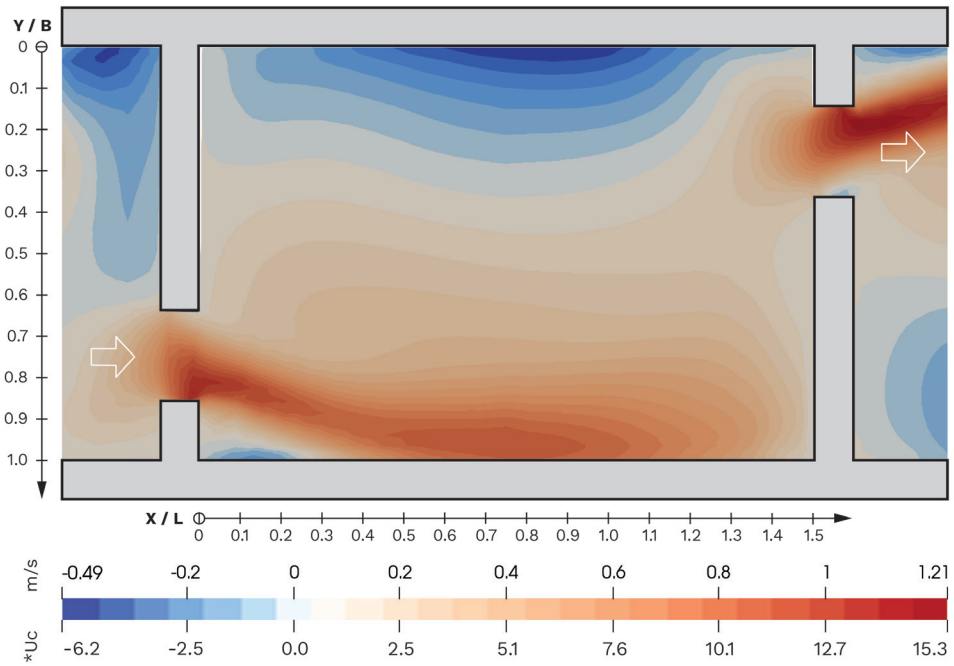

VELOCITY V_Y

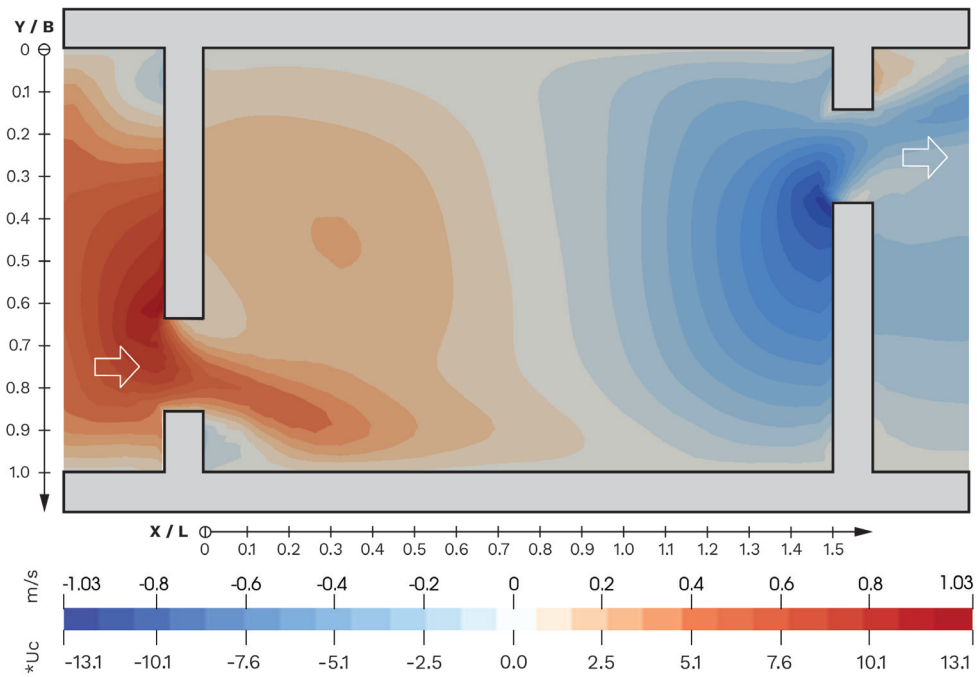

CFD LAYER 3

Laboratory flume: Version 2

Slot-width: 16.7 cm
Discharge: 42 l/s

VELOCITY W_Z

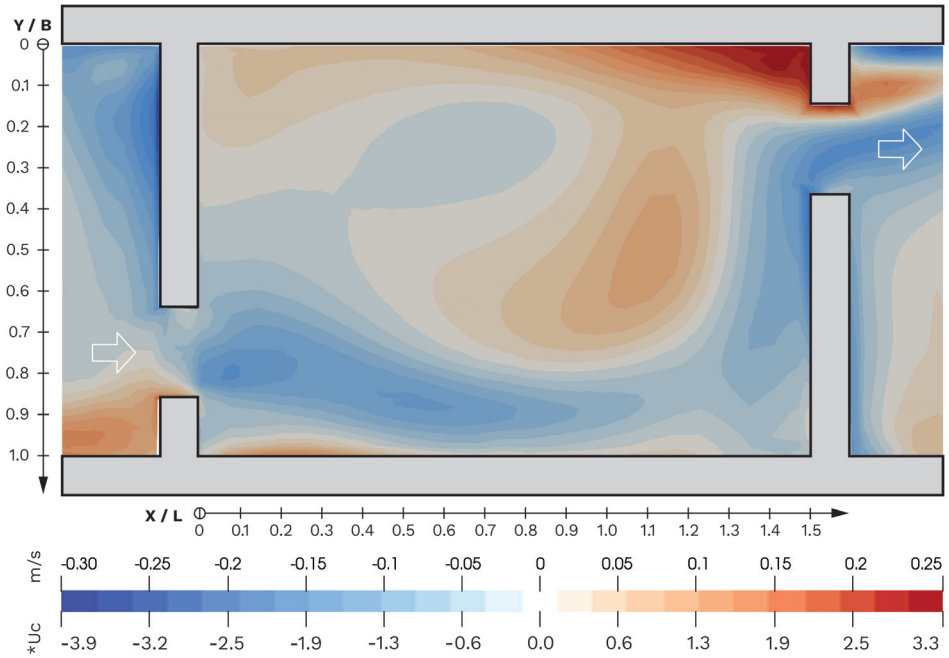

CFD VERTICAL

Laboratory flume: Version 2

Slot-width: 16.7 cm
Discharge: 42 l/s

VELOCITY MAGNITUDE

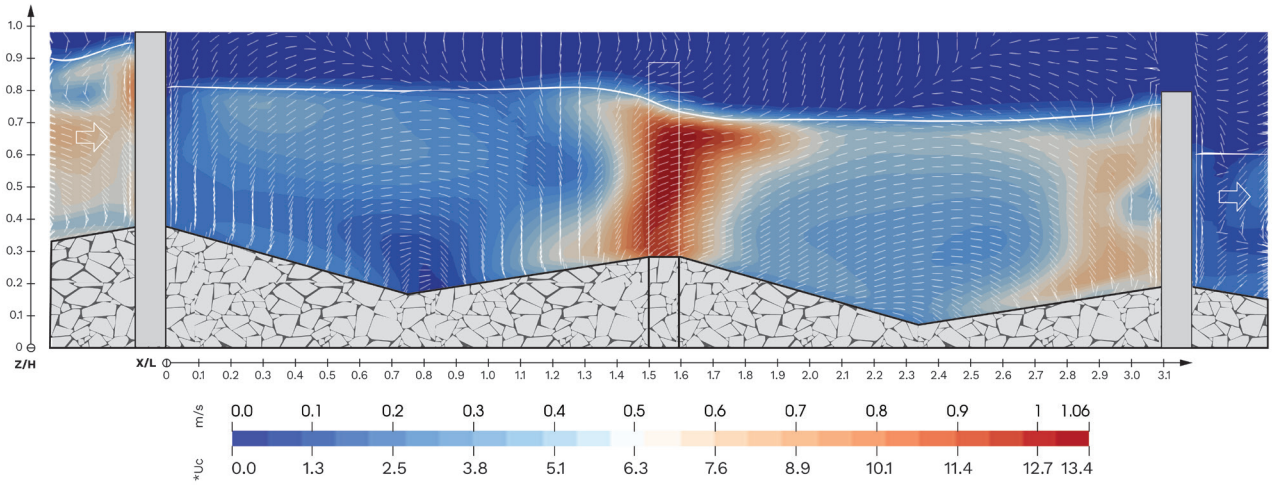

TURBULENT KINETIC ENERGY (TKE)

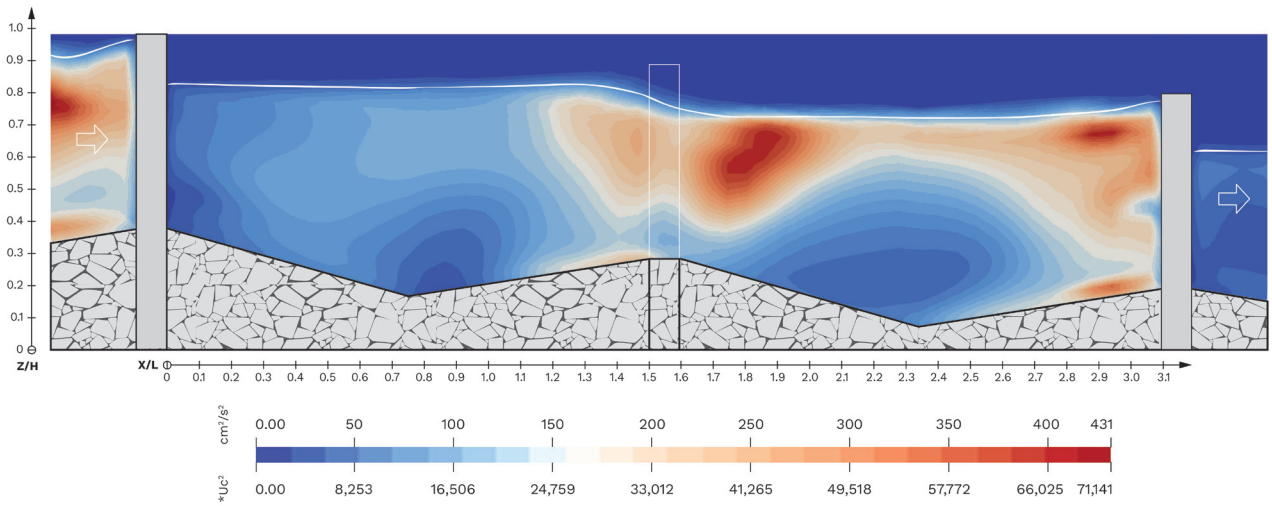

CFD VERTICAL

Laboratory flume: Version 2

VELOCITY U_X

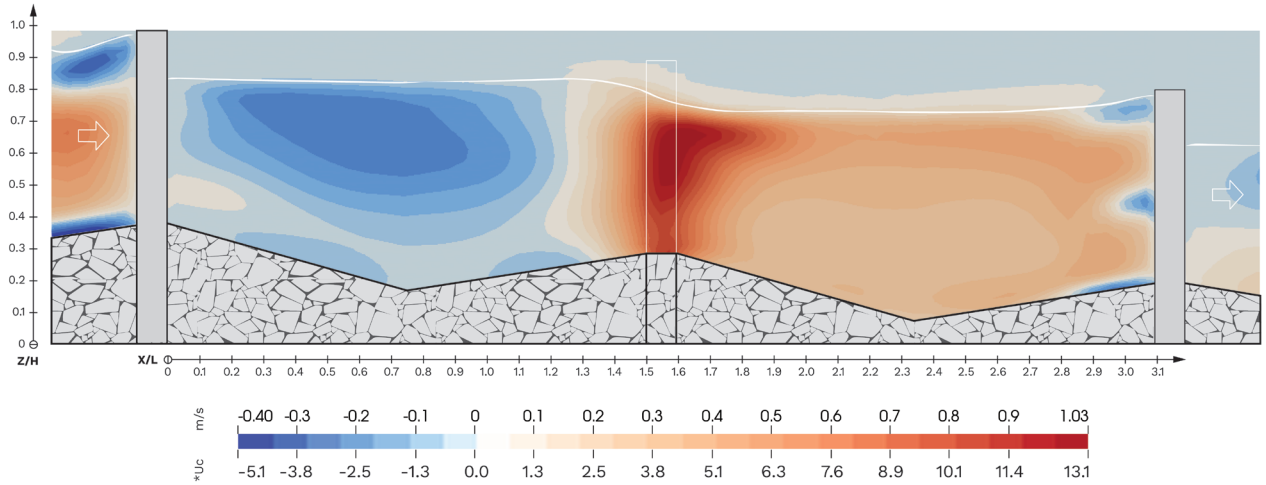

VELOCITY Y_V

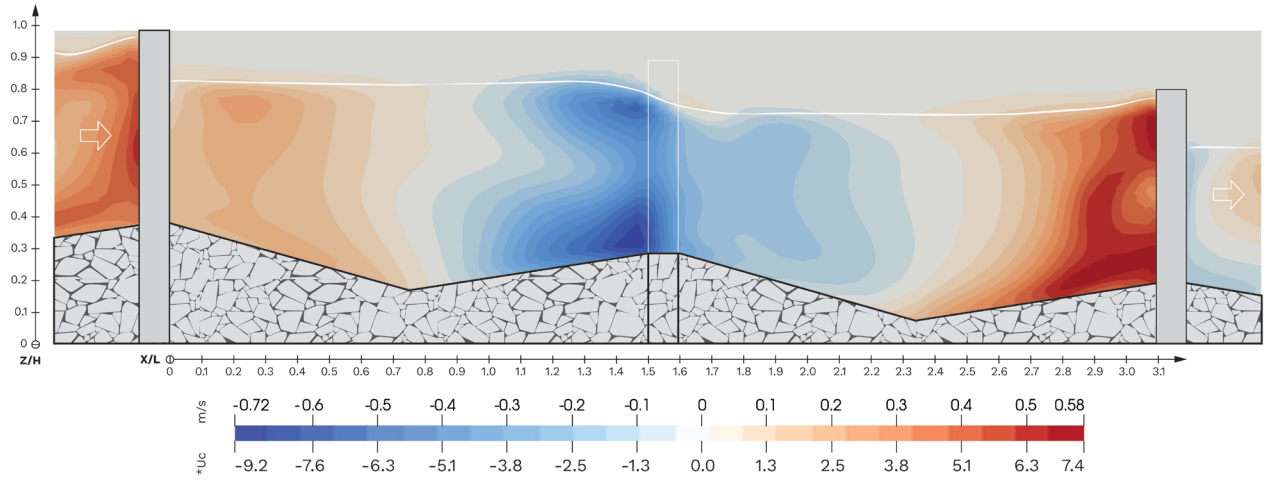

VELOCITY W_Z

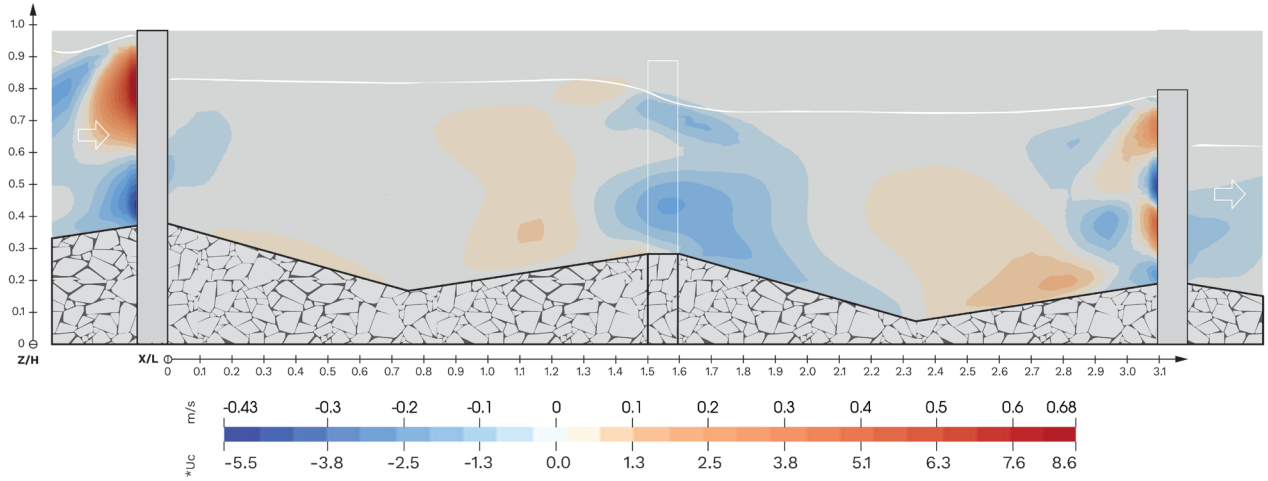

VALIDATION DATA

Laboratory flume: Version 2

Slot-width: 16.7 cm
Discharge: 42 l/s

SPANWISE LINE: X/L 0.1

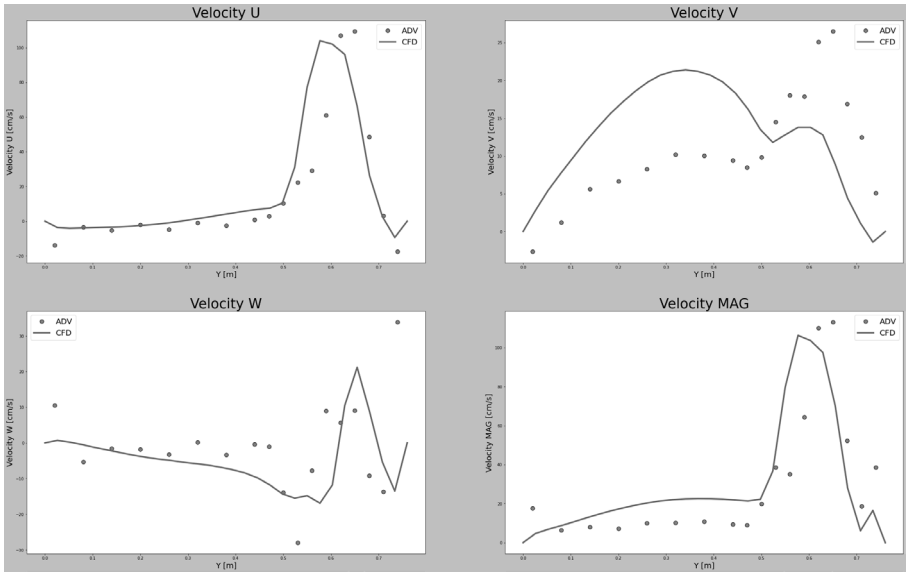

SPANWISE LINE: X/L 1.4

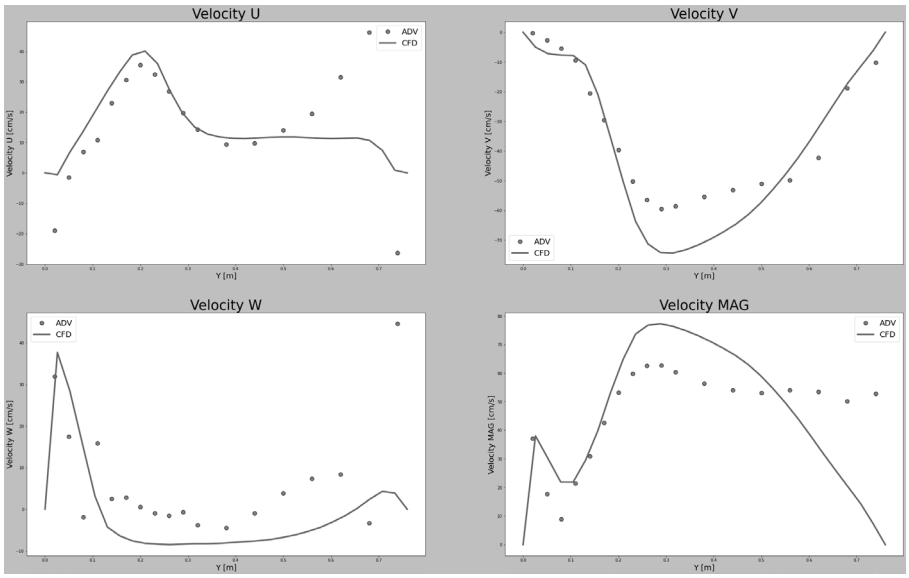

VALIDATION DATA

Laboratory flume: Version 2

Slot-width: 16.7 cm
Discharge: 42 l/s

STREAMWISE LINE: Y/B 0.75

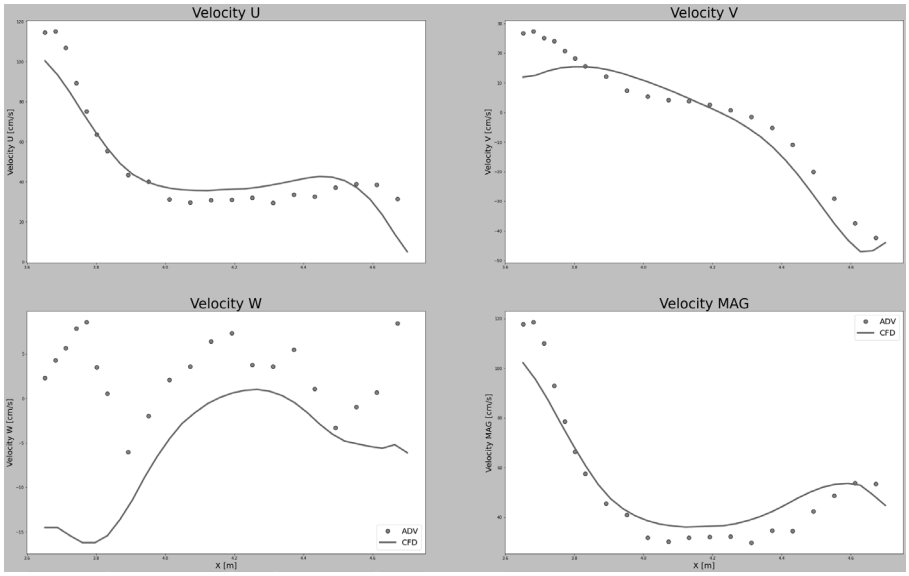

VELOCITY MAGNITUDE OVER DEPTH: WITHIN SLOT

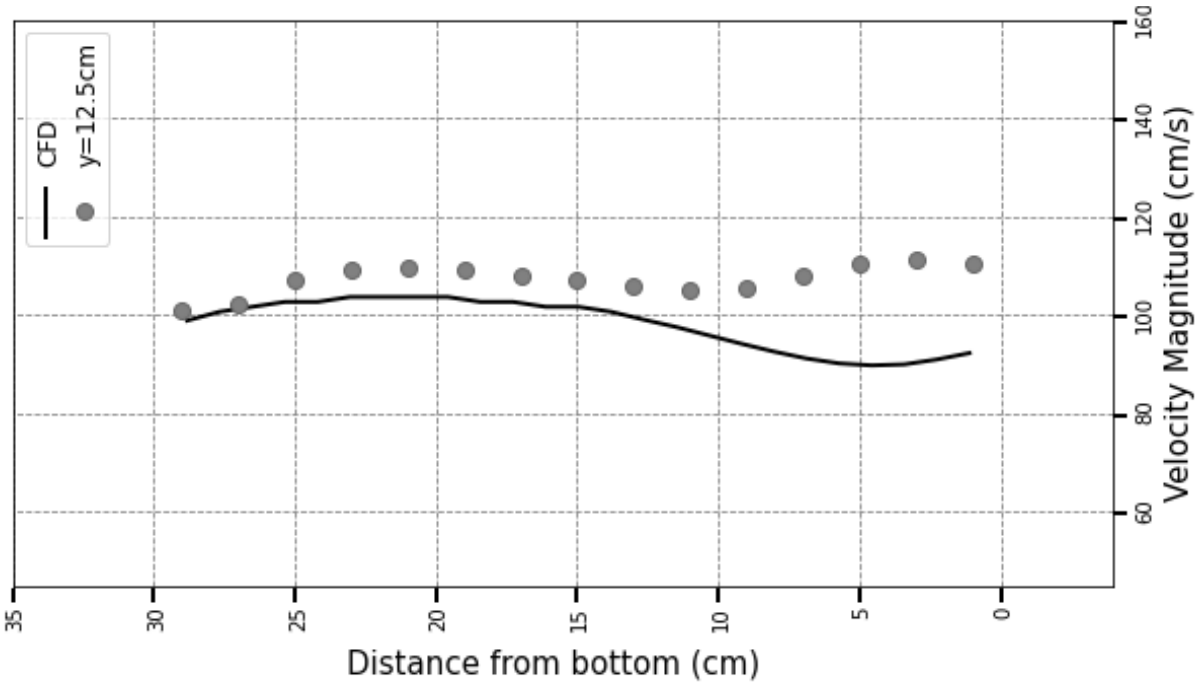

GEOMETRY

Laboratory flume

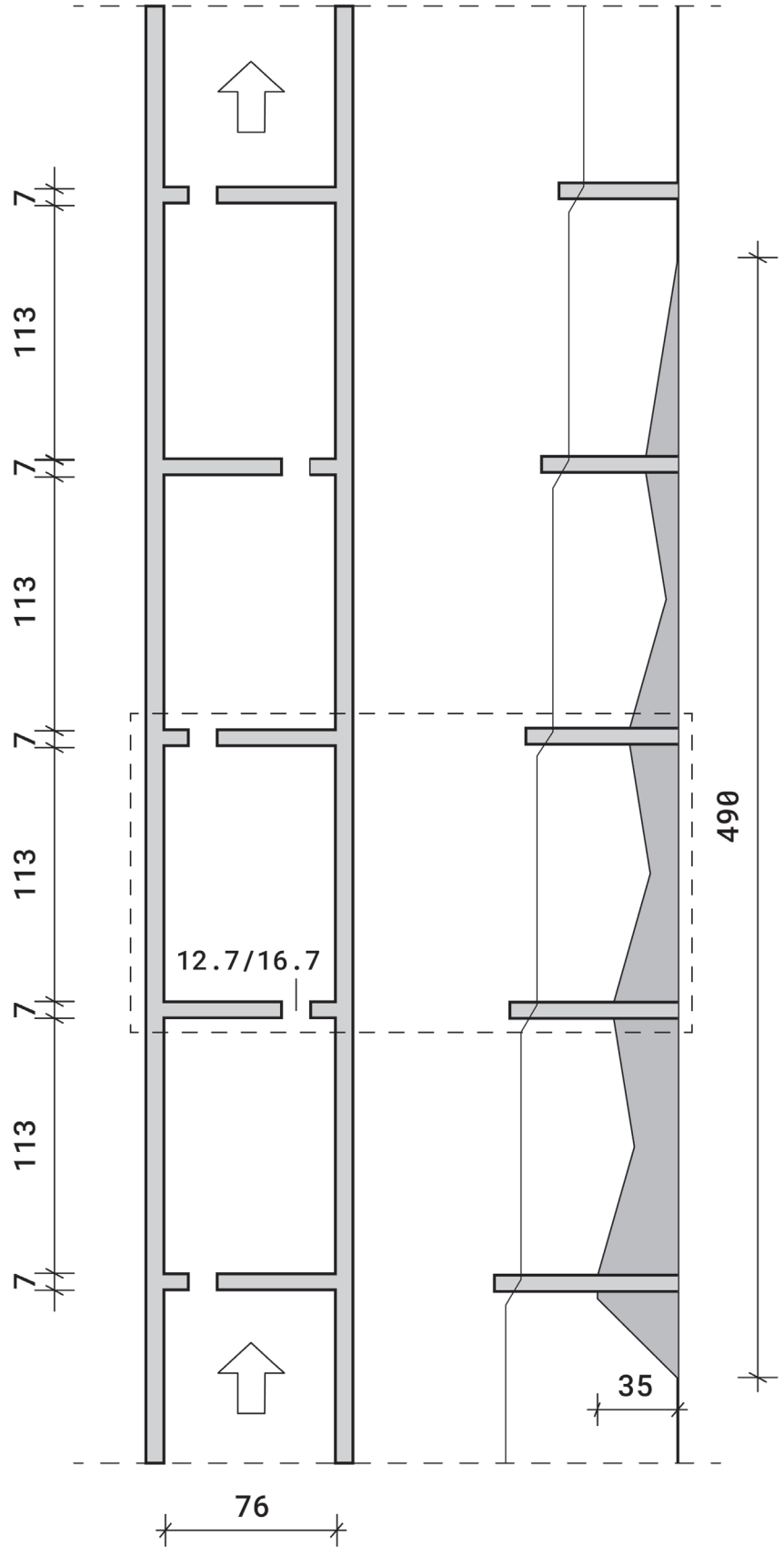

LABORATORY IMPRESSIONS

Photography

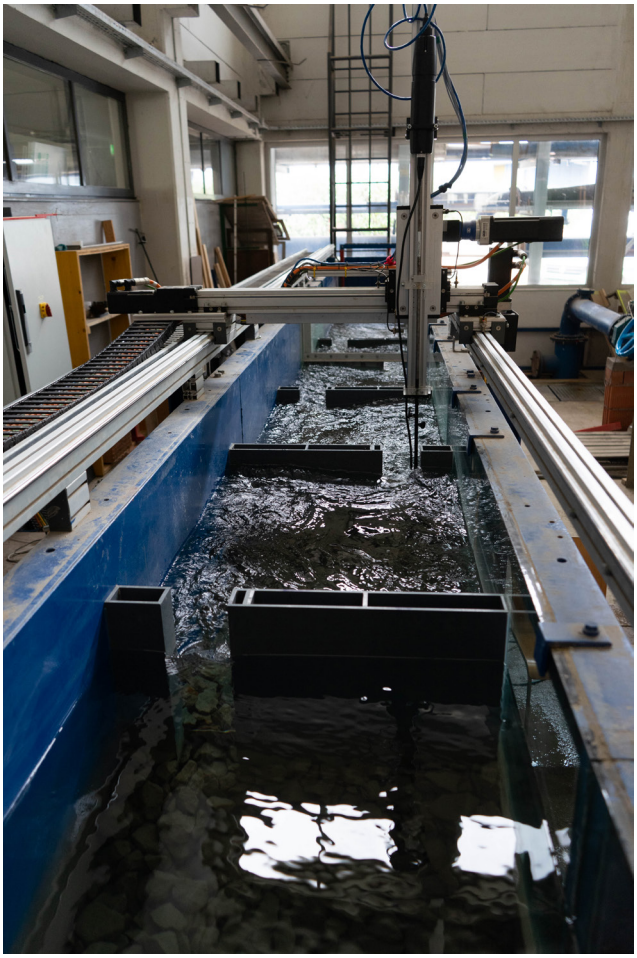

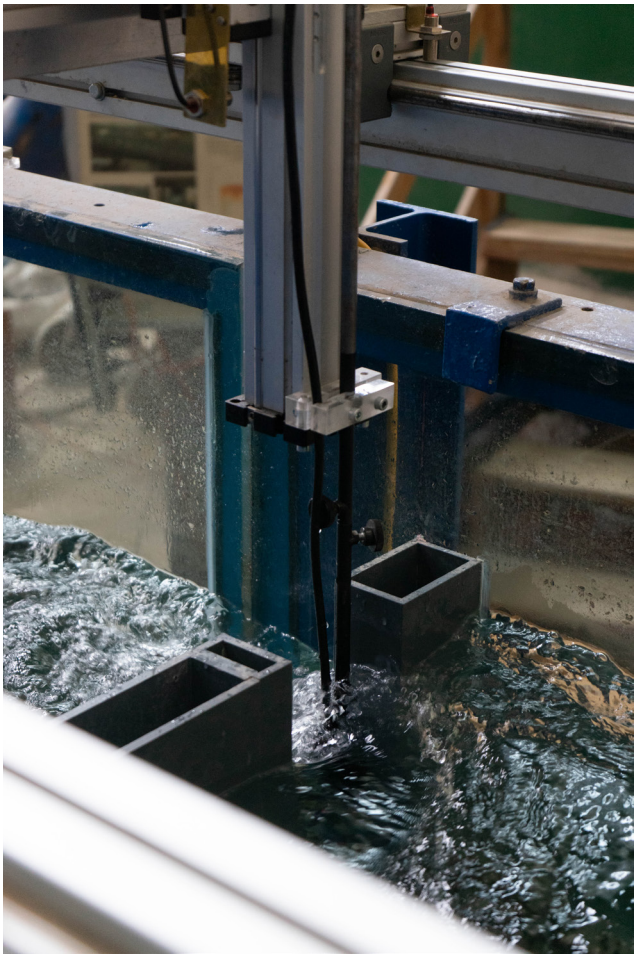

LABORATORY IMPRESSIONS

2 / 3

Photography

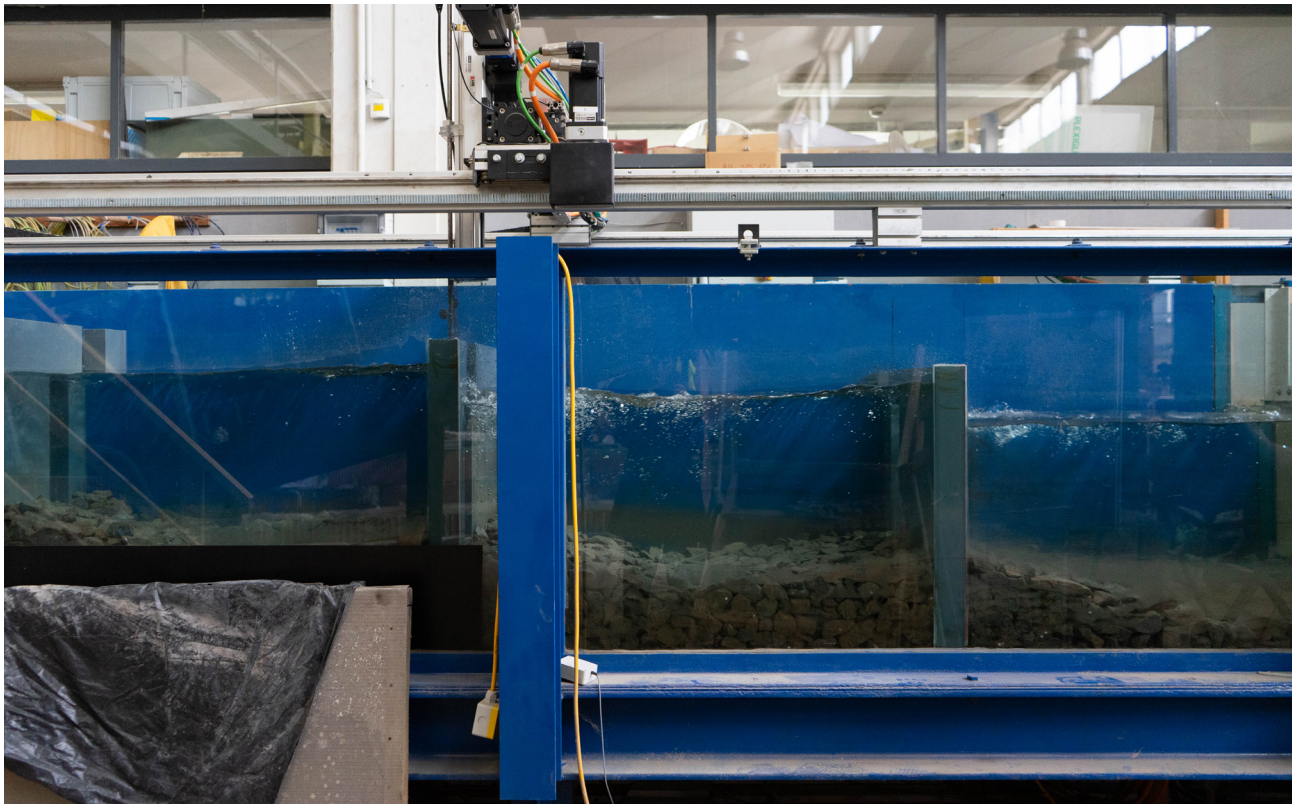

LABORATORY IMPRESSIONS

3 / 3

Photography

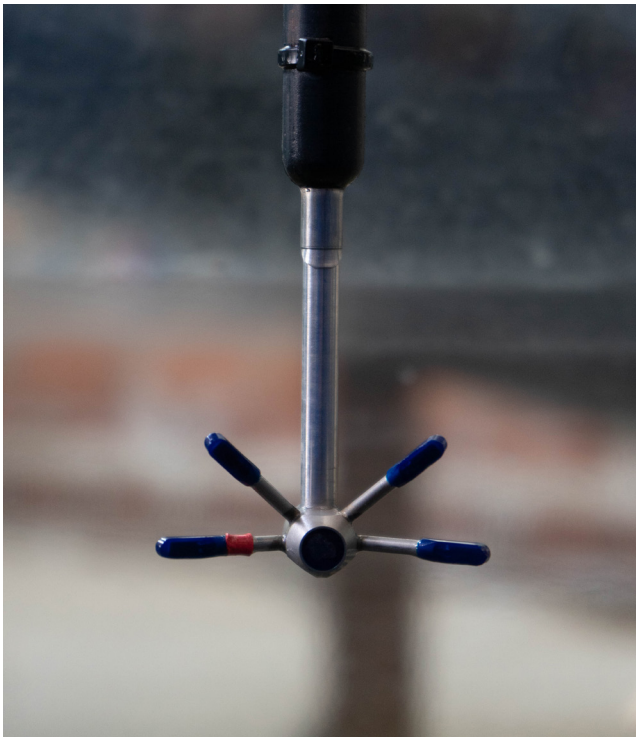

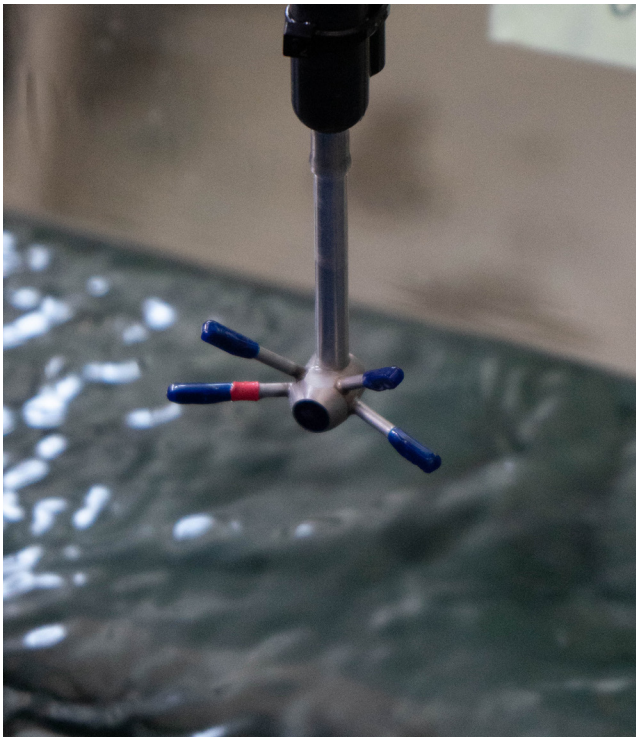

DEVELOPMENT OF A POOL AND SLOT FISHWAY
Laboratory Measurements and Numerical Simulation

AUTHOR
David Derflinger, MSc candidate
david.derflinger@hotmail.com
Geotechnical and Hydraulic Engineering

SUPERVISOR
Assoc.Prof. Dipl.-Ing. Dr.nat.techn. Josef Schneider

SUPERVISING ASSISTANT
Dr.techn. M.Sc. Shervin Shahriari

Graz, September 2021